

# UC Irvine

## UC Irvine Electronic Theses and Dissertations

### Title

The Intracellular Chlamydia Infection: Novel Considerations for the Protease CPAF and the Developmental Cycle

### Permalink

<https://escholarship.org/uc/item/49m5q47c>

### Author

Lee, Jennifer Kristine

### Publication Date

2016

### Supplemental Material

<https://escholarship.org/uc/item/49m5q47c#supplemental>

### Copyright Information

This work is made available under the terms of a Creative Commons Attribution License, available at <https://creativecommons.org/licenses/by/4.0/>

Peer reviewed|Thesis/dissertation

UNIVERSITY OF CALIFORNIA,  
IRVINE

The Intracellular *Chlamydia* Infection: Novel Considerations for the Protease CPAF and the  
Developmental Cycle

DISSERTATION

submitted in partial satisfaction of the requirements  
for the degree of

DOCTOR OF PHILOSOPHY

in Biological Sciences

by

Jennifer Kristine Lee

Dissertation Committee:  
Associate Professor Christine Sütterlin, Co-Chair  
Professor Ming Tan, Co-Chair  
Professor Grant MacGregor  
Professor Hung Fan

2016

Portions of Chapter 3 © 2015 Oxford University Press  
All other materials © 2016 Jennifer Kristine Lee

## **DEDICATION**

To

my husband,  
Steve Flores  
for his patience and understanding

my sister,  
Michelle Lee  
for her constant encouragement

my parents,  
Bill and Karen Lee  
for their loving support

my family and friends,  
for always standing by me

# TABLE OF CONTENTS

	Page
LIST OF FIGURES	v
LIST OF TABLES	vii
ACKNOWLEDGMENTS	viii
CURRICULUM VITAE	x
ABSTRACT OF THE DISSERTATION	xiii
CHAPTER 1: Background and Introduction	1
<i>Chlamydia</i> and Disease	2
<i>Chlamydia</i> Development	4
<i>Chlamydia</i> -Host Cell Interactions	7
<i>Chlamydia</i> Effectors	9
The Chlamydial Protease CPAF	10
Summary	12
CHAPTER 2: CPAF: A Chlamydial Protease in Search of an Authentic Substrate	13
Summary	15
Introduction	16
Results	19
Discussion	41
CHAPTER 3: Induction and Inhibition of CPAF Activity during Analysis of <i>Chlamydia</i> -infected Cells	52
Summary	54
Introduction	55
Results	57
Discussion	67
CHAPTER 4: Development of a CPAF Peptide Inhibitor	75
Summary	77
Introduction	78
Results	82
Discussion	94
CHAPTER 5: Insights into the Chlamydial Developmental Cycle using Three-Dimensional Electron Microscopy	101
Summary	103
Introduction	105
Results and Discussion	109

CHAPTER 6: Conclusions	169
Challenging accepted views about CPAF	172
Implications of <i>in vitro</i> CPAF activity	174
Future directions for CPAF	177
Exploring new frontiers in <i>Chlamydia</i> visualization	183
Future directions with 3D-EM	185
Cell size regulation	187
Regulators of cell fate in other systems	191
Summary	195
REFERENCES	197
APPENDIX: Materials and Methods	215

## LIST OF FIGURES

		Page
Figure 2.1	Proteolysis of centrosomal proteins in lysates of <i>Chlamydia</i> -infected cells	20
Figure 2.2	CPAF is necessary and sufficient for C-Nap1 and CPAP proteolysis <i>in vitro</i>	22
Figure 2.3	CPAF-mediated proteolysis of centrosomal proteins does not occur in intact cells	26
Figure 2.4	Golgin-84 cleavage does not occur in <i>Chlamydia</i> -infected cells when CPAF is inhibited during cell processing	27
Figure 2.5	Degradation of BH3-only proteins in <i>Chlamydia</i> -infected cells is prevented by inhibiting CPAF during cell processing	30
Figure 2.6	Cleavage of intermediate filaments in <i>Chlamydia</i> -infected cells is also dependent on cell processing	32
Figure 2.7	Proteolysis of four additional CPAF substrates is dependent on cell processing	34
Figure 2.8	CPAF is autocatalytically cleaved into its active form in <i>Chlamydia</i> -infected cells	37
Figure 2.9	CPAF localization depends on fixation method	40
Figure 3.1	Methods to inhibit CPAF activity during infected cell lysate preparation are not always effective	58
Figure 3.2	Analysis of infected cell lysates for substrate proteolysis and CPAF activity	61
Figure 3.3	Protein substrates vary in their susceptibility to CPAF-mediated proteolysis	64
Figure 3.4	CPAF activity is induced by standard cell collection methods	66
Figure 3.5	Recommended procedure for analysis of proteins in lysates from <i>Chlamydia</i> -infected cells	73
Figure 4.1	Initial screen of boronate peptides for CPAF inhibition	84

Figure 4.2	Two boronate peptides are more potent CPAF inhibitors <i>in vitro</i> than lactacystin	86
Figure 4.3	Molecular model of boronate peptide binding within CPAF active site	87
Figure 4.4	Rational design enhanced boronate peptide inhibition of CPAF	90
Figure 5.1	Novel three-dimensional electron microscopy approach to analyze chlamydial inclusions	110
Figure 5.2	Validation of 3D-EM approach compared to established chlamydial quantification methods	121
Figure 5.3	Difficulty discerning chlamydial forms using single electron micrographs	123
Figure 5.4	3D-EM overcomes limitations of 2D-EM by accurately distinguishing and quantifying chlamydial forms	125
Figure 5.5	Temporal analysis of <i>Chlamydia</i> developmental forms	127
Figure 5.6	Bang-bang mathematical modeling of chlamydial development	139
Figure 5.7	Temporal analysis of the chlamydial inclusion	141
Figure 5.8	Spatial analysis of developmental forms within the inclusion	150
Figure 5.9	Size of chlamydial forms changes over time	155
Figure 5.10	Stochastic division prior to doubling can account for RB heterogeneity	156
Figure 5.11	Proposed model of RB size regulation of chlamydial development	161

## LIST OF TABLES

		Page
Table 2.1	Summary of published CPAF substrates	31
Table 4.1	Boronate peptide compounds	83
Table 4.2	Comparison of CPAF inhibitors	95
Table 5.1	Selection of chlamydial inclusions for analysis by 3D-EM	112
Table 5.2	Individual chlamydial inclusion data	128
Table 5.3	Bang-bang time course reaction parameters	141
Table 5.4	Expected RB size over time assuming division at 1.7X original size	164

## ACKNOWLEDGMENTS

I want to express the deepest appreciation to my thesis advisors Dr. Christine Sütterlin and Dr. Ming Tan for guiding me through my Ph.D. research. My project evolved over the years, and they always helped me focus on the excitement of new scientific questions. Their enthusiasm and dedication to science and research encouraged me to work my hardest. They consistently challenged me to become a better researcher and critical thinker, and without their guidance this dissertation would not have been possible.

I would like to thank my committee members, Dr. Grant MacGregor and Dr. Hung Fan, for their valuable advice and support. Their insightful comments were critical to the development of my project. I would also like to thank Dr. Dritan Agalliu who served as a member on my advancement committee and provided important feedback about my research.

I would like to express my appreciation for Dr. German Enciso who has served as a patient guide in the field of mathematical modeling. Our conversations and regular meetings helped me approach problems from a different perspective and he brought invaluable expertise to the 3D-EM project.

My thanks go out to Dr. Mark Ellisman and Dr. Daniela Boassa at NCMIR for their assistance with 3D-EM. I am very grateful for the time and energy they put forth helping us develop a new technique. I would also like to thank Dr. Andrew Noske who taught me everything I know about segmentation and IMOD.

In addition, thank you to Dr. Rommie Amaro and Dr. Vicki Feher for collaborating on the CPAF inhibitor research. Even when the project didn't go as we had hoped, they always remained positive and resourceful.

I am grateful to have had the opportunity to work with many great people at UCI. I would especially like to thank Allan Chen and Kirsten Johnson for paving the way for the CCB group and acting as my mentors. You both taught me valuable lessons about how to succeed as a graduate student. Kirsten, I will never have another pod buddy as great as you. Our fun lunch Fridays and Bachelor Mondays helped me stay sane. In the lab I always looked to you as an example of how to be a thorough and critical scientist. I appreciate all of your advice about my research and beyond. To the current members of the Sütterlin lab - Kari Herrington, Kati Tormanen, Halim Loukil: It has been a pleasure working with you and I thank you for the support you provided to me at the bench and at lab meetings. To past Sütterlin lab members Valerian Dormoy and Breanne Karanikolas: I appreciate your helpful advice about research and career. To Tan lab members Allan Chen, Eric Cheng, Brett Hanson, Emilie Orillard, and Chris Rosario: Thank you for your continual encouragement. I will look back fondly on past CBRS meetings because of your company. Lastly, a special thank you to my undergraduate research assistants – Soroush Pairawan, Chris Chander, Tracy Lou, and Melody Guo. I could not have segmented all of those inclusions without your help! Thank you for working so diligently.

I thank Oxford University Press for permission to include copyrighted material, which was originally published in Pathogens and Disease, as part of Chapter 3 of my dissertation.

I would also like to thank the UCI Cancer Research Institute Cancer Biology Training Grant for funding as a Pre-Doctoral Fellow.

Lastly, I extend the greatest love and gratitude to my family and friends who have supported me through graduate school. You always believed in me and encouraged me, and I know I would not have succeeded without you by my side. A special thank you to my husband Steve and my sister Michelle who have seen me through the most emotionally trying times and given me the strength to persevere.

# CURRICULUM VITAE

**Jennifer Kristine Lee**

## EDUCATION

- Ph.D. in Biological Sciences, University of California, Irvine March 2016  
Dissertation Title: The Intracellular *Chlamydia* Infection: Novel  
Considerations for the Protease CPAF and the Developmental Cycle  
Advisors: Dr. Christine Sütterlin and Dr. Ming Tan
- B.S. in Biochemistry, University of California, Los Angeles June 2006

## PUBLICATIONS

Johnson KA\*, Lee JK\*, Chen AL, Tan M, Sütterlin C (2015) Induction and inhibition of CPAF activity during analysis of *Chlamydia*-infected cells. *Pathog Dis* 73(1): ftv007.  
doi:10.1093/femspd/ftv007

Chen AL\*, Johnson KA\*, Lee JK\*, Sütterlin C, Tan M (2012) CPAF: A Chlamydial Protease in Search of an Authentic Substrate. *PLoS Pathog* 8(8): e1002842.  
doi:10.1371/journal.ppat.1002842

Lee JK, Terada M, Bushong E, Thor A, Boassa D, Ellisman M, Sütterlin C, Tan M (2012) Cover image of: *Intracellular Pathogens I: Chlamydiales*. Ed. Ming Tan and Patrik Bavoil. Washington DC: ASM Press, 2012. Print.

\*equal contributions

## PRESENTATIONS

Lee JK, Boassa D, Ellisman M, Sütterlin C, Tan M. Three-Dimensional Analysis of the Chlamydial Developmental Cycle. Oral presentation at: Seventh Biennial Meeting of the Chlamydia Basic Research Society; 2015 Mar 29-Apr 1; New Orleans, Louisiana.

Johnson KA, Lee JK, Tan M, Sütterlin C. *Chlamydia*-induced centrosome and chromosomal abnormalities in infected cells. Poster presentation at: UCI Campus-Wide Symposium on Basic Cancer Research; 2013 May 4; Irvine, California.

**Lee JK**, Johnson KA, Chen AL, Tan M, Sütterlin C. Manipulations of Chlamydia-infected cells lead to CPAF activity and artifactual proteolysis of host proteins. Oral presentation at: Sixth Biennial Meeting of the Chlamydia Basic Research Society; 2013 Mar 19-22; San Antonio, Texas.

**Lee JK**, Noske A, Boassa D, Ellisman M, Tan M, Sütterlin C. 3-Dimensional Electron Microscopic Analysis of *Chlamydia*-Infected Cells. Oral presentation at: UCI School of Biological Sciences Department of Developmental and Cell Biology Retreat; 2013 Feb 28; Riverside, California.

Johnson KA, **Lee JK**, Boassa D, Molina T, Terada M, Thor A, Ellisman M, Tan M, Sütterlin C. Host centrosome morphology during infection with *Chlamydia trachomatis*. Poster presentation at: UCI Campus-Wide Symposium on Basic Cancer Research; 2012 May 5; Irvine, California.

## **HONORS AND AWARDS**

Cancer Research Institute Cancer Biology Training Grant Pre-Doctoral Fellow University of California, Irvine	2012-2013
Edward Steinhaus Teaching Award University of California, Irvine	June 2012
Howard Hughes Medical Institute (HHMI) Graduate Fellow University of California, Irvine	2010-2012

## **TEACHING AND LEADERSHIP**

California Community College Internship Program Cellular and Molecular Biology, Human Biology University of California, Irvine and Orange Coast College	2013-2014
Graduate Student Mentor Cancer Research Institute Summer Youth Fellowship Program University of California, Irvine	Spring 2013
Graduate Student Representative Department of Developmental and Cell Biology University of California, Irvine	2012-2013

Head Teaching Assistant  
Biological Sciences 93: From DNA to Organisms  
University of California, Irvine

Fall 2012

Teaching Assistant  
Biological Sciences 93: From DNA to Organisms  
University of California, Irvine

Fall 2011

## ABSTRACT OF THE DISSERTATION

The Intracellular *Chlamydia* Infection: Novel Considerations for the Protease CPAF and the Developmental Cycle

By

Jennifer Kristine Lee

Doctor of Philosophy in Biological Sciences

University of California, Irvine, 2016

Associate Professor Christine Sütterlin, Co-Chair

Professor Ming Tan, Co-Chair

*Chlamydia* are obligate intracellular bacterial pathogens with a significant impact on human health. *Chlamydia* infect eukaryotic cells, and a wide range of effects on the host cell have been attributed to a chlamydial protease, CPAF, through cleavage or degradation of numerous host proteins. We discovered that this reported proteolysis was an *in vitro* phenomenon that occurred during preparation of infected cells for protein analysis. We showed that CPAF activity was induced by detachment of *Chlamydia*-infected cells from a cell culture monolayer and that this protease remained active in cell lysates resulting in artifactual proteolysis. Chlamydial phenotypes attributed to CPAF were still observed when we took precautions to prevent *in vitro* proteolysis. Our findings challenged the prevailing model about the function of CPAF during the chlamydial infection and its intracellular targets. In a second project, we studied the unusual chlamydial developmental cycle with a novel three-dimensional electron microscopy (3D-EM) method. During the intracellular infection, the bacterium converts within the chlamydial inclusion from an infectious, but non-dividing, elementary body (EB) into a reticulate body (RB)

that divides repeatedly by binary fission before converting back into EBs to infect new cells. We analyzed each *Chlamydia*-infected cell with several hundred two dimensional EM slices and used computational methods to reconstruct the three-dimensional images of the chlamydial inclusions. The results provided the first comprehensive analysis of the developmental cycle, including the number, size, and location of each EB, RB, and intermediates of RB replication and RB-to-EB conversion. We described for the first time that RB volume progressively decreases as RB number increases, indicating that RBs divide before doubling in size. However, we did not observe RBs below a minimum size, leading us to postulate that RBs below a size threshold convert into an EB. We propose a new model of chlamydial development in which RB-to-EB conversion is regulated by RB size because several rounds of RB replication are required for the RB to become small enough to convert into an EB. In this model, RB size acts as a timer and provides a mechanism to delay RB-to-EB conversion until the RB pool has expanded.

# **Chapter 1**

## **Background and Introduction**

## ***Chlamydia* and Disease**

Bacteria of the family *Chlamydiaceae* are non-motile gram-negative obligate intracellular pathogens that infect eukaryotic host cells. Within the *Chlamydiaceae* family is a single genus, *Chlamydia*, containing nine species that exhibit a diverse range of host cell infectivity, tissue tropism, and disease. *C. muridarum*, *C. pecorum*, *C. suis*, *C. abortus*, *C. felis*, and *C. caviae* infect animals ranging from mice to cattle. Chlamydial infections cause various diseases in animals including conjunctivitis and pneumonia (1). *C. psittaci* primarily infects birds, but this organism is classified by the Centers for Disease Control (CDC) as a category B bioterrorism agent due to its ease of transmission to humans through aerosolized particles (2). Although rare, *C. psittaci* infection in humans causes psittacosis, a respiratory infection leading to severe pneumonia and possible death. *C. pneumoniae* and *C. trachomatis* are human pathogens that are the causative agents of respiratory, ocular, and genital tract infections (1). *C. pneumoniae* and *C. trachomatis* significantly impact worldwide health by causing hundreds of millions of infections annually (3).

*C. pneumoniae* infects lung epithelial cells of the upper and lower respiratory tract and is a causative agent of community acquired pneumonia. *C. pneumoniae* causes about 10% of the pneumonia cases in adults worldwide (4). Persistent *C. pneumoniae* infections have also been associated with other chronic illnesses including asthma (5) and atherosclerosis (6).

*C. trachomatis* strains are classified into serovars based on antibody response to the chlamydial major outer membrane protein (OmpA) (7). *C. trachomatis* serovars A-C infect epithelial cells of the conjunctiva and cause trachoma, a keratoconjunctivitis. Approximately 84 million people worldwide have active trachoma and if left untreated, these infections can lead to inflammation and scarring of the upper eyelid, eventually resulting in blindness (8). *C.*

*trachomatis* ocular infections are the number one cause of infectious blindness worldwide (9). These infections are particularly common in less developed countries where lack of running water and sanitation, as well as limited access to treatment, contributes to recurring infections that may result in developing blindness (8, 10).

*C. trachomatis* infections of the genital tract are the most common notifiable disease in the United States, with over 1.4 million cases reported to the CDC in 2014 (11). *C. trachomatis* serovars D-K infect columnar epithelial cells of the genital mucosa causing an infection that is often asymptomatic (12). *C. trachomatis* lymphogranuloma venereum (LGV) serovars L1-L3 are also associated with sexually transmitted infections but are more invasive than serovars D-K, causing systemic infections in the lymph nodes (7). If left untreated, chlamydial genital infections in men can lead to epididymitis and inflammation of the urethra. For women, chronic or untreated *Chlamydia* infections can result in long-term complications including pelvic inflammatory disease, which can lead to ectopic pregnancy and infertility (3).

*C. trachomatis* genital infections have also been associated with human papillomavirus (HPV) as a co-factor for development of cervical cancer (13-16). Interestingly, although HPV infection is a necessary cause of cervical cancer (17), only a small percentage of HPV infections progress into carcinomas suggesting co-factors like *Chlamydia* may modulate tumorigenic potential. Additionally, sero-epidemiological studies show that *Chlamydia* infection is independently associated with increased incidence of cervical squamous cell carcinoma when controlling for other co-factors (14, 18, 19). *C. trachomatis* infection caused transformation of 3T3 cells in culture resulting in anchorage independence and increased colony formation, which are features of cancer cells (20). Centrosome abnormalities, spindle defects, and chromosome segregation errors are all phenotypes in *Chlamydia*-infected cells that could provide a potential

mechanism by which *Chlamydia* contributes to cervical carcinogenesis (21, 22). Centrosome amplification in particular has been shown play a role in tumorigenesis by promoting aneuploidy and malignant transformation (23). In our lab, we have been particularly interested in *Chlamydia*-induced centrosome amplification as a potential mechanistic link between *Chlamydia* infection and cervical cancer, and in Chapter 2 we describe a study investigating whether centrosomal regulator proteins are altered during a chlamydial infection.

## ***Chlamydia* Development**

All chlamydial species are characterized by a biphasic intracellular developmental cycle, which is unique compared to other bacteria. *Chlamydia* alternate between two major developmental forms: elementary bodies (EBs), which are small infectious forms, and reticulate bodies (RBs), which are larger non-infectious, metabolically active forms (24). Early development is characterized by entry of an infectious EB into the host cell and conversion into an RB. During mid-cycle, RBs replicate by binary fission. Finally, late in the developmental cycle RBs convert back into EBs through a transitional form known as the intermediate body (IB) (25). The developmental cycle concludes with release of infectious progeny from the host cell. Although the chlamydial developmental cycle is well described based on qualitative observation, little is known about the quantitative relationships between chlamydial forms or the regulatory mechanisms that govern the transitions between developmental stages.

### **Attachment and entry**

A chlamydial infection begins with an infectious EB. EBs are small electron dense forms approximately 0.3  $\mu\text{m}$  in diameter with highly cross-linked outer membranes, providing structural rigidity and osmotic stability for survival outside of the host cell (26). Initial

attachment of EBs to the host cell surface is mediated by electrostatic interactions with host heparin sulfate-containing glycosaminoglycans (27). Secondary adhesion of EBs to the host cell surface is accomplished by binding of a chlamydial surface protein to a host cell receptor. There appear to be multiple mechanisms by which secondary adhesion can be mediated, and several candidate chlamydial and host proteins have been implicated in this process including OmpA, OmcB, and Pmps on the chlamydial side (28), and mannose-6-phosphate receptor and protein disulfide isomerase on the host cell side (29, 30). Chlamydial species differ in their expression of adhesins, and specific interactions between particular chlamydial adhesins and host cell receptors may account for the tissue tropism differences between chlamydial species (28, 29).

Binding is followed by uptake, but the exact mechanism by which *Chlamydia* enters the host cell is unclear. Classic receptor-mediated endocytosis was originally thought to facilitate internalization of the infectious EB, but it was later found that *Chlamydia* entry was not dependent on clathrin-coated vesicle formation (31, 32). *Chlamydia* uptake was not inhibited in mutant cell lines defective in clathrin-mediated endocytosis or when cells were treated with RNAi against clathrin itself (32). There is conflicting data suggesting dynamin, an endocytic pathway GTPase, may be important for chlamydial uptake (32, 33). Thus, *Chlamydia* may enter host cells by an unusual receptor-mediated mechanism that uses some, but not all, components of the endocytic pathway. Actin is clearly important to the process of EB internalization because actin depolymerizing agents like cytochalasin D inhibit host cell uptake of EBs from a variety of chlamydial species (32). EB attachment at the host cell surface induces local actin remodeling that results in *Chlamydia* entry into the cell by a phagocytic-like mechanism (34). Together the data suggest that *Chlamydia* enter host cells by receptor-mediated phagocytosis.

### **Establishment of the chlamydial inclusion**

Once inside the host cell, *Chlamydia* reside within a membrane bound compartment called the chlamydial inclusion. The initial inclusion originates from the host plasma membrane that was used to internalize the EB, but *Chlamydia* modify the membrane by inserting inclusion membrane proteins (Incs) within two hours of infection (35). Inc proteins share little sequence homology with each other besides a common bilobed hydrophobic domain. Although the specific functions of Incs are largely uncharacterized, they have been proposed to mediate effects on the host cell based on their localization within the inclusion membrane exposed to the host cytosol (36).

The inclusion is a specialized membrane compartment that is protected from fusion with the lysosome (37). Inclusions lack markers of early and late endosomes, such as transferrin receptor and mannose 6-phosphate receptor. Lysosomal markers like acid phosphatase and LAMP1 and 2 are also absent from chlamydial inclusions (37). The exclusion of these markers from the inclusion membrane suggests that *Chlamydia* dissociate from the endocytic pathway and avoid fusion with the lysosome. Inclusions are, however, fusogenic with a subset of exocytic vesicles from which the bacteria intercept host sphingomyelin and cholesterol traveling from the Golgi apparatus to the plasma membrane (38, 39). Curiously, host proteins are absent from the chlamydial inclusion membrane suggesting fusion with post-Golgi vesicles or direct contact with the Golgi or endoplasmic reticulum is not used as a source of membranes for the growing inclusion (40).

### **Bacterial growth, replication, and conversion**

The EB differentiates into a metabolically active RB within 1-8 hours post infection (hpi) (41). RBs are about one micrometer in diameter and are less electron dense than EBs because

their DNA is decondensed. During the mid-cycle of *Chlamydia* development, RBs replicate by binary fission. Then following a period of rapid bacterial cell division, RBs begin to asynchronously convert back into EBs (24). The mechanisms that regulate the processes of chlamydial replication and conversion are largely unknown.

### **Bacterial exit**

At the end of the chlamydial developmental cycle, EBs that have accumulated within the inclusion are released from the host cell by either lysis or extrusion. During the lysis process, inclusion rupture is followed by nuclear then plasma membrane rupture releasing infectious progeny into the environment while killing the host cell (42). Lysis is coordinated by cysteine proteases that mediate inclusion rupture and involves host intracellular calcium signaling for plasma membrane rupture (42). Alternatively, extrusion is a packaged release mechanism during which a portion of the inclusion protrudes and detaches from the host cell while leaving the cell intact (43). Extrusion requires the formation of an actin coat surrounding the inclusion. Actin recruitment appears to be directed by a secreted bacterial effector and utilizes host actin-associated signaling pathways (44). In experiments of *Chlamydia*-infected cell monolayers, lysis and extrusion occur at near equivalent frequencies (42).

A typical chlamydial developmental cycle takes 48-72 hours, depending on the species of *Chlamydia* and host cell. By the end of the intracellular infection, an average of 1000 chlamydiae are contained in each infected host cell (45).

## ***Chlamydia*-Host Cell Interactions**

*Chlamydia* interact intimately with the host cell throughout the developmental cycle and induce numerous host-pathogen interactions to support the infection. Initial establishment of the

chlamydial inclusion requires chlamydial transcription and translation, although the precise molecular mediators and mechanisms are unknown (46). *Chlamydia* then utilize host cell microtubules and dynein to migrate to the microtubule organizing center (MTOC) of the host cell and establish their intracellular niche. Interestingly, inclusion trafficking is independent of dynactin, the dynein cargo binding and activator complex, and it has been postulated that an unknown chlamydial protein may function in its place (21). Perinuclear positioning places *Chlamydia* in a prime location for interactions with nutrient-rich compartments of the host cell, like the Golgi apparatus and the endoplasmic reticulum.

Since *Chlamydia* have lost the ability to synthesize many essential building blocks (47), they must intercept intracellular trafficking pathways to acquire energy and nutrients from the host cell. *Chlamydia* inclusions interact with mitochondria (25) and require host cell ATP for survival which they import using nucleotide transporters (48). The chlamydial genome also encodes several amino acid transporters to procure host cell amino acids and oligopeptides (48). *Chlamydia* induce Golgi fragmentation into ministacks surrounding the chlamydial inclusion to aid in lipid acquisition (49). Sphingomyelin and cholesterol are obtained by intercepting host cell exocytic vesicles traveling from the Golgi apparatus to the plasma membrane (39, 50), and other host-derived ceramides are acquired by direct contact with the endoplasmic reticulum (51).

After establishing trafficking of all the essential macromolecules for bacterial growth, *Chlamydia* need to ensure the host cell survives long enough to complete the chlamydial developmental cycle. The stability of the chlamydial inclusion is thought to be maintained by a scaffold of actin and intermediate filaments that surround the inclusion (52). *Chlamydia* also protect their intracellular niche by making host cells resistant to apoptosis (53).

The mechanism by which *Chlamydia* are able to modulate host processes and induce these phenotypes is thought to be by delivering chlamydial effectors into the host cell.

## ***Chlamydia* Effectors**

*Chlamydia* effectors are proteins that interact with the host cell to modulate cellular processes. For example, *Chlamydia*-encoded Tarp (translocated actin recruiting phosphoprotein) is translocated into the host cell to promote bacterial uptake by recruiting actin to the site of bacterial entry and stimulating internalization. Tarp tyrosine phosphorylation, which is thought to be mediated by a host kinase, initiates a signal transduction cascade that results in actin remodeling (54). Incs represent a major class of effector proteins that localize to the inclusion membrane and can interact with host cell proteins. Approximately 40 putative Incs have been identified based on the presence of a characteristic hydrophobic domain (45). Several Incs interact with Rab-GTPases, which are important regulators of host vesicular transport (55). Other Incs contain SNARE-like motifs that can bind to host SNARE proteins (important in membrane fusion) and recruit them to the chlamydial inclusion (56). Effectors can also be enzymes. ChlaDUB1 and ChlaDUB2 are predicted cysteine proteases with deubiquitinating activity that are proposed to play a role in subverting host cell immune response by stabilizing I $\kappa$ B $\alpha$  and inhibiting NF- $\kappa$ B transcription (54). In order for these chlamydial effectors to interact with host cell pathways, they must be secreted from the bacteria and translocated across the inclusion membrane to reach the host cell cytosol.

There are two pathways that *Chlamydia* use to deliver chlamydial effectors to the host cell: the type III secretion (T3S) system and the type II secretion (T2S) system. The T3S system is commonly used by Gram-negative pathogenic bacteria (including *Yersenia*, *Shigella*, and

*Salmonella*) to secrete virulence proteins into host cells. The type III secretion apparatus is composed of a conserved set of 20 proteins, which assemble into a complex at the bacterial membrane (57). The mechanism by which the T3S system delivers effectors into the host cell resembles a syringe, thus the T3S machinery is often referred to as the injectisome. The basal structure is a pore complex that passes through the inner and outer bacterial membrane (58). Attached to the base is a hollow chlamydial needle complex through which effectors travel with the help of translocator proteins. The T3S apparatus can deliver effectors within the inclusion membrane, into the inclusion lumen, or directly into the host cell cytosol (59). Chlamydial T3S effectors display little sequence homology with one another and have mostly been identified by their ability to be secreted by heterologous T3S machinery (59). Tarp and several inclusion membrane proteins are secreted by the T3S system (32, 60, 61).

The type II secretion system is also commonly employed by Gram-negative bacteria to deliver proteins to the extracellular environment. T2S exports effectors across the inner bacterial membrane utilizing a Sec translocase and delivers them into the periplasmic space. Effectors then exit the bacterial periplasm by passing through type II machinery that forms a pore in the outer membrane (62, 63). T2S effectors can be identified by an N-terminal signal peptide sequence that is cleaved by signal peptidases upon crossing the inner membrane (63). Two chlamydial effector proteases contain predicted N-terminal signal peptides and have been proposed to utilize the T2S system: tail-specific protease (Tsp) and CPAF (63).

## **The Chlamydial Protease CPAF**

CPAF (chlamydial protease or proteasome-like activity factor) is a chlamydial enzyme that has been proposed to be a major virulence factor in *Chlamydia*-infected cells (64). This

protease is conserved across chlamydial genomes and has been shown to be produced by five chlamydial species as well as the environmental *Parachlamydia*, suggesting its importance for chlamydial survival (65).

CPAF is an atypical serine protease containing a water-mediated catalytic triad (66). It is synthesized as an inactive zymogen with an auto-inhibitory amino acid sequence obstructing its active site. Autocatalytic cleavage into N- and C-terminal fragments activates the protease by removing the inhibitory segment and allowing the functional active site to assemble (66). CPAF activation is induced by the formation of transient homodimers that leads to the required series of autocatalytic cleavage events that occur in *trans* (66, 67).

The studies presented in this dissertation call into question the role of CPAF as a major chlamydial virulence factor. CPAF had been proposed to cleave or degrade numerous host protein substrates (64, 68), and a wide range of *Chlamydia*-induced phenotypes including Golgi fragmentation, host cell resistance to apoptosis, cytoskeletal remodeling, and evasion of host immune response were attributed to CPAF-mediated proteolysis (49, 52, 69-73). The data we will present here, however, show that previously reported CPAF-mediated proteolysis occurred *in vitro* rather than within *Chlamydia*-infected cells. Subsequently, another group has provided genetic evidence that CPAF activity is not required for a number of *Chlamydia*-induced phenotypes previously attributed to CPAF-mediated proteolysis (74). Our studies have led to a reappraisal of CPAF and the role that this protease plays during the chlamydial infection is currently unclear.

## Summary

The aim of this dissertation is to contribute to the understanding of the intracellular *Chlamydia* infection. In Chapter 2, our investigations of CPAF-mediated proteolysis as a potential mechanism of centrosome amplification unexpectedly led to a re-evaluation of CPAF substrates and function. We found that proteolysis of 11 published CPAF substrates was due to *in vitro* activity in infected cell lysates rather than enzymatic activity during the intracellular infection. In Chapter 3 we evaluated methods used to inhibit *in vitro* CPAF activity and identified experimental manipulations that artifactually induce CPAF activity. In Chapter 4, we identified boronate peptides as a novel class of CPAF inhibitors and described our use of molecular modeling to design CPAF inhibitors with enhanced activity and selectivity. In Chapter 5, we developed a novel three-dimensional electron microscopy approach to study the intracellular *Chlamydia* infection. Our results provide the first comprehensive quantitative analysis of the chlamydial inclusion and its bacterial contents over the course of the developmental cycle and lead us to propose chlamydial size as a regulator of development.

## **Chapter 2**

# **CPAF: A Chlamydial Protease in Search of an Authentic Substrate**

## Contributions

The work described in this chapter was the result of a close collaboration between Jennifer Lee, Kirsten Johnson, and Allan Chen. All experiments were discussed and designed as a team effort. Allen Chen contributed to experiments described in Figures 2.4 and 2.5. Kirsten Johnson conducted experiments in Figures 2.1, 2.3, and 2.4. Figure 2.1 was prepared by Kirsten Johnson. Jennifer Lee was responsible for all other experiments and figures. The work described in this chapter has been published (75) (with Allen Chen, Kirsten Johnson, and Jennifer Lee as equally contributing first authors).

## Summary

The chlamydial protease CPAF has been proposed to be a major virulence factor during an intracellular *Chlamydia* infection. CPAF was reported to cleave or degrade numerous host proteins, thereby altering multiple cellular processes. However, in this study, we demonstrated that CPAF activity present in lysates of infected cells leads to *in vitro* proteolysis. CPAF activity can persist in lysates because standard methods that inhibit other enzymes are ineffective against this protease. We investigated previously published CPAF substrates and discovered that these proteins were unaltered when CPAF activity was inhibited during cell processing. Thus, previously reported proteolysis was due to CPAF enzymatic activity in cell lysates rather than in intact cells.

When precautions were taken to prevent *in vitro* CPAF activity, *Chlamydia*-infected cells continued to display characteristic phenotypes that had previously been attributed to CPAF-mediated proteolysis of specific host protein substrates. In the absence of detectable proteolysis of these proteins, it is unlikely that CPAF is responsible for inducing these effects on the infected cell, and other mechanisms likely mediate these phenotypes.

Our findings suggest that previously described CPAF-mediated proteolysis occurred *in vitro* and raise concerns about the classification of CPAF as a major virulence factor that modulates the majority of *Chlamydia*-host interactions. The data presented provides the basis for a re-characterization of the role of CPAF during a chlamydial infection.

## Introduction

*Chlamydia*-infected cells display numerous characteristic phenotypes and many of these alterations have been proposed to provide a benefit to *Chlamydia* during the intracellular infection. For example, Golgi reorganization around the chlamydial inclusion is consistently observed in *Chlamydia*-infected cells and has been proposed to facilitate lipid acquisition from the host cell (49). *Chlamydia*-infected cells also exhibit resistance to apoptosis, which is likely important for bacterial growth and reproduction (53, 76). Centrosome defects are another consequence of a *Chlamydia* infection, although, unlike the previous two examples, it is unclear whether these alterations provide any benefit to chlamydiae (21, 22).

Centrosomes are important cellular organelles that act as the major microtubule-organizing center to regulate cell shape, polarity, and motility. During mitosis, centrosomes assemble the bipolar spindle that regulates chromosome segregation (77). Eukaryotic cells possess one or two centrosomes depending on their stage in the cell cycle. Centrosome duplication occurs during S-phase and is coordinated by several regulatory proteins, including kinases like Plk4 and structural proteins like HsSAS-6. Proper centrosome duplication prior to mitosis is crucial for the formation of the bipolar spindle and to ensure that each daughter cell will inherit one centrosome (78).

*Chlamydia* dysregulate both the position and number of centrosomes within infected cells. First, perinuclear centrosome positioning is disrupted in *Chlamydia*-infected cells. Centrosomes have been found to associate with the chlamydial inclusion in a dynein-dependent manner throughout the course of an infection (21). *Chlamydia*-infected cells also have more than the normal number of one to two centrosomes (21, 22). These *Chlamydia*-induced amplified centrosomes result in formation of multipolar spindles during mitosis and chromosome

segregation errors (21). Centrosome amplification is a hallmark of cancer cells and provides a possible mechanistic link between *Chlamydia* genital infections and cervical cancer (13, 18, 19, 23). Production of supernumerary centrosomes depends on the normal host duplication machinery and requires progression through S-phase of the cell cycle (22). Based on these findings, we hypothesized that the mechanism by which *Chlamydia* induces centrosome amplification is by modulating the normal host cell duplication machinery via a chlamydial effector.

One potential chlamydial effector is CPAF, which is a chlamydial enzyme with a proposed role as a major virulence factor mediating important host-pathogen interactions(64). CPAF-mediated proteolysis has been proposed to be the mechanism for an extensive array of *Chlamydia*-specific phenotypes, and the functions of the protein substrates in the absence of infection have often been used as support for the mechanisms. For instance, CPAF-mediated cleavage of golgin-84 (a Golgi apparatus structural protein) was proposed to promote Golgi reorganization around the growing chlamydial inclusion. Immunoblots of infected cell lysates showed golgin-84 proteolysis occurred concomitantly with Golgi structural changes, and inhibitor treatments and over-expression experiments were used to show that cleaved golgin-84 was necessary and sufficient for Golgi reorganization (49, 69). Similar experiments have been utilized to show that CPAF-mediated proteolysis of other host protein substrates leads to phenotypes observed in *Chlamydia*-infected cells (70, 72, 73).

In this chapter, we examine whether centrosomal proteins are proteolytically altered during a chlamydial infection in a quest to determine the mechanism of *Chlamydia*-induced centrosome amplification. Although several centrosomal proteins are proteolytically processed within infected cell lysates, we determine that the observed proteolysis is due to *in vitro* CPAF

enzymatic activity. Upon further investigation, we demonstrate that the reported proteolysis of 11 published CPAF substrates was due to CPAF enzymatic activity within cell lysates rather than in intact cells. However, we still observe characteristic host-pathogen interactions in *Chlamydia*-infected cells in the absence of detectable proteolysis of the specific host protein substrates that were proposed to mediate the phenotypes. Our findings indicate that these *Chlamydia*-induced phenotypes, including centrosome amplification, are likely to be mediated by mechanisms other than CPAF-dependent proteolysis of the proposed host protein substrates. Our results invite a reappraisal of previously identified CPAF substrates and re-interpretation of models involving the function of this chlamydial protease during the intracellular infection.

## Results

### **Proteolysis of multiple centrosomal proteins in lysates of *Chlamydia*-infected cells**

In an attempt to determine the mechanism of centrosome amplification in *Chlamydia*-infected cells, we examined whether host cell centrosomal proteins were altered during a *Chlamydia* infection. We prepared lysates from *Chlamydia*-infected cells by trypsinizing the cells from the monolayer and lysing the cell pellet in RIPA buffer containing a protease inhibitor cocktail – a standard technique which has been utilized in other studies (49, 53, 69, 79). Several centrosomal proteins including C-Nap1, CPAP, HsSAS-6, Cep170, Cep192, and Plk4 were cleaved or degraded within *Chlamydia*-infected cell lysates. Immunoblots of lysates from a time course of infected HeLa cells showed that full-length forms of the proteins were gradually converted into smaller sized fragments or degraded beginning at 21-24 hpi (Fig. 2.1 and data not shown). This timing of proteolysis was consistent with the observed cleavage and degradation of other CPAF substrates in previous studies and with the expression pattern of CPAF protease (72, 73, 80). Thus, we investigated whether CPAF was the protease responsible for the cleavage and degradation of these centrosomal proteins.

### **CPAF mediates proteolysis of centrosomal proteins**

We focused on two specific centrosomal proteins and found that CPAF was necessary and sufficient for their proteolysis *in vitro*. C-Nap1 is a centriole linker protein that regulates centrosome cohesion (81), and CPAP is a protein that regulates centriole length (82). We focused on these proteins because alterations of either protein in the absence of infection results in abnormal centrosome phenotypes (81-83), making them interesting candidates with potential roles in *Chlamydia*-induced centrosome amplification.

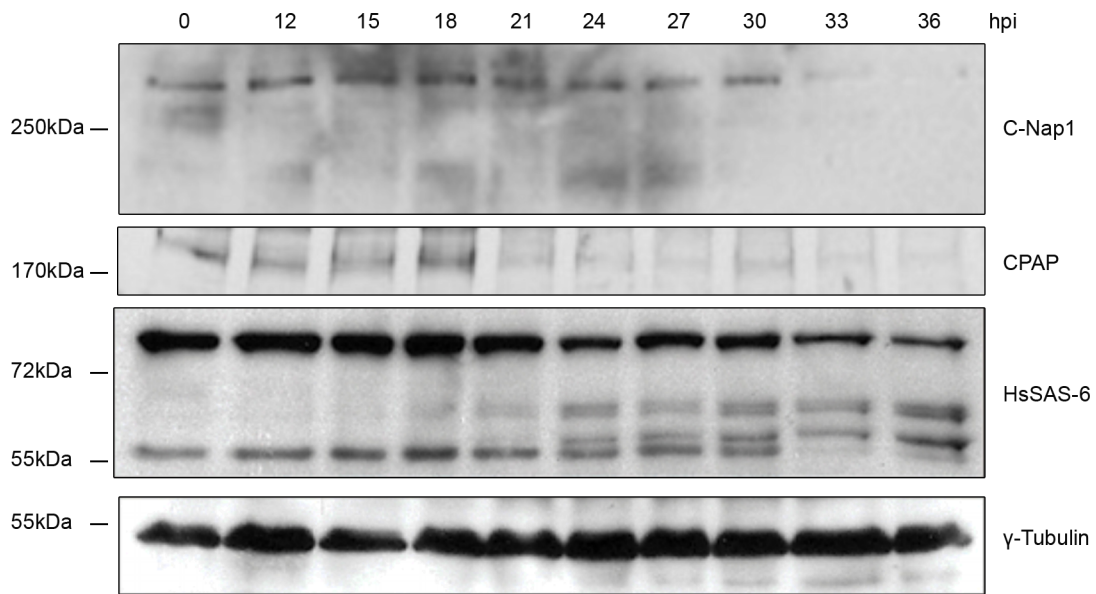


**Figure 2.1. Proteolysis of centrosomal proteins in lysates of *Chlamydia*-infected cells**

*Chlamydia*-infected cells were harvested between 12 and 36 hours post infection by trypsinization from the monolayer followed by lysis in RIPA buffer. Total cell lysates were separated by SDS-PAGE and blots were probed with antibodies to C-Nap1, CPAP, HsSAS-6 and  $\gamma$ -tubulin (loading control).

First, we determined whether a chlamydial factor was responsible for the observed proteolysis of C-Nap1 and CPAP. We set up a cell-free degradation assay in which uninfected lysate (as a source of host proteins) was incubated with a small amount of infected lysate (as a source of chlamydial factors), and the reaction was analyzed by immunoblot. Our results indicated that an enzyme was present within infected cell lysates that proteolytically processed C-Nap1 and CPAP in a dose-dependent manner (Fig. 2.2A).

We then utilized the CPAF inhibitor lactacystin (73) to address our hypothesis that CPAF was the chlamydial enzyme responsible for the observed proteolysis. Cleavage of C-Nap1 and degradation of CPAP in the cell-free degradation assays was abrogated in a concentration-dependent manner by treatment with lactacystin (Fig. 2.2B). Since lactacystin also inhibits the proteasome, we tested another proteasomal inhibitor MG132 and found that treatment with this compound did not prevent proteolysis of C-Nap1 or CPAP (data not shown). These findings implicate CPAF in the proteolysis of these centrosomal proteins.

Using a modified version of the cell-free degradation assay, we demonstrated that recombinant CPAF was sufficient to reproduce the specific cleavage and degradation patterns of C-Nap1 and CPAP that we observed in infected cell lysates (Fig. 2.2C). Furthermore, CPAF was necessary for the observed proteolysis of these proteins since immunodepletion of CPAF from infected lysates using specific antibodies abrogated C-Nap1 and CPAP proteolysis (Fig. 2.2D). We concluded from these experiments that CPAF was the enzyme that proteolytically processed C-Nap1 and CPAP during a chlamydial infection.

CPAF also appeared to mediate proteolysis of the other identified centrosomal proteins HsSAS-6, Cep170, Cep190, and Plk4. An enzyme within infected lysates could reproduce the characteristic cleavage and degradation patterns and lactacystin treatment abrogated the

**Figure 2.2. CPAF is necessary and sufficient for C-Nap1 and CPAP proteolysis *in vitro***

C-Nap1 data is presented in the left column and CPAP data is presented in the right column. **A)**

“Lysates”: Immunoblots of uninfected or *Chlamydia*-infected lysates probed with C-Nap1 or

CPAP antibodies. “*In vitro*”: Uninfected lysates were combined with increasing quantities of

infected lysates and incubated at 37°C for 1 hour. Immunoblots of the *in vitro* reactions were

probed with antibodies to C-Nap1 or CPAP. **B)** *In vitro* reactions as described in (A) were

supplemented with 2-4mM of the CPAF inhibitor lactacystin or DMSO as a solvent control.

Immunoblots of the *in vitro* reactions were probed with antibodies to C-Nap1 or CPAP. **C)**

Uninfected lysates were combined with infected lysates or with recombinant CPAF and

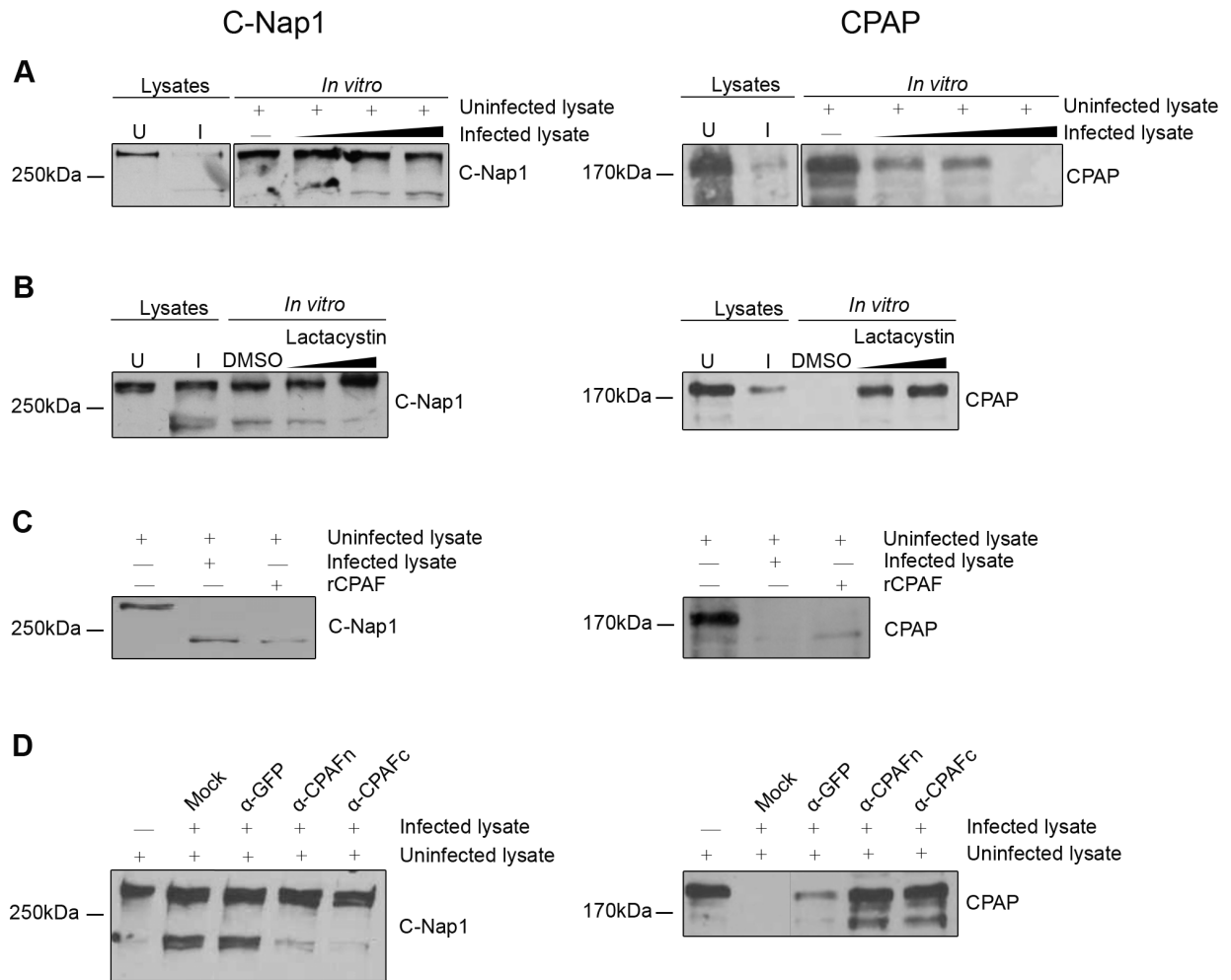
incubated at 37°C for 1 hour. Immunoblots of the *in vitro* reactions were probed with antibodies

to C-Nap1 or CPAP. **D)** Uninfected lysates were combined with infected lysates that were mock-

treated, immunodepleted with a non-specific antibody to GFP, or immunodepleted using CPAF-

specific antibodies. After incubation at 37°C for 1 hour, *in vitro* reactions were analyzed by

immunoblot with antibodies to C-Nap1 or CPAP.



proteolysis (data not shown). Furthermore, CPAF was necessary and sufficient for HsSAS-6 cleavage in studies conducted similarly to the C-Nap1 and CPAP experiments presented here (data not shown). HsSAS-6 is a critical regulator of centrosome number (84) and its role in the potential mechanism of *Chlamydia*-induced centrosome amplification was the subject of a detailed study (85).

### **CPAF-mediated proteolysis of centrosomal proteins occurs *in vitro* and not in intact cells**

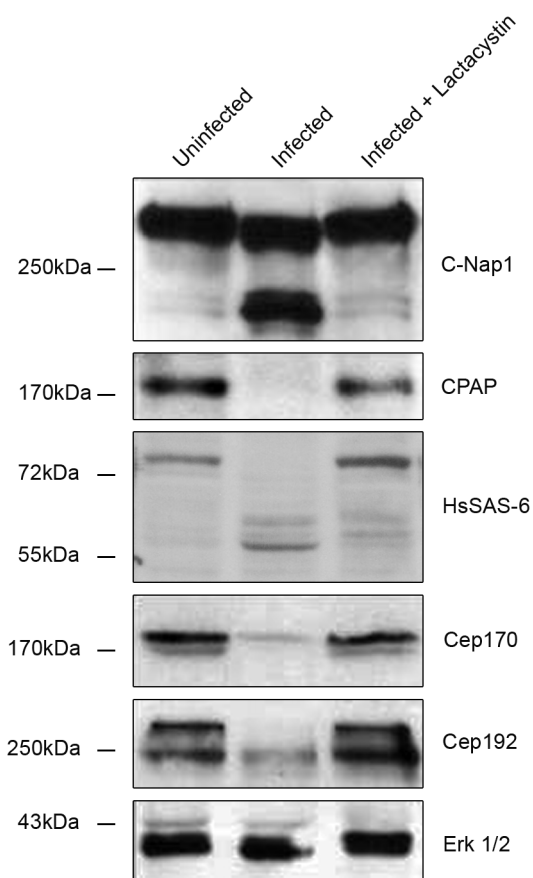
Although the discovery of numerous apparent centrosomal CPAF substrates was exciting, we questioned whether CPAF truly targets such a large population of important centrosomal regulators within an infected cell. Upon careful investigation, we found that the proteolysis of centrosomal proteins was dependent upon the method of lysate preparation. When infected cells were trypsinized from the monolayer and subsequently lysed in RIPA buffer, we observed the characteristic cleavage and degradation patterns for each substrate. However, when infected cells were prepared by other methods (such as trypsinization followed by lysis in RIPA buffer supplemented with 2% SDS, or by lysing directly in Laemmli sample buffer), we observed varying levels of proteolysis (data not shown). This variance suggested that at least some of the proteolysis that we observed using standard cell lysate preparation procedures was due to *in vitro* enzymatic activity during our experimental manipulations.

To determine the extent of proteolysis that occurred within intact *Chlamydia*-infected cells, we inhibited CPAF activity prior to cell lysis with lactacystin then examined lysates for centrosomal protein cleavage and degradation. We pre-treated *Chlamydia*-infected cells for one hour prior to lysate preparation with *clasto*-lactacystin (the active form of lactacystin), which inhibits CPAF activity during the cell collection and lysis procedures. Surprisingly, there was no detectable cleavage or degradation of C-Nap1, CPAP, HsSAS-6, Cep170, Cep 192, or Plk4 even

as late as 36 hpi when CPAF was inhibited prior to lysate preparation (Fig. 2.3). We concluded that CPAF-mediated proteolysis of centrosomal proteins was due to *in vitro* CPAF activity in our cell lysates and not to CPAF activity during the intracellular infection. Thus, proteolysis of these centrosomal proteins is unlikely to be the mechanism by which *Chlamydia* induce centrosome amplification in infected cells.

### **Re-examination of published CPAF substrates**

In light of our discovery that several centrosomal proteins were proteolytically altered by CPAF *in vitro* but not *in vivo*, we decided to re-examine other published CPAF substrates and their related host-pathogen interactions. Golgin-84 is a Golgi structural protein whose cleavage by CPAF was reported to cause Golgi reorganization in *Chlamydia*-infected cells (49, 69). When *Chlamydia*-infected cells were trypsinized followed by lysis in standard RIPA buffer, golgin-84 cleavage occurred as previously published; however, pre-treatment with *clasto*-lactacystin for one hour prior to lysate preparation prevented CPAF-mediated golgin-84 cleavage (Fig. 2.4A). An *in vitro* CPAF activity assay provided an explanation for the different results. In this assay, uninfected lysate as a source of host protein substrate (specifically golgin-84 in this case) was incubated with a small amount of *Chlamydia*-infected lysate as a source of CPAF, then the reaction was analyzed by immunoblot. The *in vitro* activity assay revealed that CPAF remained active in RIPA buffer and could cleave full-length golgin-84 in as little as 10 minutes on ice (data not shown); however, a one hour pre-treatment of an infected cell monolayer with 150  $\mu$ M *clasto*-lactacystin was sufficient to inhibit this *in vitro* CPAF activity (Fig. 2.4B). Since no golgin-84 cleavage was detected in *clasto*-lactacystin pre-treated lysates (Fig. 2.4A), we concluded that no intracellular CPAF-mediated proteolysis of golgin-84 took place up to 36 hpi. Previous reports used standard lysate preparation techniques without taking precautions to inhibit

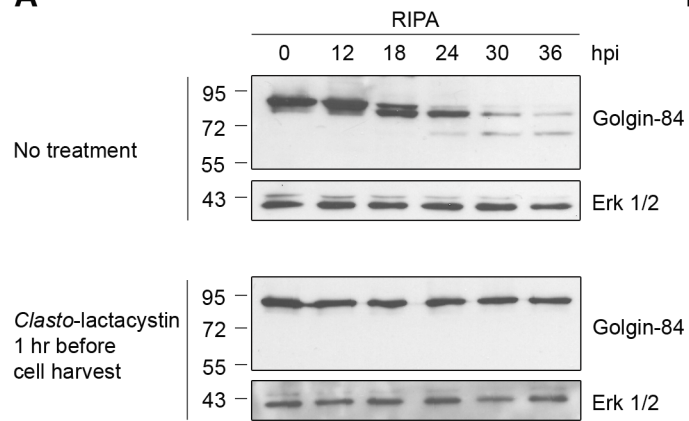
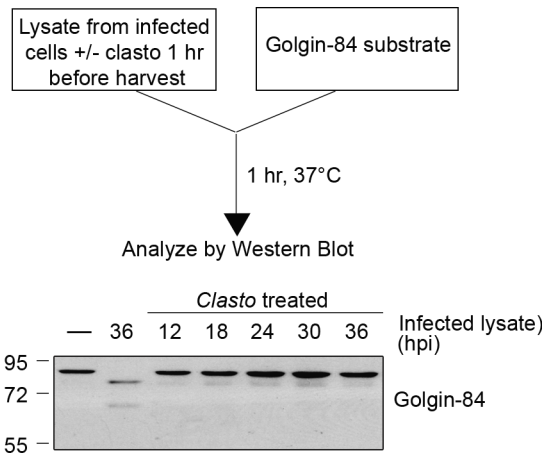
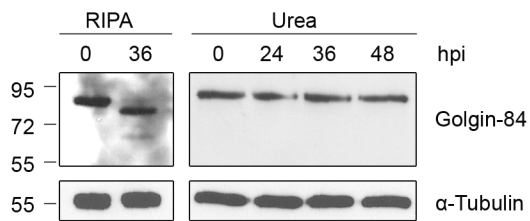
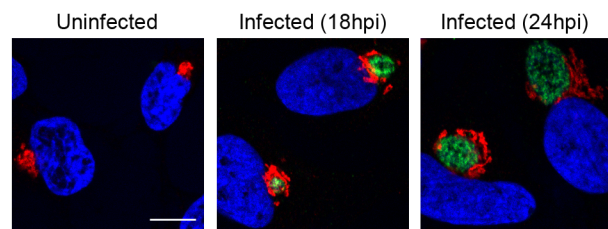


**Figure 2.3. CPAF-mediated proteolysis of centrosomal proteins does not occur in intact cells**

Lysates were prepared from uninfected cells, infected cells at 36 hpi, or infected cells at 36 hpi pre-treated for one hour prior to lysis with 150 $\mu$ M *clasto*-lactacystin. Immunoblots were probed with antibodies to C-Nap1, CPAP, HsSAS-6, Cep170, Cep192 and Erk 1/2 (loading control).

**Figure 2.4. Golgin-84 cleavage does not occur in *Chlamydia*-infected cells when CPAF is inhibited during cell processing**

**A)** Uninfected (0hpi) and infected cells at time points between 12 and 36 hpi were treated with methyl acetate as a solvent control (top panel) or 150  $\mu$ M of the CPAF inhibitor *clasto*-lactacystin (bottom panel) for 1 hour prior to cell lysis in RIPA buffer. Total cell lysates were separated by SDS-PAGE and probed with antibodies against golgin-84 or Erk 1/2 (loading control). **B)** Cell-free degradation assay testing for CPAF activity in lysates prepared from the *Chlamydia*-infected HeLa cells described in (A). Each infected cell lysate was incubated with a lysate of uninfected HeLa cells as the source of golgin-84 substrate and reactions were analyzed by immunoblotting with golgin-84 antibodies. **C)** Lysates of uninfected (0 hpi) or infected cells from different times in the infection were prepared in RIPA buffer (left panel) or by direct lysis in 8M urea (right panel), separated by SDS-PAGE and analyzed with antibodies to golgin-84 or  $\alpha$ -tubulin (loading control). **D)** Confocal images of uninfected or *Chlamydia*-infected HeLa cells examined at 18 and 24 hpi. Cells were stained with antibodies to the Golgi marker  $\alpha$ -mannosidase II (red), the chlamydial major outer membrane protein MOMP (green) and the DNA dye Hoechst 33342 (blue) to detect Golgi membranes, the chlamydial inclusions, and DNA, respectively. Scale bar, 10 $\mu$ m.

**A****B****C****D**

*in vitro* CPAF activity (49, 69); therefore, observed golgin-84 cleavage was likely due to *in vitro* CPAF activity rather than proteolysis that occurred intracellularly during the infection.

To verify that golgin-84 cleavage was not taking place intracellularly, we developed an alternative method to inhibit CPAF activity during preparation of infected cell lysates. Infected cells were lysed directly in 8M urea, which denatures proteins and globally inhibits enzymatic activity. Under these conditions, no golgin-84 cleavage was observed up to 48 hpi (Fig. 2.4C). This lack of golgin-84 cleavage was observed for *Chlamydia* infection of HeLa cells and two other human cell lines when lysed in urea (data not shown).

As cleavage of golgin-84 has been proposed to induce Golgi reorganization in *Chlamydia*-infected cells, parallel coverslips were examined by immunofluorescence to determine whether this phenotype persisted in infected cells that retained full-length golgin-84. *Chlamydia*-infected cells continued to exhibit Golgi membranes reorganized around the growing chlamydial inclusion (Fig. 2.4D), similar to previous reports (49). Therefore, Golgi reorganization occurred in the absence of detectable golgin-84 cleavage, and this phenotype is unlikely to be caused by CPAF-dependent proteolysis of this structural Golgi protein.

The resistance of *Chlamydia*-infected cells to apoptosis has been proposed to be mediated by CPAF-dependent degradation of BH3-only proteins, including Puma, Bik, and Bim (70, 79). When we examined BH3-only proteins under our conditions that inhibited CPAF *in vitro* activity (direct lysis in 8M urea), no degradation of Puma, Bik, or Bim was detected up to 48 hpi (Fig. 2.5A). Infected cells were still resistant to apoptosis, as previously reported (53), despite the lack of proteolysis of these proteins (Fig. 2.5B). Based on these results, it is doubtful that the anti-apoptotic effects of the chlamydial infection on the host cell can be attributed to CPAF-dependent degradation of BH3-only proteins Puma, Bik, and Bim.

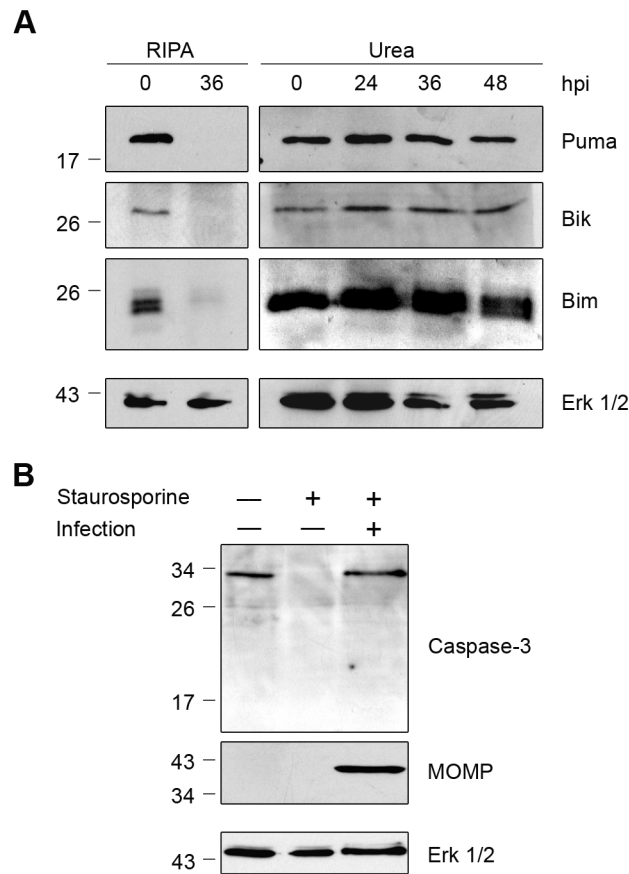


**Figure 2.5. Degradation of BH3-only proteins in *Chlamydia*-infected cells is prevented by inhibiting CPAF during cell processing**

**A)** Lysates of uninfected (0 hpi) or infected HeLa cells were prepared in RIPA buffer (left panel) or by direct lysis in 8M urea (right panel) at the indicated times, separated by SDS-PAGE, and analyzed by immunoblotting with antibodies to the pro-apoptotic BH3-only proteins Puma, Bik, or Bim. Equal loading was monitored for each blot with antibodies to Erk 1/2, but only the loading control for the Puma blot is shown as an example. **B)** Uninfected or *Chlamydia*-infected HeLa cells were treated with 1  $\mu$ M staurosporine to induce apoptosis, which was monitored by the loss of full-length caspase-3. Immunoblots of the lysates were probed with antibodies to caspase-3, MOMP (marker of *Chlamydia* infection), or Erk 1/2 (loading control).

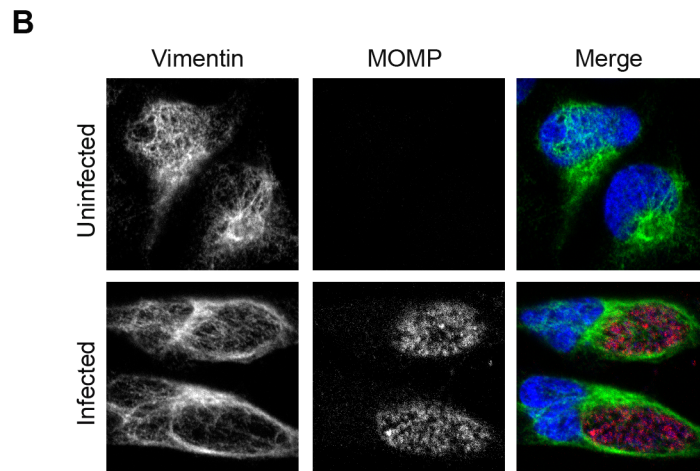
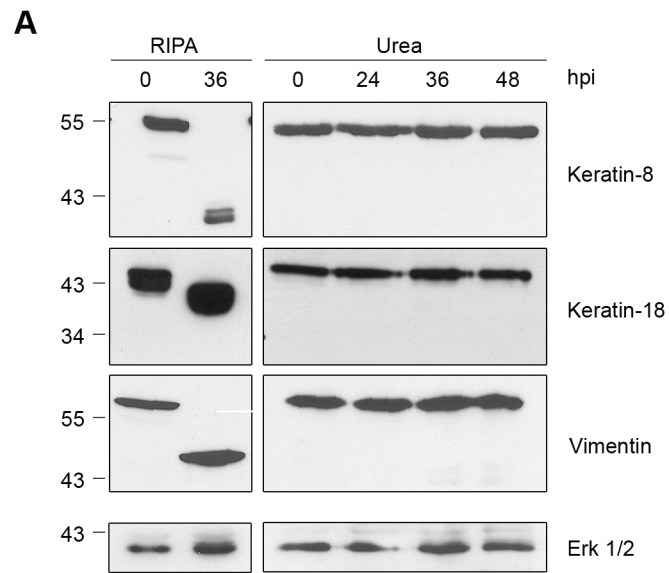
CPAF-mediated cleavage of intermediate filaments keratin-8, keratin-18, and vimentin has been implicated in the growth the chlamydial inclusion (52, 80). Similar to our previous observations of golgin-84 and BH3-only proteins, no cleavage of intermediate filaments keratin-8, keratin-18, or vimentin was detected when infected cells were lysed directly in 8M urea up to 48 hpi (Fig. 2.6A). However, cytoskeletal arrangement around the chlamydial inclusion continued to be observed in the absence of detectable proteolysis of these proteins (Fig. 2.6B).

Additional protein substrates we examined also do not appear to be altered during an intracellular *Chlamydia* infection as previously reported. These include the NFκB transcription factor subunit p65/RelA (86), the MHC transcription factor RFX5 (68, 73), the adherens junction protein nectin-1 (87), and the cell cycle protein cyclin B1 (79, 88). As with the other substrates analyzed, the proteolysis of these four proteins was only observed when *Chlamydia*-infected cells were lysed in RIPA buffer and not with direct lysis in urea (Fig. 2.7). Taken together, these studies demonstrate that the previously reported proteolysis of 11 published CPAF substrates is prevented by inhibiting CPAF activity during the processing of *Chlamydia*-infected cells (Table 2.1).

Considering the lack of detectable intracellular proteolysis of any protein substrate we examined, we wondered whether CPAF itself was autocatalytically processed into its active form in our *Chlamydia*-infected cells. CPAF is synthesized as a zymogen of 70 kDa that is converted in *trans* into active N- and C-terminal fragments via an autocatalytic cleavage reaction that requires CPAF proteolytic activity (65-67, 89, 90). Using an antibody that recognized the C-terminal fragment, we found that CPAF was in fact cleaved into its active form even when infected cell lysates were prepared in urea. Cleaved CPAF accumulated over the course of infection from 24 to 48 hpi (Fig. 2.8).

**Figure 2.6. Cleavage of intermediate filaments in *Chlamydia*-infected cells is also dependent on cell processing**

**A)** Lysates of uninfected (0 hpi) or infected HeLa cells were prepared in RIPA buffer (left panel) or by direct lysis in 8M urea (right panel) at the indicated times, separated by SDS-PAGE, and analyzed by immunoblotting with antibodies to keratin-8, keratin-18, or vimentin. Equal loading for each blot was monitored by blotting for Erk 1/2 (loading control), but only the loading control for keratin-8 is shown. **B)** Uninfected and infected HeLa cells at 30 hpi were fixed and stained with antibodies to vimentin (green), the chlamydial major outer membrane protein MOMP (red), and the DNA dye Hoechst 33342 (blue). Representative confocal images are shown. Scale bar, 10 $\mu$ m.



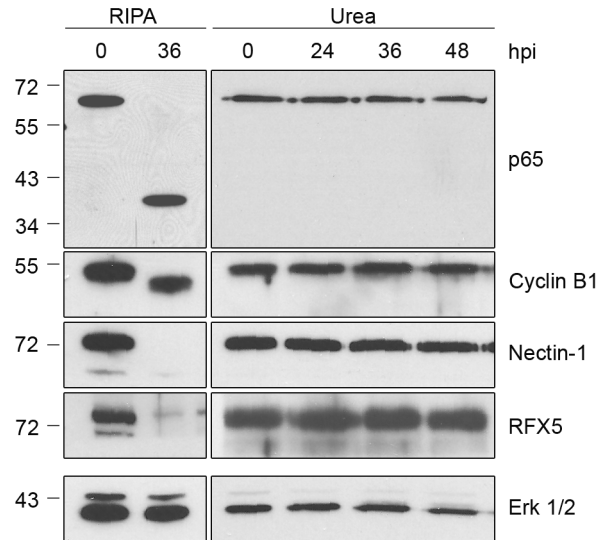


**Figure 2.7. Proteolysis of four additional CPAF substrates is dependent on cell processing**

Lysates of uninfected (0 hpi) or infected HeLa cells were prepared in RIPA buffer (left panel) or by direct lysis in 8M urea (right panel) at the indicated times, separated by SDS-PAGE, and probed with antibodies to the p65/RelA subunit of NF $\kappa$ B, cyclin B1, nectin-1, or RFX5 as indicated. Equal loading for each blot was monitored by blotting for Erk 1/2, but only the loading control for nectin-1 is shown.

**Table 2.1. Summary of published CPAF substrates**

<b>Reported Substrate</b>	<b>Reported Proteolysis</b>	<b>References</b>	<b>Proteolysis when CPAF is inhibited during cell processing</b>
<i>Host Proteins</i>			
Golgin-84	Cleavage	Christian <i>et al.</i> , 2011; Heuer <i>et al.</i> , 2009	No cleavage
Puma	Degradation	Dong <i>et al.</i> , 2005; Fischer <i>et al.</i> , 2004; Paschen <i>et al.</i> , 2008; Pirkhai <i>et al.</i> , 2006	No degradation
Bim	Degradation		No degradation
Bik	Degradation	Dong <i>et al.</i> , 2005; Pirkhai <i>et al.</i> , 2006	No degradation
Keratin-8	Cleavage	Dong <i>et al.</i> , 2004; Kumar and Valdivia, 2008	No cleavage
Keratin-18	Partial Cleavage	Kumar and Valdivia, 2008	No cleavage
Vimentin	Partial Cleavage	Kumar and Valdivia, 2008; Snively <i>et al.</i> , 2014	No cleavage (this study), late cleavage (Snively <i>et al.</i> , 2014)
p65	Cleavage	Christian <i>et al.</i> , 2010; Lad <i>et al.</i> , 2007	No cleavage
Cyclin B1	Cleavage	Balsara <i>et al.</i> , 2006; Paschen <i>et al.</i> , 2008	No cleavage
Nectin-1	Degradation	Sun <i>et al.</i> , 2008; Sun and Schoborg, 2009	No degradation
RFX5	Degradation	Zhong <i>et al.</i> , 2001; Zhong <i>et al.</i> , 2000	No degradation
Securin	Degradation	Brown <i>et al.</i> , 2012; Grieshaber and Grieshaber, 2014	No degradation
LAP-1	Partial Cleavage	Snively <i>et al.</i> , 2014	Not tested
USF-1	Degradation	Zhong <i>et al.</i> , 2001; Zhong <i>et al.</i> , 1999	Not tested
CD1d	Degradation	Kawana <i>et al.</i> , 2007	Not tested
PARP	Partial Cleavage	Paschen <i>et al.</i> , 2008; Yu <i>et al.</i> , 2010	Not tested
HMGB1	Cleavage	Yu <i>et al.</i> , 2010	Not tested
HIF-1	Degradation	Rupp <i>et al.</i> , 2007	Not tested
<i>Chlamydial proteins</i>			
CPAF	Cleavage	Huang <i>et al.</i> , 2008; Dong <i>et al.</i> , 2004	Cleavage
OmcB	Partial Cleavage	Hou <i>et al.</i> , 2012	Partial Cleavage
CT005	Degradation	Jorgensen <i>et al.</i> , 2011	Not tested
IncD (CT115)	Degradation		Not tested

IncE (CT116)	Cleavage	Jorgensen <i>et al.</i> , 2011	Not tested
IncC (CT233)	Degradation		Not tested
CT288	Degradation		Not tested
CT694	Degradation		Not tested
CT813	Cleavage		Not tested
TARP (CT456)	Degradation		Not tested

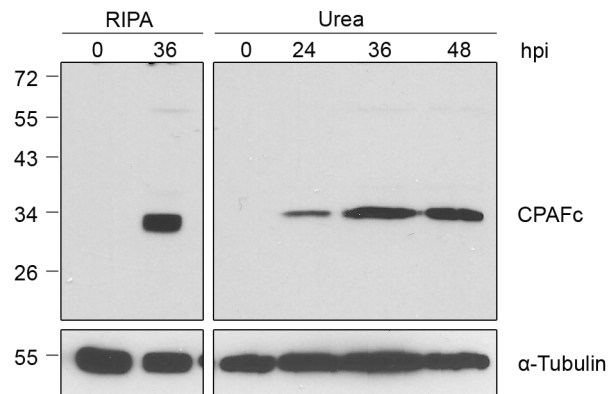


**Figure 2.8. CPAF is autocatalytically cleaved into its active form in *Chlamydia*-infected cells**

Lysates of uninfected (0 hpi) or infected HeLa cells were prepared in RIPA buffer (left panel) or by direct lysis in 8M urea (right panel) at the indicated times, separated by SDS-PAGE, and probed with antibodies to the C-terminal fragment of CPAF (CPAFc) and  $\alpha$ -tubulin (loading control).

In summary, we discovered that the reported CPAF-mediated proteolysis of 11 host proteins was due to *in vitro* activity of CPAF present in cell lysates rather than enzymatic activity during the intracellular infection. Thus, proteolysis of these proteins is not the mechanism by which *Chlamydia* induce the associated host-pathogen interactions, and CPAF is unlikely to be the virulence factor responsible for the observed phenotypes. There is still evidence that active CPAF is present within a *Chlamydia*-infected cell, but its role during an intracellular infection is unclear.

### **Evidence for CPAF translocation**

CPAF has been reported to be secreted from *Chlamydia* and translocated into the host cell cytosol (63, 68, 91), but our experiments in the previous section reveal that host protein substrates (which are capable of being altered by CPAF) are not targeted *in vivo*. We questioned why there is no detectable proteolysis in an infected cell if these host proteins are good *in vitro* substrates. We decided to re-examine whether CPAF is translocated from the inclusion into the host cytosol.

Immunofluorescence with antibodies to CPAF reveal cytosolic localization when infected cells at 48 hpi are fixed with formaldehyde (Fig. 2.9, top panels), as previously published (73). However, when the same experiment was performed using methanol fixation, CPAF was visualized within the inclusion lumen rather than the host cell cytosol (Fig. 2.9, middle panels). Fixation in a combination of ethanol and acetone showed similar localization within the inclusion lumen (Fig. 2.9, bottom panels). These observations demonstrate that the localization pattern of CPAF depends on the fixation method; therefore, it is unclear whether or not CPAF is translocated into the host cell cytosol. These results raise the possibility that lack of detectable

proteolysis of host protein substrates may be due to sequestration of CPAF within the inclusion lumen.

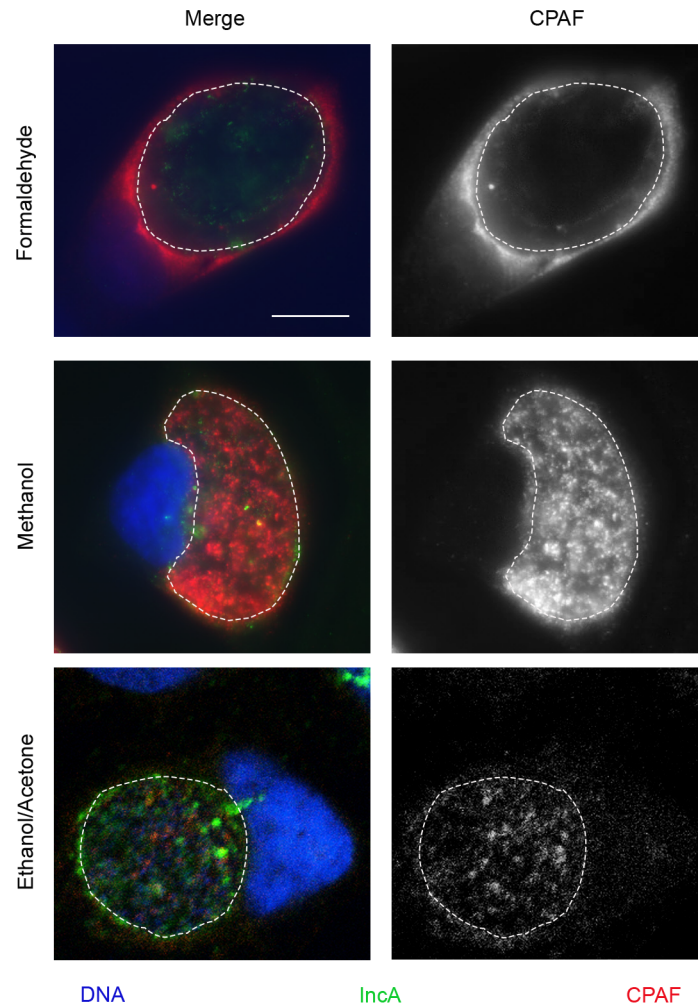


**Figure 2.9. CPAF localization depends of fixation method**

Infected HeLa cells were fixed at 48 hpi in 4% formaldehyde (top panels), 100% ice-cold methanol (middle panels), or a combination of ethanol and acetone (bottom panels) and stained with antibodies to the C-terminal fragment of CPAF (red), the inclusion membrane protein IncaA (green), and the DNA Hoechst 33342 (blue). Representative images are shown. Scale bar, 10 $\mu$ m.

## Discussion

We began this study by investigating a potential mechanism of *Chlamydia*-induced centrosome amplification. After observing that several centrosomal proteins were altered in *Chlamydia*-infected cell lysates, we tested whether CPAF was the enzyme responsible since it has been reported to cleave or degrade many other host proteins. Using a series of *in vitro* experiments, we demonstrated that CPAF was necessary and sufficient for the proteolysis. However, identification of numerous putative CPAF substrates within a small pool of critical centrosomal regulators raised red flags and led us to re-examine our findings. We discovered that the proteolysis of centrosomal proteins within infected cell lysates was artifactual and had occurred during lysate preparation rather than within intact infected cells. These findings led us to question whether *in vitro* proteolysis contributed to the observed cleavage and degradation in studies of previously identified CPAF substrates.

In this study we have shown that proteolysis of 11 published CPAF substrates is also due to *in vitro* CPAF activity. Cleavage or degradation was detected under standard lysis conditions, but pre-treatment with lactacystin or direct lysis in 8M urea, which inhibited CPAF activity during lysate preparation, prevented proteolysis. Furthermore, we did not detect proteolysis up to 48 hpi, which is much later than previous publications reported cleavage or degradation of these protein substrates. In fact, we have examined some substrates as late as 60 hpi and still detected no proteolysis (data not shown). Our results demonstrate that there is no detectable proteolysis of these reported CPAF substrates inside an infected cell during the normal course of infection.

Host-pathogen interactions attributed to CPAF were still observed when we took precautions to inhibit *in vitro* CPAF activity. Infected cells displayed Golgi reorganization, resistance to apoptosis, and restructuring of intermediate filaments even while there were no

alterations to the proteins proposed to mediate these phenotypes (golgin-84, BH3-only proteins, and vimentin, respectively). In the absence of detectable proteolysis, it is unlikely that CPAF mediates these phenotypes via cleavage or degradation of the previously identified host protein substrates. Consequently, our findings call into question CPAF's identity as a major chlamydial virulence factor whose function is to induce host-pathogen interactions.

Our immunofluorescence data raises questions about CPAF localization. Using the same CPAF antibody, we detected two different localization patterns depending on the fixation method. CPAF was detected in the host cell cytoplasm in some experiments but within the inclusion lumen in others. Determining the true localization of CPAF has important implications for identifying its *in vivo* substrates. Our results challenge the published literature about CPAF substrates and the timing and significance of their proteolysis during a *Chlamydia* infection. In light of our findings, the role of CPAF during a *Chlamydia* infection must be reconsidered.

### **Why were multiple host proteins incorrectly identified as *in vivo* CPAF substrates?**

Several lines of evidence have consistently been used to identify putative CPAF substrates. Generally, the cleavage or degradation of specific host proteins was detected by immunoblot analyses of lysates from *Chlamydia*-infected cells prepared by standard lysis procedures (52, 68-70, 79, 86, 87). The timing of proteolysis matched the timing CPAF expression, leading researchers to investigate the involvement of this chlamydial protease (72, 73, 80). These proteolytic patterns have then been reproduced *in vitro* by recombinant CPAF (52, 68, 70, 87) or *in vivo* by overexpression of CPAF in uninfected cells (69, 79, 86). The involvement of CPAF in this protein processing was then further supported by data showing that proteolysis of specific substrates can be prevented *in vitro* by a CPAF inhibitor, such as lactacystin (68, 70, 87), or by immunodepletion of CPAF from infected cell lysates (70, 80, 89,

92). These data showed that CPAF is sufficient to cause proteolysis of 16 host proteins (Table 2.1). However, they did not demonstrate that this proteolysis occurred in an infected cell. In fact, only one study (focused on the substrate nectin-1) has provided immunofluorescence data as evidence of proteolysis in intact infected cells (87).

Unique enzymatic properties of CPAF and experimental artifacts during lysate preparation led to misinterpretation that CPAF-mediated proteolysis occurred intracellularly. First, the unusual properties of CPAF contributed to its enzymatic activity in lysates of *Chlamydia*-infected cells prepared under standard conditions (lysis of cells in RIPA buffer in the presence of a standard protease inhibitor cocktail on ice). CPAF is an atypical serine protease that is not inhibited by a range of protease inhibitors found in standard cocktails (73, 93). Second, although researchers recognized the potential for *in vitro* enzymatic activity during lysate preparation to exaggerate *in vivo* proteolysis (94), they did not realize the potency of *in vitro* CPAF activity. *In vitro* CPAF activity can completely cleave or degrade host proteins within a lysate, even on ice, in as little as ten minutes. Intracellular protein substrates were misidentified because the primary evidence for CPAF-mediated proteolysis was detection of cleavage or degradation within infected cell lysates, and researchers presumed this proteolysis was occurring *in vivo* rather than *in vitro*.

The roles of host proteins in uninfected cells were used as support for the proposed effects of CPAF in mediating chlamydial phenotypes. CPAF-mediated proteolysis of host proteins with specific functions in the absence of infection led to plausible explanations for how *Chlamydia* had established particular host-pathogen interactions. However, there was no direct evidence showing that CPAF was necessary for the specific host-pathogen interactions during a chlamydial infection. Experimental limitations at the time of these studies prohibited knockout of

CPAF within infected cells. Instead, researchers demonstrated that proteolysis of the host protein substrate conferred a benefit to the chlamydial infection or was sufficient to cause the proposed phenotype in the absence of infection (49, 52, 76). These experiments, however, did not definitively show that this was the same mechanism occurring within a *Chlamydia*-infected cell. Very few people questioned whether CPAF-mediated proteolysis had occurred *in vitro* or *in vivo* because the observed chlamydial phenotypes seemed to support the idea that the proteins had been altered in the infected cells.

### **What are the intracellular substrates of CPAF?**

There are 6 other reported host and 8 reported chlamydial protein substrates that we have not tested under conditions that prevent *in vitro* CPAF activity (Table 2.1). One or more of these proteins may be *in vivo* targets of CPAF, but it is unlikely these substrates are bona fide because they were identified in a manner similar to the other *in vitro* substrates. Although the substrates we have examined only appear to be targeted by CPAF *in vitro*, their proteolysis is specific, suggesting these proteins have the potential to be *in vivo* CPAF substrates. It is possible that there is a small amount of intracellular cleavage or degradation of one or more of the purported substrates below the detection limit of immunoblots. However, if this is the case, CPAF-mediated proteolysis is minor and unlikely to cause the significant phenotypes that have been ascribed to it, such as Golgi reorganization. Alternatively, these proteins may be *in vivo* CPAF substrates under conditions in a *Chlamydia*-infected cell that have not yet been elucidated. For example, the identified CPAF substrates may be cleaved intracellularly but only very late in infection. Our studies have only examined proteolysis up to 48 hpi, prior to the time when the majority of infected cells begin to lyse.

Since our study was published, two proteins have been reported to be CPAF substrates late in the chlamydial infection when precautions were taken to inhibit *in vitro* CPAF activity. Snavelly *et al.* propose that vimentin and LAP-1 are *in vivo* CPAF substrates at late times in the infection based on their experiments in which cleaved vimentin and LAP-1 were detected within *Chlamydia*-infected lysates that were prepared taking precautions to inhibit *in vitro* CPAF activity. Although they used a method to minimize artifactual CPAF-mediated proteolysis, experiments lacked controls to definitively demonstrate that the observed proteolysis occurred intracellularly. Specifically, infected cell lysates were not tested to see if they contained any *in vitro* CPAF activity. The low level of vimentin and LAP-1 proteolysis they detected could be explained by *in vitro* proteolysis taking place in the lysates or *in vivo* proteolysis within the intact infected cells. Live-cell imaging using tagged vimentin and LAP-1 correlated loss of signal with CPAF-mediated proteolysis, but did not directly test whether cleavage by CPAF caused the loss of signal observed by microscopy (74).

In our hands, vimentin seems an unlikely *in vivo* cleavage substrate. Vimentin cleavage products were only detected when *in vitro* CPAF activity was found in the lysate (using an *in vitro* activity assay). Infected lysates in which *in vitro* CPAF activity was completely inhibited contained no detectable cleaved forms of vimentin even as late as 60 hpi (data not shown), which is 12 hours beyond the time when cleavage products were first detected by Snavelly *et al.* (74). Thus, we have no evidence that vimentin is a bona fide substrate *in vivo*. We have not, however, attempted to examine LAP-1.

### **What are the mechanisms of the chlamydial phenotypes previously attributed to CPAF?**

Chlamydial genetic tools were unavailable at the time of our study, but a CPAF-deficient mutant *Chlamydia* strain has since been generated and utilized to demonstrate that CPAF is not

required for many of the cellular phenotypes associated with *Chlamydia* infection (74). HeLa cells infected with CPAF-deficient *Chlamydia* displayed characteristic chlamydial phenotypes, including Golgi reorganization, activation of NFκB, and protection from apoptosis. This data provides genetic evidence that CPAF and CPAF-mediated proteolysis are not necessary for these host-pathogen interactions.

The mischaracterization of the role of CPAF as a major virulence factor largely stemmed from the identity of its proposed substrates. The identity of each protein substrate in the absence of an infection was used as support for the role of CPAF in mediating a specific host-pathogen interaction. Considering phenotypes like Golgi reorganization and resistance to apoptosis are observed in *Chlamydia*-infected cells lacking CPAF, there must be other mechanisms to account for these characteristic chlamydial phenotypes. What, then, are the mechanisms of the numerous host-pathogen interactions previously attributed to CPAF-mediated proteolysis?

We initially began investigating CPAF because we were interested in the mechanism of *Chlamydia*-induced centrosome amplification. We found that although CPAF cleaved or degraded numerous centrosomal proteins, the proteolysis occurred *in vitro* and therefore was not the mechanism of the centrosome abnormalities observed in infected cells. Instead, centrosome amplification may be caused by *Chlamydia* dysregulation of the E3 ubiquitin ligase APC/C (anaphase-promoting complex/cyclosome) (85). APC/C has two co-factors, Cdc20 and Cdh1, that regulate its activation and confer specificity toward different protein substrates during the cell cycle (95). APC<sup>Cdh1</sup> substrates, including centrosomal regulator HsSAS-6, are stabilized in G1 of infected cells (85), and overexpression of HsSAS-6 in uninfected cells is sufficient to cause centrosome amplification (96). The mechanism by which *Chlamydia* modulates APC<sup>Cdh1</sup>

activity is still under investigation. *Chlamydia* does not appear to alter Cdh1 protein levels (85), but may dysregulate Cdh1 activity and interaction with the APC complex.

Similarly, other phenotypes previously attributed to CPAF-mediated proteolysis likely occur due to mechanisms independent of CPAF. For example, Golgi reorganization may be induced by Rab-mediated regulation of Golgi structural proteins rather than golgin-84 cleavage. Rabs, small GTPases that are key regulators of cellular trafficking, have been shown to be actively recruited to the chlamydial inclusion and are necessary for *Chlamydia*-induced Golgi fragmentation (97-99). Relocalization of Rabs could destabilize normal Golgi structure by dysregulating golgin protein localization (100). An alternative mechanism for *Chlamydia*-induced resistance to apoptosis could be stabilization of anti-apoptotic factors rather than degradation of pro-apoptotic factors. Anti-apoptotic protein cIAP-2 is upregulated during a chlamydial infection, and, along with its heteromeric binding partners cIAP-1 and X-linked IAP, is required to maintain apoptosis resistance in infected cells (101). Intermediate filament reorganization around the chlamydial inclusion does not require CPAF-mediated proteolysis of vimentin, but instead may be accomplished through a mechanism involving F-actin. Vimentin cage formation requires RhoA-dependent F-actin ring assembly, suggesting a possible mechanism by which the F-actin surrounding the inclusion recruits full-length vimentin protein (52). Another intracellular parasite, *Toxoplasma gondii*, resides in a parasitophorous vacuole similar to *Chlamydia* and has been proposed to modulate vimentin rearrangement via a secreted parasite protein, although no candidate protein has been identified (102).

### **Where is CPAF localized?**

Our studies in this chapter provide a possible explanation for the lack of intracellular CPAF-mediated proteolysis: CPAF may not be translocated into the cytosol. We found that

CPAF localization to the host cytosol is dependent on fixation method. Infected cells fixed in methanol or a combination of ethanol and acetone exhibited CPAF staining in the inclusion lumen rather than in the host cytosol. Upon close examination, an earlier publication with methanol fixed infected cells seems to validate our findings. *Chlamydia*-infected cells fixed in methanol and stained with a CPAF-specific antibody show inclusion localization, although the published micrographs are of low magnification (87). In light of our conflicting experimental results, what is the true localization of CPAF?

Revisiting the methods that were used to demonstrate cytosolic localization, none of them completely excludes the possibility that CPAF resides in the inclusion lumen. Several immunofluorescence studies using antibodies toward CPAF showed localization in the host cell cytosol beginning at 24 hpi (63, 67, 68, 91, 103-106), but the majority of the experiments relied on the same fixation and permeabilization method (paraformaldehyde followed by saponin treatment) (63, 67, 68, 91, 104-106). Furthermore, the pattern of CPAF staining was often asymmetrical in nature, as if protease had leaked out of one pole of the inclusion (63, 103-106). Others have demonstrated that this type of staining pattern can be indicative of immunofluorescence experimental artifacts in which protein extraction or relocalization obscures the *in vivo* localization (107). Thus, it is possible that CPAF was not translocated into the host cytosol but rather leaked out of the inclusion due to experimental artifacts.

CPAF was also visualized in the cytosol when cells were infected with *Chlamydia* transformed with flag-tagged CPAF, but even these experiments were susceptible to immunofluorescence artifacts since they relied on fixation and antibody staining rather than live-cell imaging (108). Unlike immunofluorescence studies with endogenous CPAF, though, flag-tagged CPAF demonstrated both inclusion and cytosolic localization. CPAF puncta within the

inclusion did not colocalize with antibodies to chlamydial organisms, suggesting CPAF was secreted from the bacteria but contained in a vesicle-type structure inside the inclusion lumen. Diffuse flag-CPAF in the cytosol could have been the result of fixation artifacts or could indicate a small amount of translocation into the host cell.

A comparative proteomics study found CPAF outside of bacterial organisms within infected cell lysate (91). CPAF was clearly secreted from chlamydial organisms, but the CPAF-containing infected cell lysate fraction included inclusion lumen contents as well as host cytosol (91). Thus, these results do not exclude the possibility that CPAF lies within the inclusion lumen.

There is biochemical support for CPAF secretion from chlamydial organisms, but not translocation into the host cell cytosol. CPAF is secreted across the inner bacterial membrane into the bacterial periplasm in a Sec-dependent manner (63). From there, it is unknown how CPAF exits the outer bacterial membrane and inclusion membrane to access the host cell cytosol. Outer membrane vesicle budding has been proposed, but there is little experimental evidence supporting this model (63). CPAF staining in puncta may represent CPAF-containing vesicle structures, but it has not been specifically investigated (108). Localization of CPAF within outer membrane vesicles (OMVs) could explain why host cell substrates are protected from CPAF-mediated proteolysis (63).

If CPAF is localized within the inclusion, it is unlikely that the protease accesses host protein substrates, which would explain our data that reported CPAF substrates are not cleaved or degraded intracellularly during a normal infection. However, it is possible that CPAF is translocated into the host cytosol late in the infection resulting in proteolysis of yet undisclosed host protein substrates or of those previously identified, albeit at much later times than previously reported. Regardless, the true localization of CPAF over the course of the chlamydial

infection would greatly help in identifying CPAF's *in vivo* substrates and the timing of their proteolysis.

Snaveley *et al.* have proposed that CPAF resides within the inclusion for the majority of the intracellular infection and is only released late in the infection by inclusion rupture, rather than active translocation. Once released into the host cytosol, CPAF could target host protein substrates, potentially facilitating host cell lysis. Vimentin and LAP-1 have been proposed to be *in vivo* CPAF substrates at this late time, but we have been unable to confirm these observations (at least for vimentin) based on immunoblot analysis. Live-cell imaging of tagged forms of vimentin and LAP-1 was used to indirectly demonstrate CPAF release into the host cytosol; however, these studies would need to be repeated using *Chlamydia* transformed with a tagged form of CPAF to be able to monitor CPAF localization directly and definitively support this model (74).

### **How to determine the role of CPAF?**

Since our initial studies, CPAF-deficient mutant *Chlamydia* strains developed by Snaveley *et al.* have helped us learn more about the role of CPAF during a chlamydial infection. Using chemical mutagenesis and whole genome sequencing, the authors identified two null mutant strains with nonsense mutations in the *cpa* gene preventing production of CPAF protein. Surprisingly, cells infected with the CPAF-null *Chlamydia* were able to complete a successful infection in 48 hours, although mutant infected cells displayed a threefold decrease in infectious progeny compared to controls. These results demonstrate that CPAF is not essential for a chlamydial infection, but suggest a role for this protease in the production of infectious progeny (74).

The CPAF-mutant strain is a helpful genetic tool for studying CPAF function, but it cannot answer all questions about the function of this protease. It is useful for assessing if CPAF is necessary for a phenotype of chlamydial infection and for avoiding artifactual CPAF effects during protein analysis of infected cell lysates. It can also help with determining whether CPAF is involved in protein proteolysis (although it does not distinguish *in vitro* from *in vivo* proteolysis). The mutant cannot, however, be modulated to determine the timing of CPAF involvement in *Chlamydia* phenotypes or protein proteolysis.

Despite the ambiguity surrounding CPAF's intracellular substrates, there is still evidence this potent protease plays a role in chlamydial infection. CPAF is conserved among chlamydial species (65), and our studies have demonstrated that CPAF is made during an infection and cleaved into its active form (Fig. 2.8). However, identification of *in vivo* CPAF substrates will be challenging because experiments must be conducted and analyzed with caution to distinguish *in vitro* proteolysis from intracellular proteolysis. Even experiments that utilize the CPAF-mutant will be paired with isogenic control strains that do encode CPAF, thus precautions must still be taken to inhibit *in vitro* CPAF activity. Clearly, chlamydial researchers need a reliable strategy for inhibiting *in vitro* CPAF activity to avoid contaminating results with experimental artifacts. In the next chapter we investigate the effectiveness of various methods to inhibit *in vitro* CPAF activity.

## **Chapter 3**

### **Induction and Inhibition of CPAF Activity during Analysis of *Chlamydia*-infected Cells**

## **Contributions**

The work described in this chapter was the result of the continuing collaboration between Jennifer Lee, Kirsten Johnson, and Allan Chen. All experiments were discussed and designed as a team effort. Allen Chen and Kirsten Johnson contributed to experiments described in Figure 3.1 and 3.2. Jennifer Lee was responsible for all other experiments and figures. The work described in this chapter has been published (109) (with Kirsten Johnson and Jennifer Lee as co-first authors).

## Summary

Studies of the chlamydial protease CPAF have been complicated by difficulties in distinguishing bona fide intracellular proteolysis from *in vitro* proteolysis. This confounding issue has been attributed to CPAF activity in lysates from *Chlamydia*-infected cells. In this study, we evaluated methods to inhibit *in vitro* CPAF-mediated proteolysis and identified several experimental conditions that reduce their effectiveness. The amount of *in vitro* proteolysis in a lysate was variable and depended on factors such as the specific substrate and the time in the intracellular infection. Additionally, we demonstrated that artifactual CPAF activity is induced before cell lysis by standard cell detachment methods, including trypsinization. Protein analysis of *Chlamydia*-infected cells therefore requires precautions to inhibit CPAF activity during both cell detachment and lysate preparation, followed by verification that the cell lysates do not contain residual CPAF activity. These concerns about artifactual proteolysis extend beyond studies of CPAF function because they have the potential to affect the analyses of host and chlamydial proteins from *Chlamydia*-infected cells.

## Introduction

CPAF is a potent protease that retains significant enzymatic activity *in vitro* within infected cell lysates, which has made it difficult to distinguish *in vivo* from *in vitro* proteolysis. Intracellular CPAF substrates were mainly misidentified because studies analyzed proteolysis by immunoblots using standard lysate preparation methods, which are insufficient to inhibit *in vitro* CPAF activity. CPAF is resistant to standard protease inhibitor cocktails (73, 110) and active at 4°C (75). Furthermore, the time of lysate preparation (as little as 10 minutes) is sufficient for CPAF to completely cleave or degrade proteins *in vitro* (75). Although *in vitro* CPAF activity within cell lysates had been suspected prior to our findings (88), the extent to which *in vitro* activity contributed to observed proteolysis was thought to be minimal. Our data presented in the previous chapter demonstrates that *in vitro* proteolysis due to CPAF activity within lysates is substantial and greatly misrepresents the intracellular protein profile. Therefore, methods to effectively inhibit CPAF activity during lysate preparation are essential for any studies of proteins within chlamydial lysates.

Several methods have been proposed to inhibit CPAF *in vitro* activity during lysate preparation. The first method is pre-treatment of infected cells with *clasto*-lactacystin prior to cell collection and lysis (75). *Clasto*-lactacystin, the active form of lactacystin, is a cell-permeable proteasome inhibitor that has been shown to inhibit CPAF (66, 68, 72, 73). Alternatively, direct lysis in 8M urea non-specifically denatures all proteins rendering CPAF inactive (75). Similarly, direct lysis in hot 1% SDS also acts to globally denature proteins and inhibit CPAF activity (74). Though these methods have been employed as a precaution against *in vitro* CPAF activity, the effectiveness of each method had not been examined in detail.

In this study, we compare these three common methods used to prevent CPAF-mediated proteolysis during lysate preparation. Our results reveal that each method has specific limitations that reduce effective inhibition of *in vitro* CPAF activity. Experimental variables including preparation of buffers, time in the infection, and protein substrate being analyzed affect the amount of *in vitro* CPAF activity detected within a lysate. We also show for the first time that artifactual CPAF activity is induced before cell lysis by standard cell detachment methods. Based on our findings, we outline an approach for preventing and checking for CPAF activity during protein analysis of *Chlamydia*-infected cells.

# Results

## **Experimental methods to inhibit *in vitro* CPAF activity are not completely effective**

Pre-treatment with *clasto*-lactacystin can inhibit CPAF *in vitro* activity, but we found that the level of inhibition achieved is variable from experiment to experiment. Infected cells must be pre-treated for 60 minutes prior to lysate preparation to completely inhibit CPAF activity (Fig. 3.1A). Pre-treatment is necessary as *clasto*-lactacystin added directly to the lysis buffer is insufficient for complete CPAF inhibition (Fig. 3.1B). Additionally, there is variation between lots of *clasto*-lactacystin (74, 111) so each batch must be tested for the optimal treatment time and concentration (Fig. 3.1C).

Direct lysis in 8M urea is a method used to non-specifically inhibit CPAF activity during lysate preparation that does not require pre-treatment of the infected cells. We found that direct lysis in denaturing urea is effective to inhibit CPAF, but only when the concentration of urea is 8M, not less (Fig. 3.1D). Moreover, 8M urea solution must be prepared fresh to ensure reliable CPAF inhibition (Fig. 3.1E).

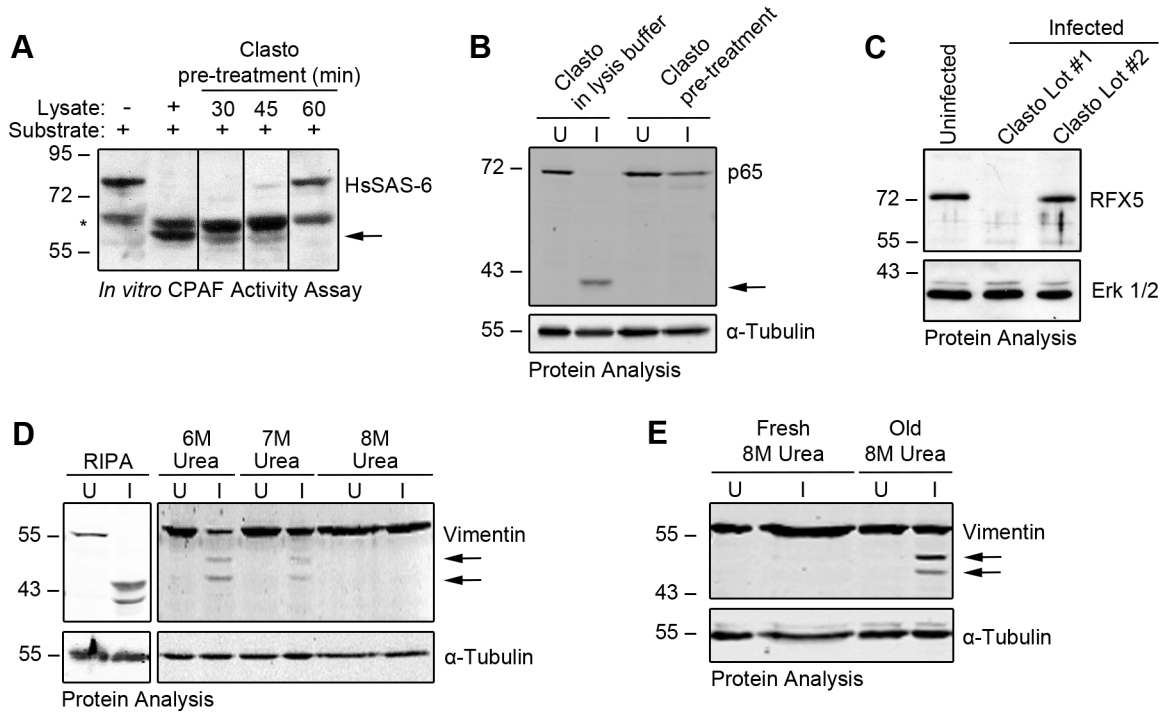
Direct lysis in hot 1% SDS was proposed by others as another method to non-specifically denature proteins and inhibit CPAF activity within cell lysates (74). Although this method is adequate to completely inhibit CPAF activity early in infection, it becomes less effective later in infection (Fig. 3.2F-G), which could indicate that there is more CPAF in a late-stage *Chlamydia*-infected cell or that CPAF becomes more difficult to inhibit at late times.

## **An *in vitro* CPAF activity assay is required to assess whether residual enzymatic activity remains in cell lysates**

Without verification that lysates are free of CPAF activity, subsequent protein analyses cannot be interpreted because any observed proteolysis could have taken place *in vivo* within

**Figure 3.1. Methods to inhibit CPAF activity during infected cell lysate preparation are not always effective**

**A)** *Chlamydia*-infected HeLa cells were pre-treated with 150 $\mu$ M *clasto*-lactacystin for 30, 45, or 60 min prior to collection at 36 hpi by trypsinization and lysis in RIPA buffer. Infected cell lysates were tested for CPAF activity in an *in vitro* activity assay (outlined in Fig. 3.2A), which was analyzed by Western blotting with antibodies to the host protein HsSAS-6. The first lane with uninfected cell lysate alone shows uncleaved HsSAS-6. A cross-reacting band is marked with a '\*'. **B)** Uninfected and infected cells were collected by trypsinization at 48 hpi, and lysed in RIPA buffer containing 150 $\mu$ M *clasto*-lactacystin. Alternatively, infected cells were pre-treated with 150 $\mu$ M *clasto*-lactacystin for 60 min prior to lysate preparation in RIPA buffer. Proteolysis of p65 as a substrate was monitored in the lysates by Western blot analysis with p65 antibodies, with  $\alpha$ -tubulin serving as a loading control. **C)** Uninfected and infected cells were pre-treated with two different batches of *clasto*-lactacystin at 150 $\mu$ M for 60 min and then lysed in RIPA buffer. Lysates were assayed by Western blot for RFX5 degradation with antibodies to RFX5 or Erk 1/2 as a loading control. **D)** Monolayers of uninfected and infected cells at 48 hpi were either collected by trypsinization and lysed in RIPA buffer or lysed directly in urea at the indicated concentrations. **E)** Monolayers of uninfected and infected cells at 48 hpi were lysed directly in fresh or old solutions of 8M urea. For D) and E), lysates were analyzed for vimentin proteolysis by Western blotting with vimentin antibodies. HsSAS-6, p65, and vimentin proteolysis products are indicated with arrows.

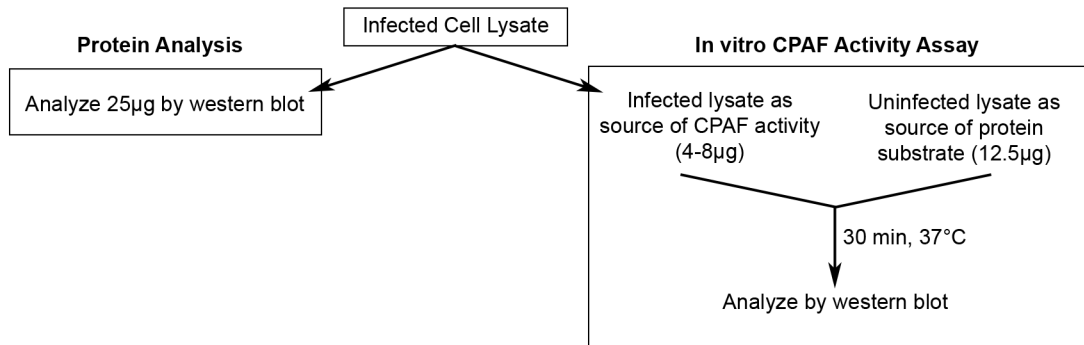
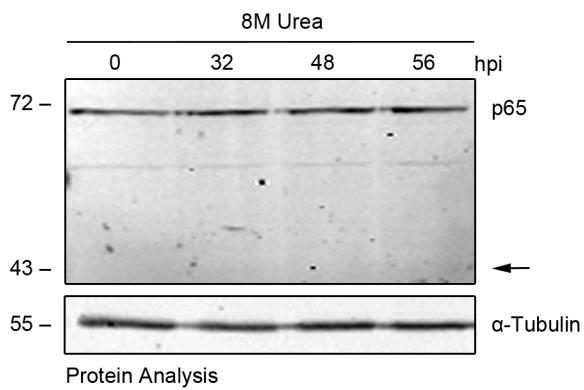
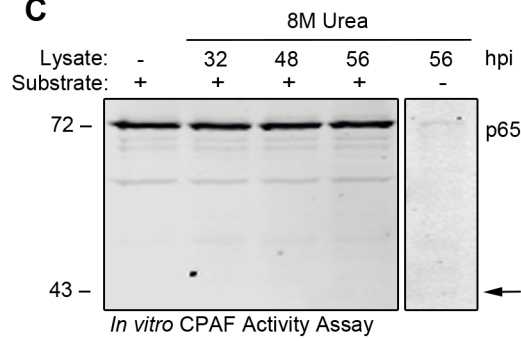
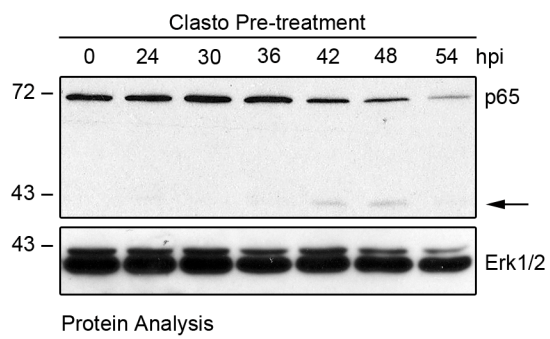
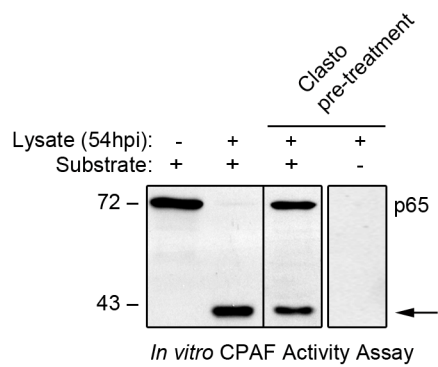
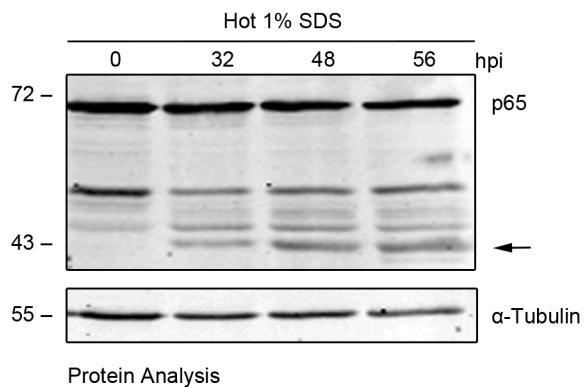
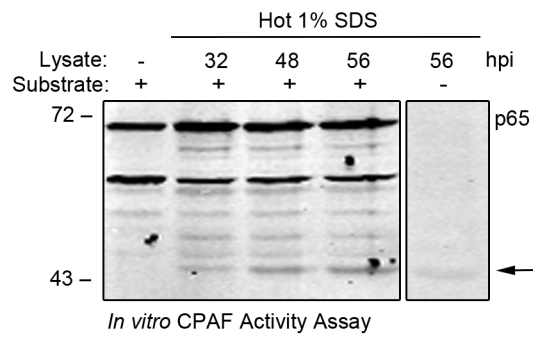


infected cells or *in vitro* during lysate preparation. Thus, an *in vitro* CPAF activity assay is required for each infected cell lysate in every experiment to ensure complete inhibition of CPAF was achieved prior to interpretation of any proteolysis within the lysates (Fig. 3.2A). In the assay, a small amount of infected cell lysate (containing potential CPAF activity) is incubated with uninfected cell lysate (as a source of host protein substrates) and the reaction is analyzed by immunoblot for CPAF-mediated proteolysis. Any detectable proteolysis indicates that *in vitro* CPAF activity is present within the infected lysate. We propose that this *in vitro* assay should be conducted for each experiment since there is variability in CPAF inhibition with all three methods we examined: direct lysis in 8M urea, lysis in RIPA buffer after pre-treatment with *clasto*-lactacystin, and direct lysis in hot 1% SDS.

The utility of the *in vitro* assay for interpretation of proteolysis within infected cell lysates can be illustrated using p65, a published CPAF substrate (86) which we have found is cleaved *in vitro* by CPAF (75). When p65 proteolysis was examined in infected cell lysates prepared with each of three methods to inhibit *in vitro* CPAF activity, three different results were obtained. In 8M urea there was no apparent cleavage up to 56 hpi (Fig. 3.2B), lysates pre-treated with *clasto*-lactacystin showed p65 cleavage beginning at 42 hpi (Fig. 3.2D), and lysates prepared in 1% SDS contained cleaved p65 at 32 hpi (Fig. 3.2F). If these infected cell lysates were analyzed in isolation, the *clasto*-lactacystin treated and 1% SDS lysates would suggest that p65 is cleaved during a chlamydial infection. However, when the infected lysates were subjected to an *in vitro* CPAF activity assay, we determined that these two methods did not completely inhibit residual *in vitro* CPAF activity in this experiment. *Clasto*-lactacystin treated and 1% SDS lysates showed residual CPAF *in vitro* activity present in 54 hpi and 32 hpi lysates, respectively (Fig. 3.2E, Fig. 3.2G) while 8M urea lysates displayed no detectable *in vitro* CPAF activity at

**Figure 3.2. Analysis of infected cell lysates for substrate proteolysis and CPAF activity**

**A)** Procedure to examine proteolysis and CPAF activity in an infected cell lysate. ‘Protein Analysis’ refers to Western blot analysis of infected cell lysates for cleavage or degradation of a protein of interest. The ‘*In vitro* CPAF Activity Assay’ measures any residual CPAF activity present in the infected cell lysate. **B)** At the indicated times in the *Chlamydia* infection, cells were lysed directly in 8M urea, followed by protein analysis of the lysates by Western blotting with antibodies to p65. **C)** Lysates from Fig 3.2B were also assayed for CPAF activity against p65 using the *in vitro* assay. **D)** Uninfected and infected cells were pre-treated with 150 $\mu$ M *clasto*-lactacystin for 60 min prior to lysis in RIPA buffer at the indicated times in the *Chlamydia* infection. Lysates were examined for p65 proteolysis by Western blot analysis. **E)** Lysates from the 54 hpi time point of Fig. 3.2D were tested in the *in vitro* CPAF activity assay for p65 cleavage. **F)** Cells at the indicated times in the *Chlamydia* infection were lysed in hot 1% SDS buffer, followed by protein analysis of the lysates for p65 cleavage. **G)** Lysates from Fig. 3.2F were tested for residual CPAF activity against p6 in the *in vitro* CPAF activity assay. Expected p65 cleavage products in the Western blots are indicated with arrows. For Fig. 3.2C, E, and G, the same amounts of representative infected cell lysates that were used in the *in vitro* assay were included to demonstrate that it does not contain detectable amounts of the p65 cleavage product. Thus, the appearance of p65 cleavage products in the *in vitro* assays testing *clasto*-lactacystin pre-treated (Fig. 3.2E) and hot 1% SDS (Fig. 3.2G) infected cell lysates indicate that these lysates contain residual CPAF activity.

**A****B****C****D****E****F****G**

any time (Fig. 3.2C). Thus, p65 cleavage observed at late times in the *clasto*-lactacystin pre-treated and hot 1% SDS lysates likely occurred *in vitro* within the lysate rather than within intact cells. 8M urea was effective at completely inhibiting residual CPAF activity within the infected cell lysates at all times tested and no p65 cleavage was observed in these samples. These studies demonstrate that proteolysis within a *Chlamydia*-infected lysate cannot be correctly interpreted unless the lysate is free of *in vitro* proteolytic activity toward that protein.

### **Proteins vary in their susceptibility to CPAF**

Conditions that are sufficient to inhibit CPAF activity toward one substrate may not be adequate for another substrate. We performed an *in vitro* activity assay assessing CPAF activity from the same set of lysates toward two different substrates: vimentin and p65 (52, 86). Pre-treatment with *clasto*-lactacystin inhibited most, but not all, *in vitro* CPAF activity toward vimentin while urea and hot SDS preparation methods were sufficient to completely inhibit residual CPAF activity toward vimentin in this experiment. In contrast, residual activity toward p65 was detected in all three lysates (Fig. 3.3). These results suggest that p65 is a more sensitive CPAF substrate than vimentin, and that CPAF activity toward one protein substrate is not indicative of activity toward another. These findings have implications when applying the *in vitro* CPAF assay to protein analysis of an infected lysate. Specifically in this experiment, if any vimentin proteolysis were observed in the 8M urea or 1% SDS lysates it could be interpreted as occurring intracellularly since there was not detectable residual CPAF activity within these lysates; however, any cleavage of p65 could have occurred in intact infected cells, during lysate preparation, or both because of residual activity toward this protein in the lysates. Our findings also illustrate the necessity of performing an *in vitro* assay to check for residual CPAF activity in each experiment. In this experiment 8M urea did not completely inhibit *in vitro* CPAF activity

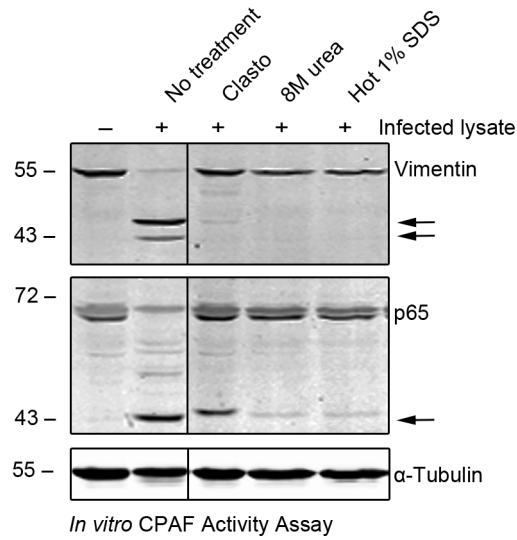


**Figure 3.3. Protein substrates vary in their susceptibility to CPAF-mediated proteolysis**

Lysates of infected cells at 48 hpi were prepared by three methods (pre-treatment with *clasto*-lactacystin followed by lysis in RIPA buffer, direct lysis in 8M urea, or direct lysis in hot 1% SDS) and were examined for residual CPAF activity in the *in vitro* activity assay. Reaction mixtures were examined for vimentin and p65 by Western blot analysis. Cleavage products in the Western blots are indicated with arrows.

toward p65 (Fig. 3.3), even though it had in a previous experiment (Fig. 3.2C). Without verification that an infected-cell lysate is free from CPAF activity toward a specific protein of interest, one cannot interpret whether proteolysis detected in immunoblots occurred during the intracellular infection, *in vitro* within the lysate, or a combination of the two. Furthermore, it is important to evaluate the same protein substrate in both protein analysis and *in vitro* activity assay since proteins vary in their susceptibility to CPAF.

### **CPAF activity is induced by standard cell collection methods**

We discovered that the experimental manipulation of collecting *Chlamydia*-infected cells from a monolayer induces CPAF activity. Many standard lysis procedures involved collecting and pelleting infected cells prior to adding lysis buffer (49, 69, 71, 76, 79, 80, 86, 88, 92, 103, 112), but no study had specifically addressed whether these operations could lead to *in vitro* CPAF-mediated proteolysis. We discovered that cell collection by trypsin, accutase, or mechanical scraping followed by lysis in 8M urea (to inhibit CPAF activity in the lysate) produced a small level of vimentin cleavage compared to direct lysis in 8M urea, which had no detectable proteolysis (Fig. 3.4A). Vimentin cleavage did not likely result from CPAF activity in the lysates as they tested negative for residual activity in the *in vitro* assay (Fig. 3.4B). Putting these findings together, it appears that artifactual CPAF-mediated cleavage in these samples occurred during cell collection but before cell lysis. These experiments provide evidence that CPAF activity can be induced by experimental manipulations and cause proteolysis within intact infected cells. If lysates contain residual CPAF activity, *in vitro* proteolysis can continue during lysate preparation, exaggerating the artifactual cleavage or degradation. Thus, protein analysis of *Chlamydia*-infected cells requires precautionary methods to inhibit CPAF activity during cell collection as well as within the lysate.

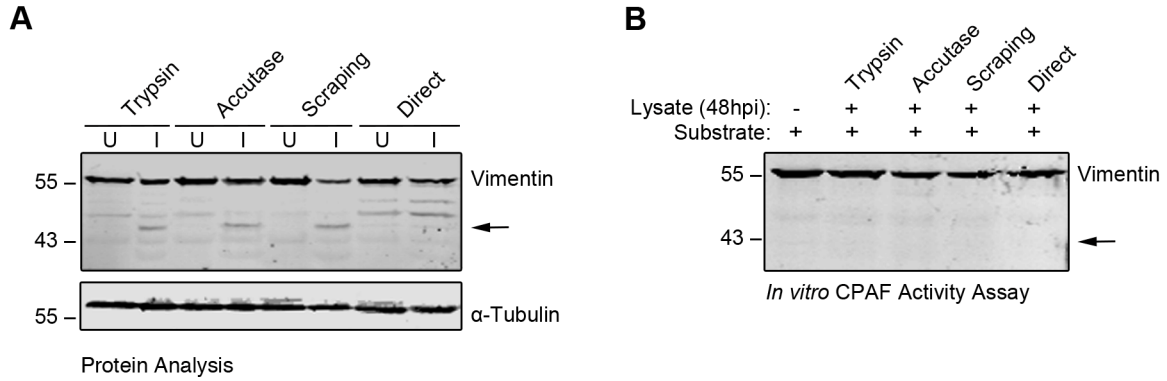


**Figure 3.4. CPAF activity is induced by standard cell collection methods**

**A)** Uninfected and infected cells were detached at 48 hpi by treatment with trypsin or accutase, or by scraping, and then pelleted and lysed in 8M urea. In parallel, cells were lysed directly in 8M urea. Lysates were analyzed for vimentin proteolysis by Western blotting, with  $\alpha$ -tubulin serving as a loading control. **B)** Infected cell lysates from Fig. 3.4A were tested in the *in vitro* CPAF activity assay and reactions were examined by Western blot analysis with antibodies to vimentin. Expected cleavage products in the Western blots are indicated with arrows.

## Discussion

In this chapter we have shown that methods to inhibit *in vitro* CPAF activity during lysate preparation are not completely reliable, and artifactual proteolysis can occur despite the precautions taken. To ensure an infected lysate does not contain residual CPAF activity, an *in vitro* activity assay should be conducted prior to analysis of any proteolysis. This assay should be performed with the protein of interest, since substrates vary in their susceptibility to CPAF. Additionally, the *in vitro* assay needs to accompany each experiment because we found that the level of CPAF inhibition is variable between lysates, even when utilizing the same lysate preparation method. Our results indicate that artifactual CPAF activity may also occur prior to cell lysis because experimental manipulations to remove infected cells from a monolayer, including trypsinization, induced CPAF activity. Thus, artifactual CPAF-mediated proteolysis may be experimentally induced within intact cells by the cell collection procedure. This finding indicates that inhibition of CPAF activity after cell lysis will not completely prevent artifactual proteolysis. Together, our findings about experimental induction of CPAF and residual *in vitro* activity within lysates provide an explanation for why chlamydial researchers had difficulty distinguishing *in vitro* from *in vivo* proteolysis in previous studies, and why intracellular CPAF substrates were misidentified.

### **Why are methods to inhibit *in vitro* CPAF activity during lysate preparation variable?**

Although chlamydial researchers are now taking precautionary measures to inhibit CPAF activity during lysate preparation (74, 105), problems persist with interpretation of proteolysis within infected cell lysates because the methods are not always completely effective. Some groups have added CPAF inhibitors like lactacystin to cells after they have been harvested to

prevent *in vitro* CPAF activity (79, 91). However, treatment with an inhibitor at the time of lysis is too late to prevent CPAF-mediated proteolysis that has already occurred during cell collection.

Even when infected cells are pre-treated with *clasto*-lactacystin there are several factors that affect its efficacy. There is variability between batches of this chemical compound (74, 111), so using treatment conditions that have been established in previous experiments does not guarantee reliable CPAF inhibition. Batch variation is likely due to lactacystin's sensitivity to long-term storage. Lactacystin spontaneously converts into *clasto*-lactacystin  $\beta$ -lactone, which is the active form of the compound that inhibits CPAF and the proteasome (66, 113, 114). Once *clasto*-lactacystin forms, it can either bind to and inhibit CPAF or be hydrolyzed to the inactive product dihydroxy acid (115). The complex kinetics of lactacystin stability make it difficult to regulate the effective concentration and ensure complete CPAF inhibition in each experiment. The challenges of storing and testing each batch of lactacystin prior to conducting any experiments are not only inconvenient but also costly. Therefore, alternative methods to inhibit *in vitro* CPAF activity during analysis of *Chlamydia*-infected cell lysates are preferred.

Direct lysis in 8M urea can successfully denature CPAF and prevent its activity within lysates. In contrast to lactacystin pre-treatment, the lysis solution is applied to infected cells directly on the monolayer, avoiding cell collection that leads to artifactual CPAF induction. 8M urea then continues to inhibit CPAF activity within lysates to prevent *in vitro* proteolysis. One consideration with this method is that the urea solution must be prepared freshly. Cyanate is in equilibrium with urea in solution, and storage of urea solutions at room temperature may develop a significant concentration of cyanate ions (116). Factors such as the concentration of urea, pH, and temperature of the solution affect the equilibrium (117), but any accumulation of cyanate effectively reduces the concentration of urea. As urea solutions less concentrated than 8M do not

completely inhibit *in vitro* CPAF activity (Fig. 3.1D), we recommend that solutions be prepared on the same day that they are to be used. Even with such safeguards, it is still necessary to test each lysate for residual CPAF activity using the *in vitro* assay because even fresh 8M urea may not completely inhibit all CPAF activity in every instance. In our experience, fresh 8M urea generally provides reliable CPAF inhibition for lysates prepared prior to 48 hpi; however, experiments in which *Chlamydia*-infected cells were lysed between 48-60 hpi did not have consistent inhibition (data not shown). We reason that as the infection progresses more CPAF protease is made, and it becomes more difficult to achieve complete inhibition of enzymatic activity at these late times.

Direct lysis in hot 1% SDS buffer is another method that prevents artifactual induction because it is applied directly to the monolayer and denatures CPAF to inhibit *in vitro* activity. Like direct lysis in 8M urea, this method can effectively inhibit CPAF activity at early and mid times in the chlamydial infection but becomes less effective at late times. These observations support our speculation that large quantities of CPAF that accumulate during infection are difficult to completely denature. Additionally, we suspect that when 1% SDS has cooled from boiling prior to addition to the cell monolayer it is less effective at inhibiting CPAF (data not shown).

### **Why is an *in vitro* CPAF activity assay necessary?**

Snavely *et al.* reported partial proteolysis of vimentin and LAP-1 at late times in the intracellular *Chlamydia* infection (74). They took precautions to inhibit CPAF activity during lysate preparation by directly lysing *Chlamydia*-infected cells in hot 1% SDS, but the lysates were not verified to be free of CPAF activity. Although they demonstrated in another experiment that 1% SDS was sufficient to inhibit recombinant CPAF activity toward vimentin, the

experimental lysates themselves were not examined directly. Without this important control, the presence of residual CPAF activity in the lysates cannot be ruled out and thus it is not clear if vimentin and LAP-1 proteolysis is an experimental artifact. In our hands, immunoblots have also revealed vimentin cleavage late, but importantly in each instance residual CPAF activity was detected in the lysates using the *in vitro* activity assay. Experiments in which we successfully inhibited all residual CPAF activity did not contain cleaved vimentin forms (data not shown). Thus, there is a high likelihood that vimentin proteolysis detected in immunoblots by Snavely *et al.* occurred *in vitro* rather than intracellularly. This example illustrates the difficulty in interpreting proteolysis without verifying that the specific lysates being examined are free of residual CPAF activity using an *in vitro* activity assay.

#### **How does cell harvesting induce artifactual CPAF activity?**

It was surprising to find that CPAF activity is experimentally induced by standard cell harvesting methods, and it is unclear how physical detachment of the infected cells could produce this artifact. We detected the CPAF<sub>c</sub> fragment within infected cell lysates prepared in 8M urea beginning at 24 hpi (Fig. 2.8), suggesting that CPAF is already activated (90) and can cleave substrates prior to cell harvest. Furthermore, we do not believe that direct enzymatic processing of CPAF by trypsin or accutase causes the artifactual activation since mechanical scraping of cells from the monolayer led to the same CPAF artifacts as enzymatic detachment methods. Perhaps the artifact introduced by cell harvesting is the release of active CPAF to access proteins it does not normally have contact with inside the infected cell. In chapter 2, we provided evidence suggesting CPAF may be localized in the inclusion lumen rather than the host cell cytosol. Physical stress on the infected cells inflicted during cell harvesting could trigger

partial or complete disruption of the inclusion membrane, releasing active CPAF into the host cell cytosol where it could then cleave and degrade host cell proteins.

Cell harvesting has been shown to physically and chemically alter cells in the absence of a *Chlamydia* infection. Enzymatic and mechanical methods of cell collection can physically damage cells (118) and have also been shown to have deleterious effects on cell morphology, behavior, and chemical make up (119). Standard treatments like trypsinization and mechanical scraping affect the IR spectra of collected cells, including peaks corresponding to amide groups (120), suggesting these types of manipulations could lead to different protein profiles in *Chlamydia*-infected cells. These observations lend support to a model in which the stress of host cell detachment from the monolayer results in the release of active CPAF allowing it to now access and artifactually cleave or degrade numerous protein substrates.

Cell detachment-induced CPAF activity could help explain our results from another experiment in which we attempted to examine infected cells after trypsinization. We trypsinized *Chlamydia*-infected monolayers at mid to late stages in the infection and attempted to replat cells rather than collect them for lysis. The trypsinized infected cells did not re-adhere to the cell culture dish and exhibited rounded, floating, shrunken, and blebbing phenotypes characteristic of apoptosis (121, 122) (data not shown). Early stage *Chlamydia*-infected cells, however, were able to re-adhere and continued to grow when replated. The timing of the differences in these two populations of cells correlated with the expression pattern of CPAF. One reason CPAF-containing infected cells may not have been able to survive after trypsinization is that cell detachment released active CPAF into the host cytosol and proteolytically processed many substrates. Even though the infected cells remained intact, the treatment had a devastating effect on the cells that they could not recover from, perhaps an extensive level of CPAF-mediated

proteolysis. It would be interesting to repeat this experiment with CPAF-deficient mutant *Chlamydia* to determine whether CPAF is required for these phenotypes after cell detachment.

### **How shall we proceed with studies of CPAF and infected cell lysates?**

In this study, we have demonstrated that artifactual CPAF-mediated proteolysis is the result of a combination of induction of CPAF activity during cell harvesting and *in vitro* activity within cell lysates. Therefore protein analysis of *Chlamydia*-infected cells requires precautions to inhibit CPAF activity during both cell detachment and lysate preparation. Based on our experiments, the most reliable method appears to be direct lysis in 8M urea, but we discovered that no method was 100% effective at inhibiting CPAF *in vitro* activity in every experiment. Thus, it is critical to verify that each lysate does not contain residual CPAF activity. We propose that in all studies of *Chlamydia*-infected cell lysates researchers utilize precautionary methods to inhibit CPAF activity during cell collection and an assay to reveal whether detected proteolysis could be due to residual CPAF activity within cell lysate (Fig. 3.5).

Artifactual CPAF-mediated proteolysis has broad implications for studies of *Chlamydia*-infected cells. Clearly, artifactual proteolysis can obscure studies of CPAF function, specifically identification of intracellular substrates; but concerns extend beyond studies of CPAF because artifactual proteolysis has the potential to affect analyses of many host and chlamydial proteins from *Chlamydia*-infected cells. Cell detachment is a standard step in many protocols to prepare *Chlamydia*-infected cells for protein and proteomic analysis by approaches such as flow cytometry, mass spectrometry, protein affinity chromatography, and biochemical studies. If CPAF activity is not inhibited during the preparation of *Chlamydia*-infected cells for these experiments, artifactual CPAF activity could alter the protein landscape and mislead chlamydial researchers about the true situation in an infected cell.

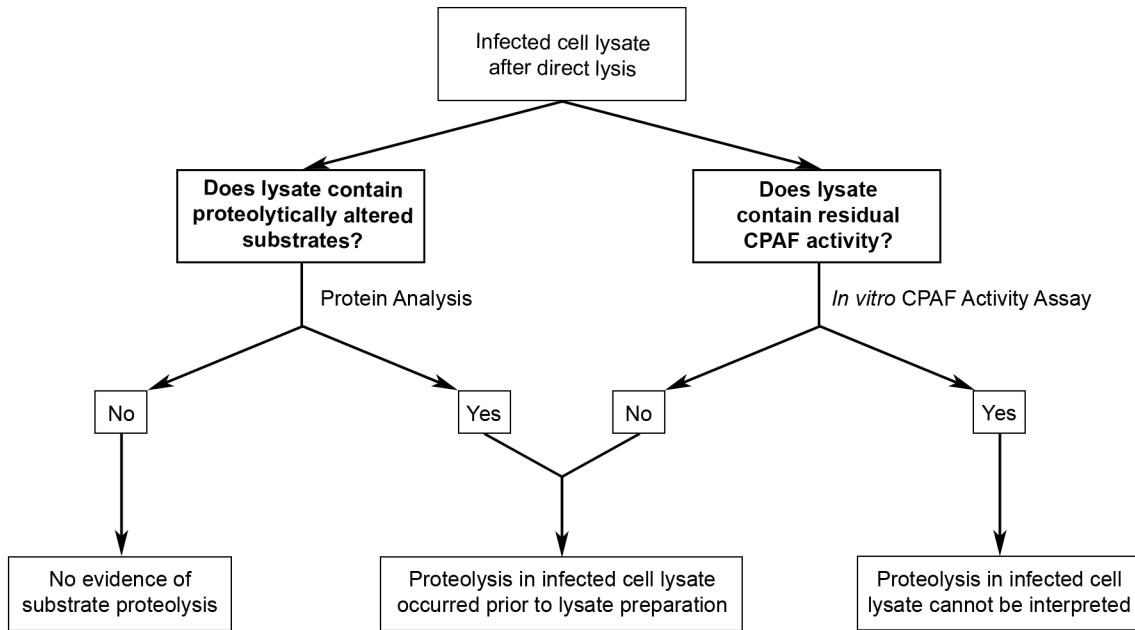


**Figure 3.5. Recommended procedure for analysis of proteins in lysates from *Chlamydia*-infected cells**

We propose that infected cell lysates, which are analyzed for cleavage or degradation of a protein of interest (‘Protein analysis’), should also be tested for the presence of residual CPAF activity (‘*In vitro* CPAF Activity Assay’). This parallel analysis should examine the same substrate as the protein analysis and be performed for each lysate. If the *in vitro* CPAF assay reveals residual CPAF activity in the infected lysate, any observed proteolysis in this lysate cannot be interpreted because it will be unclear whether the proteolysis occurred in the *Chlamydia*-infected cell, during lysate preparation, or both.

Unfortunately, the methods to inhibit CPAF activity during cell harvesting and lysis are not compatible with all downstream analyses. For example, direct lysis of infected cells in denaturing urea or SDS solutions can effectively prevent artifactual CPAF activity, but these lysates are not useful for enzyme activity assays (for example kinase or phosphatase assays) since proteins were globally denatured during lysate preparation.

Treatment of infected cells with a CPAF inhibitor is a useful approach to inhibit artifactual CPAF activity in experiments that cannot be conducted under strongly denaturing conditions. Although *clasto*-lactacystin is the most well-characterized CPAF inhibitor, we have found that there are many variables effecting its reliability; therefore, a more dependable inhibitor would be an invaluable tool for future studies of *Chlamydia*-infected cells and to help determine CPAF's function. In the next chapter we use a chemical modeling approach to design a novel peptide inhibitor of CPAF.

## **Chapter 4**

### **Development of a CPAF Peptide Inhibitor**

## Contributions

The work described in this chapter was the result of collaboration between Jennifer Lee, Victoria Feher, Rommie Amaro, Timon Mönig, Anna-Laura Schmitz, and Markus Kaiser. Timon and Anna-Laura synthesized the peptide compounds. Victoria performed the molecular modeling and prepared Figure 4.3. Jennifer conducted all other experiments and prepared the remaining figures.

## Summary

Although several peptide and small molecule inhibitors of CPAF activity have been identified, none of these compounds is ideal for studying CPAF function in *Chlamydia*-infected cells. The main issue with current CPAF inhibitors is that they lack potency and specificity. As we have explored in the previous two chapters, CPAF has an especially persistent enzymatic activity that is not easily inhibited. Caution must be taken to ensure compounds effectively inhibit all enzymatic activity to avoid *in vitro* artifacts. Furthermore, currently available CPAF inhibitors have off-target effects on other enzymes that are present within *Chlamydia*-infected cells. An ideal inhibitor would be selective for CPAF with little affinity for other proteases.

In this chapter we identify novel boronate peptide inhibitors of CPAF. We demonstrate for the first time that boronate heptapeptides can inhibit CPAF activity *in vitro* and establish molecular modeling as an approach to determine CPAF-peptide structure activity relationships. Our studies reveal substrate binding pocket features of the CPAF active site that can be utilized to design boronate peptides with enhanced binding affinity and specificity for CPAF. Our observations in this study demonstrate the promise of boronate peptides as strong and specific inhibitors of CPAF.

## Introduction

CPAF is highly resistant to standard protease inhibitors, which has made it an especially difficult enzyme to study. Although CPAF is classified as a serine protease (due to the presence of a catalytic serine in its active site), CPAF is atypical in that its catalytic triad contains a glutamic acid residue in place of the typical aspartic acid residue (66, 123). The altered catalytic triad is a likely reason that many standard serine protease inhibitors do not inhibit CPAF. For instance, phenylmethylsulphonyl fluoride (PMSF), which inactivates virtually all serine proteases by reacting with the catalytic serine, is ineffective against CPAF (73, 123). The reaction between PMSF and the serine protease is usually stabilized by hydrogen binding within the active site, but the altered topology of CPAF's active site prevents these stabilizing intermolecular forces (66). Another serine protease inhibitor, aprotinin, also does not inhibit CPAF (73).

One effective inhibitor against CPAF is lactacystin, a small molecule inhibitor of the proteasome. Interestingly, lactacystin was the only one of a panel of proteasomal inhibitors that inhibited CPAF. Peptide aldehyde inhibitors of the proteasome, such as MG132, MG115, and PSI, did not display any inhibitory activity toward CPAF (73). In neutral pH solutions, lactacystin spontaneously converts to *clasto*-lactacystin  $\beta$ -lactone, which is the membrane-permeable active form of the compound. *Clasto*-lactacystin reacts with the active site threonine of the proteasome resulting in the acylation of the catalytic hydroxyl (124). The mechanism of CPAF inhibition by lactacystin is thought to occur similarly to the proteasome despite their different catalytic residues (66). Lactacystin is a strong inhibitor of CPAF because it binds irreversibly, but there are several reasons why lactacystin is not the optimal tool to use in CPAF studies. First, off-target effects of lactacystin on the proteasome complicate the interpretation of

any studies in which lactacystin is being used as a CPAF inhibitor. Second, as we have discussed in the previous chapters, lactacystin is not a reliable inhibitor of CPAF because its inhibitory activity varies depending on the preparation and source of the compound (109). Inconsistencies with lactacystin have led researchers to search for alternative CPAF inhibitors.

Heuer *et al.* identified z-WEHD-fmk (benzyloxycarbonyl-Typ-Glu-His-Asp-fluoromethyl ketone) as a CPAF inhibitor (49). z-WEHD-fmk is a synthetic peptide aldehyde inhibitor of the caspase family of cysteine proteases. The tetrapeptide sequence “WEHD” confers specificity for caspases -1, -4, and -5 (125). Although the mechanism by which z-WEHD-fmk inhibits CPAF is unknown, treatment *in vitro* or of infected cells prevented CPAF-mediated cleavage of golgin-84, keratin-8, and vimentin (49, 69). This small peptide inhibitor is soluble and cell permeable without any reported cytotoxic effects, making it a good candidate for use in studies of *Chlamydia*-infected cells. Unfortunately, though, since z-WEHD-fmk was designed to inhibit caspases it lacks specificity for CPAF.

An anti-CPAF peptide was designed by the Valdivia group in an attempt to develop a selective CPAF inhibitor. Their approach utilized knowledge of CPAF structure and activation to rationally design a peptide that would have strong binding affinity for CPAF. Activation of the CPAF zymogen requires removal of an internal 40 amino acid sequence, known as the auto-inhibitory segment, which obstructs the substrate binding pocket in the inactive zymogen (66). The anti-CPAF peptide was designed to contain a 25 amino acid sequence resembling the auto-inhibitory segment so that it would compete for substrate binding in the active protease and emulate the inactive zymogen conformation. The CPAF-specific inhibitory peptide inhibited recombinant CPAF in an *in vitro* assay and the addition of a nona-arginine C-terminal tail conferred cell permeability to the peptide (93, 126). The anti-CPAF peptide, with or without the

arginine sequence, was a more potent CPAF inhibitor than lactacystin *in vitro* (126). Since the anti-CPAF peptide was designed by taking advantage of the unique mechanism of CPAF activation, the peptide likely exhibits some specificity toward CPAF (93). However, subsequent studies suggested it has off-target effects. Anti-CPAF treated cells lost inclusion integrity and experienced caspase-1-dependent cell death, whereas cells infected with the CPAF-null mutant did not display these phenotypes (74, 93). These observations suggest that the anti-CPAF peptide interacted with additional molecular targets besides CPAF within an infected cell. Although no obvious toxicity with anti-CPAF was initially reported, the observed caspase-1-dependent cell death upon treatment with anti-CPAF that is not observed in CPAF-null infected cells is troubling. Shortcomings of the available CPAF inhibitors necessitate the development of an inhibitor that is both potent and specific for CPAF.

Molecular modeling has been a successful strategy for inhibitor design in other systems. Structure-based drug design methods identify favorable and unfavorable interactions between a potential inhibitor and target binding site and maximize beneficial interactions to increase binding affinity (127). Molecular modeling approaches have been utilized to identify anti-malarial cysteine protease inhibitors (127), to design specific non-peptide small molecule inhibitors of the MDM2-p53 interaction in cancer cells (128), and to enhance selectivity of inhibitors for specific isoforms of histone deacetylases (129).

Boronate peptides represent a promising class of inhibitors whose potential for CPAF binding could be explored using molecular modeling. Boronate peptides competitively inhibit serine proteases by forming a tetrahedral adduct with the hydroxyl group of the catalytic serine (130, 131). The inhibitory strength and selectivity can be modulated by altering the boronate peptide sequence for optimal binding to the active site of the protease of interest (132). This

strategy was employed to develop selective boronate peptide inhibitors for thrombin (a trypsin-like protease) (133). Boronate peptides have also been pursued as potent and selective proteasome inhibitors (124, 134). Additionally, boronate peptides are well tolerated in animal models, demonstrating their potential for use *in vivo* (135, 136).

In this study, we show that boronate peptides demonstrate inhibitory activity against CPAF. We utilized molecular modeling and a rational design approach to make particular amino acid changes to boronate peptides in order to create a specific CPAF inhibitor. Our findings establish molecular modeling as a valuable approach to learn about features of the CPAF active site and demonstrate that boronate peptides have the potential to be strong and selective CPAF inhibitors.

# Results

## Boronate peptides inhibit CPAF protease activity *in vitro*

We investigated a panel of boronate peptide compounds as potential CPAF inhibitors. The peptides we tested were designed as inhibitors of another serine protease, HTRA1. HTRA1 contains a typical serine protease catalytic triad (serine-histidine-asparatic acid) and complexes with the boronate peptide inhibitor through a tetrahedral adduct at the catalytic serine residue (137). We hypothesized that boronate heptapeptides that inhibit HTRA1 may have some inhibitory effect on CPAF since it is also a serine protease, albeit with a modified catalytic triad.

We screened 13 boronate heptapeptide compounds (Table 4.1) for CPAF inhibition using an *in vitro* CPAF activity assay similar to the assay we developed to detect residual CPAF activity within infected cell lysates. In the *in vitro* assay, a small amount of infected cell lysate as a source of CPAF was incubated with uninfected HeLa cell lysate as a source of host protein substrate p65. Boronic peptide compound was added to the reaction and the mixture was incubated for 30 minutes before results were analyzed by Western blot. Detection of p65 cleavage into its characteristic smaller sized fragment was indicative of active CPAF while maintenance of full-length p65 showed CPAF was inhibited. We found that all of the boronate peptides we tested demonstrated some inhibitory activity toward CPAF at 10  $\mu$ M (Fig. 4.1). Each compound was able to completely or partially inhibit CPAF-mediated p65 cleavage in contrast to the solvent and non-specific peptide controls where no inhibition was observed. From our studies of CPAF activity, we knew that CPAF demonstrates cleavage and degradation activities and substrates exhibit different sensitivities to CPAF proteolysis (see Chapter 3). Therefore, we also tested the boronate peptides' ability to inhibit CPAF-mediated degradation of nectin-1 in a similar *in vitro* assay in which nectin-1 acted as the host protein substrate. For the *in vitro*

**Table 4.1. Boronate peptide compounds**

<b>Name</b>	<b>Sequence</b>
TM375	MGKASPV-B(OH) <sub>2</sub>
TM231	DRYMKQV-B(OH) <sub>2</sub>
TM232	DRMIKQV-B(OH) <sub>2</sub>
TM233	DRMMKQV-B(OH) <sub>2</sub>
TM234	DRYMRQV-B(OH) <sub>2</sub>
TM237	DRYIRYV-B(OH) <sub>2</sub>
TM238	DRYIKYV-B(OH) <sub>2</sub>
TM243	DPMFKLV-B(OH) <sub>2</sub>
TM244	DRMIKYV-B(OH) <sub>2</sub>
TM247	DRMIRYV-B(OH) <sub>2</sub>
TM248	DRYMRYV-B(OH) <sub>2</sub>
TM249	DRMMRYV-B(OH) <sub>2</sub>
TM250	DRMMRQV-B(OH) <sub>2</sub>
TM401	SLFYSP-Norleucine-B(OH) <sub>2</sub>
TM402	DRYIRY-Norleucine-B(OH) <sub>2</sub>
TM403	DRYWRYYV-B(OH) <sub>2</sub>
TM404	DRFIRYV-B(OH) <sub>2</sub>
TM405	DRFWRY-Norleucine-B(OH) <sub>2</sub>

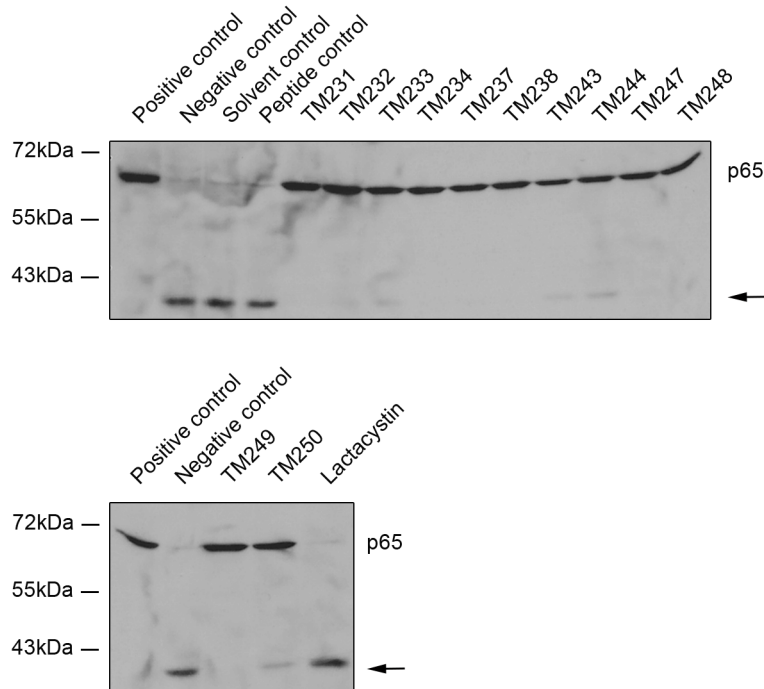


**Figure 4.1. Initial screen of boronate peptides for CPAF inhibition**

Boronate peptides were tested for their ability to inhibit CPAF in an *in vitro* reaction. Uninfected HeLa cell lysate (as a source of host proteins) was incubated with infected cell lysate (as a source of CPAF) in the presence of 10  $\mu$ M of each boronate peptide. Positive control for complete inhibition was a reaction containing uninfected lysate only. Negative control for inhibition was uninfected and infected lysate, without any inhibitor. Solvent control contained uninfected and infected lysates with DMSO. Peptide control was a reaction containing a boronate heptapeptide without specificity for serine protease HTRA1. Reactions were separated by SDS-PAGE and blots were probed with antibodies to p65. Arrow indicates p65 cleavage product.

nectin-1 assay, loss of the band representing full-length protein indicated CPAF activity was present in the reaction. By titrating the concentrations of boronate peptides in our *in vitro* assay and examining different CPAF substrates, we identified the top candidates as lead compounds for the design of a CPAF-specific boronate peptide inhibitor (data not shown).

Of the 13 boronate heptapeptides in our original screen, compounds TM237 and TM247 demonstrated the highest level of CPAF inhibition. 20  $\mu\text{M}$  of these peptides partially inhibited degradation of CPAF substrate nectin-1 *in vitro* (Fig. 4.2). In contrast, the same concentration of *clasto*-lactacystin did not inhibit CPAF activity toward nectin-1 at all – the protein was completely degraded *in vitro*. In fact, 300  $\mu\text{M}$  *clasto*-lactacystin was required to completely protect nectin-1 from degradation (Fig. 4.2).

### **Molecular modeling of boronate peptides to improve activity and specificity**

We performed molecular modeling of each of the tested boronate heptapeptides within the CPAF active site to elucidate important structure activity relationships that could be exploited in the rational design of a CPAF inhibitor. Each boronate peptide was fitted into the CPAF active site and overlaid with CPAF's auto-inhibitory segment, which served as a reference sequence with strong binding within the CPAF substrate binding pocket (Fig. 4.3). When we compared models of boronate peptides that demonstrated differential inhibitory activity toward CPAF, we were able to predict the positions and identities of residues that were critical for binding. Through these studies we identified important contact residues in the substrate binding domain that could be utilized to enhance inhibitor binding to CPAF or impart selectivity of the inhibitor for CPAF over the proteasome.

Our analysis of the pocket features of the CPAF active site revealed three key positions that could be modulated to develop a more potent and selective inhibitor. The residue in the P1

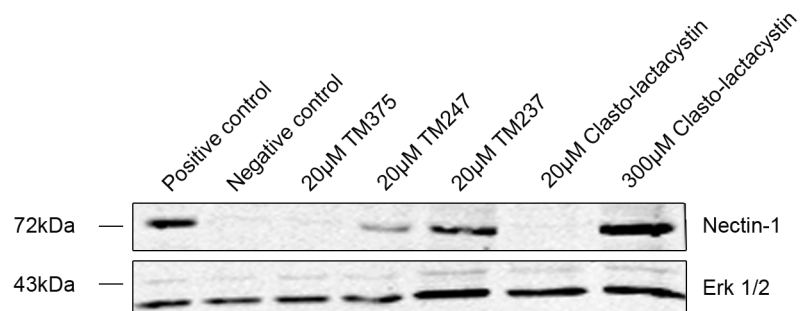


**Figure 4.2. Two boronate peptides are more potent CPAF inhibitors *in vitro* than lactacystin**

Uninfected HeLa cell lysate was incubated with infected cell lysate in the presence of 20 µM of each boronate peptide (or *clasto*-lactacystin where indicated). Reactions were separated by SDS-PAGE and analyzed by probing with antibodies to nectin-1 and Erk 1/2 (loading control).

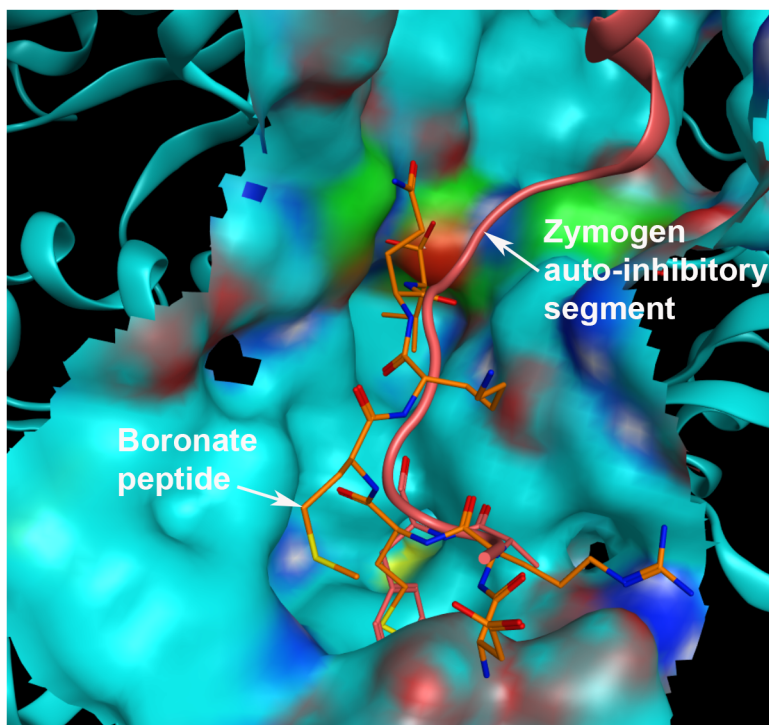


**Figure 4.3. Molecular model of boronate peptide binding within CPAF active site**

Boronate peptides (TM233 is shown as an example) were modeled into the catalytic groove of the CPAF active site overlaid with the CPAF auto-inhibitory segment of the zymogen. Peptides were fit by using Rotamer Explorer MOE to minimize Van der Waals clashes at each P site, then minimized to represent the lowest energy conformation using a multi-step process. The boronate peptide is shown in ball and stick structure (orange) and the zymogen auto-inhibitory sequence is shown in ribbon structure (red). The CPAF catalytic groove is represented by its electrostatic surface. Blue indicates positively charged regions, red indicates negatively charged regions, and yellow represents hydrophobic regions.

position of the boronate peptide is in a likely position for strong intermolecular forces with CPAF residues. In the CPAF zymogen, Met264 is a critical residue that mediates the interaction between the auto-inhibitory amino acid sequence and CPAF. Met264 interacts with the hydrophobic pocket created by CPAF residues Val378, Cys500, Gly525, and F527 (66). A peptide with a M264E mutation was no longer able to bind CPAF, illustrating the importance of this methionine residue (66). From our modeling data, P1 of the boronate peptide was in the same position within the CPAF binding pocket as this critical methionine residue of the CPAF zymogen. The original panel of boronate heptapeptides all contained valine at P1, and we reasoned including a methionine residue at P1 instead would create a boronate peptide with stronger binding to CPAF. However, due to synthesis issues, a norleucine residue was utilized to mimic a methionine at the P1 position. Norleucine is an analog of methionine, which contains a carbon instead of a sulfur atom in its side chain.

The P4 position is rather flexible and could be optimized to increase inhibitor specificity by diminishing peptide binding to the proteasome while maintaining strong binding to CPAF. The binding pockets of both the proteasome and CPAF accommodate bulky residues at this position. The boronic peptide-based proteasomal inhibitor bortezomib contains a phenylalanine residue that mediates interactions in the chymotrypsin-like and caspase-like active sites in the 20S proteasome (138). Within the CPAF active site, Van der Waals forces mediate interactions of bulky residues Phe268, Trp269, and Tyr276 of the zymogen auto-inhibitory sequence (66). The strongest CPAF inhibitor from the original screen, compound TM237, contained an isoleucine residue at this P4 position which we proposed be replaced with bulky tryptophan. Tryptophan will fit into the active site of CPAF but may be too large to be accommodated by the 20S proteasome thus potentially imparting selectivity for CPAF.

We determined that the P5 position could be utilized to provide additional intermolecular forces with CPAF residues and stabilize boronate peptide binding to the active site. The two most active compounds in our screen, TM237 and TM247, differed only in the residue at position P5. TM237 contained a tyrosine at P5 while TM247 contained a methionine. Since TM237 was a more potent CPAF inhibitor, we reasoned that the benzene ring was likely better at facilitating the Van der Waals forces binding the peptide to the CPAF active site. Thus, we hypothesized that changing the residue at P5 from tyrosine to phenylalanine (removing a hydrophilic hydroxyl group) may improve Van der Waals interactions in the hydrophobic pocket of the CPAF active site.

Using our findings about the CPAF pocket features, we synthesized 5 boronate peptide compounds with amino acid changes we predicted would strengthen binding to CPAF or diminish binding to the proteasome. We made all of our amino acid changes using TM237 as a starting compound since it was the most potent CPAF inhibitor identified from our initial screen. Valine at P1 was replaced by norleucine in peptide TM402. Isoleucine at P4 was replaced by tryptophan in TM403. Tyrosine at P5 was replaced by phenylalanine in TM404. All three amino acid changes at P1, P4 and P5 were introduced in TM405. We also constructed a zymogen-like boronate peptide containing the first seven amino acid residues of the anti-CPAF peptide conjugated to a boronic acid warhead as a control. (For the complete sequences of each peptide see Table 4.1.) We synthesized these peptides in small quantities for *in vitro* testing of CPAF inhibition.

### **Rationally designed boronate peptides have increased activity against CPAF *in vitro***

We evaluated the designed CPAF boronate peptide inhibitors using the *in vitro* assay toward nectin-1 (Fig. 4.4A). The lead compound TM237, the zymogen-like control TM401,

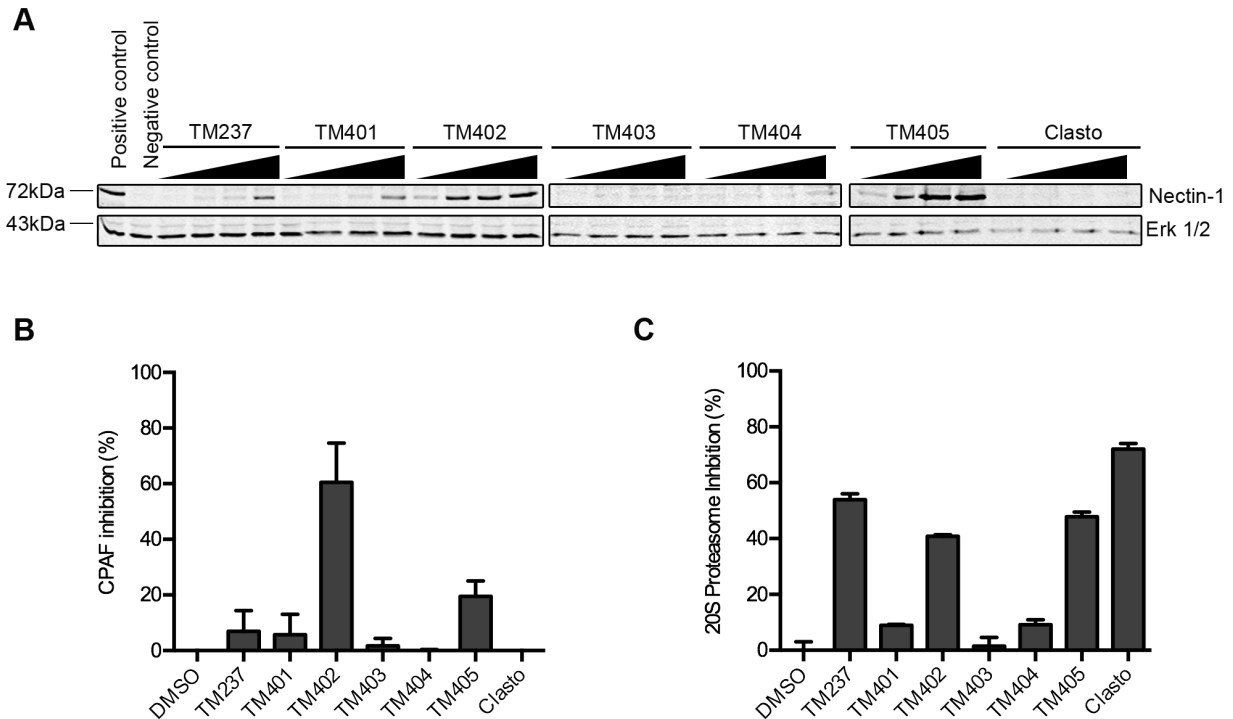


**Figure 4.4. Rational design enhanced boronate peptide inhibition of CPAF**

**A)** *In vitro* CPAF inhibition assays with designed boronate peptides. Reactions of uninfected cell lysates, infected cell lysates, and 0.3-10  $\mu$ M boronate peptides were separated by SDS-PAGE and probed with antibodies against nectin-1 or Erk 1/2 (loading control). **B)** Quantification of CPAF inhibition at 3  $\mu$ M. Nectin-1 band in each lane was normalized to loading control Erk 1/2 then compared to the positive control (complete inhibition of CPAF) to calculate CPAF inhibition. Error bars represent standard deviation from three independent experiments. **C)** Quantified results from a 20S proteasome activity assay using 3  $\mu$ M of each compound. Uninfected lysate as a source of host proteasomes was incubated with fluorogenic substrate LLVY-AMC in the presence of 3  $\mu$ M inhibitor. Percent proteasomal inhibition was calculated by comparing reaction signal to purified 20S proteasome as a positive control. Error bars represent standard deviation from three independent experiments.

TM402, and TM405 each demonstrated concentration dependent inhibition of CPAF between 0.3-10  $\mu$ M. Two of our designed compounds, TM402 and TM405, were more active CPAF inhibitors than our lead compound TM237. To compare the relative strength of these inhibitors, we quantified the level of CPAF inhibition detected in the *in vitro* assay in the presence of 3 $\mu$ M of each compound. The amount of nectin-1 protein remaining after each reaction was calculated as a percentage of the positive control (starting amount of nectin-1 in the *in vitro* reaction) and used to represent the level of CPAF inhibition (Fig. 4.4B). The zymogen-like peptide TM401 demonstrated 5.7% CPAF inhibition, which was comparable to our lead boronate peptide compound TM237 that exhibited 7.0% CPAF inhibition. TM405 inhibited 19.5% of CPAF activity while TM402 demonstrated the strongest CPAF inhibition at 60.5% (Fig. 4.4B). In contrast, *clasto*-lactacystin at 3 $\mu$ M was unable to inhibit any CPAF activity in this *in vitro* assay. Interestingly, TM403 and TM404 did not inhibit CPAF when used at 0.3-10  $\mu$ M in the *in vitro* assay (Fig. 4.4A and 4.4B). These results were not anticipated based on our modeling predictions and may indicate that the predicted peptide conformations we used for our models were not representative of the *in vivo* orientations.

The results of our *in vitro* CPAF assay show that two of our rationally designed boronate peptides (TM402 and TM405) are novel inhibitors of CPAF and that we can enhance inhibition in a logical way by understanding structure activity relationships gleaned from molecular modeling.

### **Rationally designed boronate peptides have reduced activity against the 20S proteasome**

To examine the specificity of our boronate peptide inhibitors, we tested their inhibitory activity against the proteasome. We used a 20S proteasome activity assay in which uninfected HeLa cell lysate as a source of proteasome was incubated with fluorogenic substrate in the

presence of the boronate peptide compounds. Fluorescent signal produced from proteasome-mediated cleavage of the substrate was used to quantify the amount of proteasome inhibition (Fig. 4.4C). 3  $\mu$ M of *clasto*-lactacystin, a known proteasomal inhibitor, inhibited 80% of proteasomal activity. All six of the boronate peptide inhibitors were less potent proteasomal inhibitors than lactacystin, but they still demonstrated measurable effects in this *in vitro* assay. Lead compound TM237 inhibited 53.9% of proteasome activity (Fig. 4.4C). Of the designed compounds, inhibition of CPAF correlated with inhibition of the proteasome. TM402 and TM405 exhibited the strongest CPAF inhibition and also the strongest proteasome inhibition (40.8% and 47.9%, respectively) compared to TM403 and TM404 which demonstrated very little CPAF or proteasome inhibition (1.5% and 9.2%, respectively) (Fig. 4.4C). These results emphasize that similarities between CPAF and the proteasome active sites may make it difficult to identify an inhibitor that will only bind one of these enzymes selectively. Notably, though, the zymogen-like peptide TM401 demonstrated only modest proteasomal inhibition (9%) (Fig. 4.4C), suggesting that there may be features within the CPAF auto-inhibitory segment that have yet to be exploited to design boronate peptides with further reduced proteasome inhibition. When comparing TM402 and TM405 to lead compound TM237, the amino acid changes introduced to TM237 enhanced inhibitory activity toward CPAF and reduced proteasomal binding. Together our studies support rational design based on molecular modeling as an effective approach toward a more potent and selective CPAF inhibitor.

### **Boronate peptides are more active than existing CPAF inhibitors**

Boronate peptide inhibitors are more active and selective for CPAF than lactacystin. Compared to lactacystin, approximately thirty-fold lower concentrations of peptide compounds were required to inhibit *in vitro* CPAF activity toward two substrates, p65 (cleavage) and nectin-

1 (degradation) (Fig. 4.2 and data not shown). Additionally, boronate peptides were less active toward the proteasome than lactacystin (Fig. 4.4C), demonstrating that they are more specific inhibitors of CPAF than lactacystin.

Boronate peptide inhibitors also appear to be better CPAF inhibitors than the anti-CPAF peptide sequence. We did not directly compare our boronate peptides to the anti-CPAF peptide itself, but instead used a truncated sequence of the zymogen (upon which the anti-CPAF peptide is based) attached to a boronic acid warhead. This way, all compounds we compared were of the same sequence length (heptapeptides). Our designed boronate peptides TM402 and TM405 were stronger inhibitors of CPAF than the zymogen-like sequence in our *in vitro* experiments (Fig. 4.4A and 4.4B), suggesting that we have developed peptides with better binding to CPAF than the anti-CPAF peptide sequence.

## Discussion

In this chapter we validate the use of boronate peptides as potent CPAF inhibitors. Our *in vitro* experiments demonstrated that boronate heptapeptides inhibit CPAF at relatively low concentrations and are stronger CPAF inhibitors than two other commonly used CPAF inhibitors, lactacystin and the anti-CPAF peptide. Furthermore, boronate peptides exhibited less inhibition of the 20S proteasome than lactacystin, suggesting that these compounds had improved selectivity for CPAF.

Molecular modeling of boronates within the CPAF active site provided insights into the pocket features that could be utilized to design CPAF-specific inhibitors. We identified positions P1, P4, and P5 of the boronate peptide as residues that could be optimized for CPAF binding. Specifically, we found that a methionine analog, norleucine, is sufficient to substitute for the critical methionine residue at the P1 position. When comparing rationally designed compounds containing this amino acid change to the lead boronate compound, we found that norleucine in the P1 position resulted in stronger inhibition of CPAF and reduced inhibition of the 20S proteasome. Although molecular modeling suggested that substitutions at P4 and P5 could enhance CPAF binding and minimize proteasomal binding, amino acid changes we introduced at these positions did not improve CPAF inhibition. Nevertheless, our initial experiments validated a rational design approach toward the development of an inhibitor with strong and selective activity toward CPAF.

### Comparison of boronate peptides to other CPAF inhibitors

How do boronate peptides stack up against the other established CPAF inhibitors (Table 4.2)? In terms of inhibitory activity toward CPAF, boronate peptides appear to be more active than lactacystin and the anti-CPAF peptide *in vitro*. Since our boronate peptides are not cell

**Table 4.2. Comparison of CPAF inhibitors**

<b>Inhibitor</b>	<b>Type</b>	<b>Activity</b>	<b>Specificity</b>	<b>Cell Permeability</b>
Lactacystin	Small molecule	20-150 $\mu$ M (Zhong <i>et al.</i> , 2000; Johnson <i>et al.</i> , 2015)	Off-target effects on the proteasome	Yes
z-WEHD-fmk	Peptide	80 $\mu$ M (Heuer <i>et al.</i> , 2009)	Off-target effects on caspases	Yes
Anti-CPAF peptide	Peptide	200-fold greater than lactcystin <i>in vitro</i> (Bednar <i>et al.</i> , 2011)	Unknown	Yes
Boronate peptides	Peptide	10 $\mu$ M <i>in vitro</i>	Off-target effects on the proteasome	No

permeable, however, we have not been able to test whether they are better CPAF inhibitors within *Chlamydia*-infected cells. One weakness of boronate peptides as CPAF inhibitors is that they also inhibit the proteasome; however, specificity is a problem with all of the other established CPAF inhibitors as well (Table 4.2). Lactacystin inhibits the proteasome, z-WEHD-fmk inhibits caspases, and there is experimental evidence suggesting the anti-CPAF peptide has off-target effects on a yet uncharacterized molecule(s) (74, 93). Another drawback of boronate peptides as CPAF inhibitors is that they are not cell permeable. Lactacystin, z-WEHD-fmk, and the anti-CPAF peptide can all enter *Chlamydia*-infected cells thus they can be used to inhibit CPAF in cell culture experiments, whereas the current forms of the boronate peptides are limited to *in vitro* use.

### **Strategies to develop better boronate peptide CPAF inhibitors**

Molecular modeling could be used to design the next generation of CPAF boronate peptide inhibitors with improved selectivity for CPAF over the proteasome. For example, lead compound TM237 and zymogen-like TM401 both demonstrated modest CPAF inhibition, but TM401 had less inhibitory effect on the 20S proteasome. By comparing the fit of these peptides within the proteasome active site we may identify the amino acids in TM237 that mediate proteasome binding and substitutions at these positions in TM401 that reduce proteasomal binding.

To facilitate the testing of additional candidate CPAF inhibitors, we could develop a high throughput *in vitro* assay that is simpler to perform. Our current *in vitro* assay, which we used in this study, is too time-intensive to assess more than 10 compounds at a time; however, the assay could be adapted into a format in which the reactions are run and analyzed in a 96-well plate. For example, we could use a fluorogenic substrate that was used to demonstrate inhibitory

activity of the anti-CPAF peptide (126). A synthetic peptide substrate with an anthranilic acid moiety was constructed based on the vimentin sequence surrounding the cleavage site between Ser72 and Ser 73. Upon cleavage, a fluorescent signal was produced that served as a measure of CPAF activity (126). *In vitro* screening of compounds is a useful assessment of CPAF inhibition, but this type of analysis does not reveal potential cell cytotoxic or off-target effects that may be a problem within *Chlamydia*-infected cells. Thus, it will also be necessary to test any future boronate peptide CPAF inhibitor in a cell culture model.

### **Strategies for boronate peptide cell permeability**

The boronate heptapeptides we designed are not cell permeable, but they could be modified so that they can enter a *Chlamydia*-infected cell. For example, an HIV-TAT protein transduction domain or related arginine oligopeptide sequence could be added to the C-terminus of the peptides to induce uptake. The HIV-TAT domain has been used as a vector to deliver many proteins into cells via an endocytic mechanism (139). In the case of *Chlamydia*-infected cells, nona-arginine added to the C-terminus of the anti-CPAF peptide successfully delivered the peptide within infected cells without disrupting inhibitory activity (93, 126). It is unclear, however, whether the addition of a C-terminal sequence on our relatively short boronate heptapeptides would influence binding of the inhibitors to the CPAF active site.

An alternative method to deliver the boronate peptide inhibitors into cells without chemical covalent coupling is with the cell-penetrating peptide Pep-1 (140). Pep-1 non-covalently complexes with protein, peptide, or antibody cargo in solution and, upon crossing the cell membrane, disassembles the complex freeing the cargo within the cell (141). Preliminary experiments with the Chariot transfection reagent (Active Motif), a proprietary solution based on Pep-1, successfully transfected  $\beta$ -galactosidase protein into *Chlamydia*-infected cells within 2

hours (data not shown). Visualization of  $\beta$ -galactosidase with specific antibodies showed that the protein was localized in the host cell cytosol as well as within the chlamydial inclusion (data not shown), providing proof of principle that Chariot may be a useful strategy to deliver a boronate peptide CPAF inhibitor into an infected cell.

### **Boronate peptides as CPAF visualization tools**

A potent, selective boronate peptide could serve not only as a CPAF inhibitor, but also as a marker to determine where CPAF localizes within an infected cell. Boronate peptides could be adapted to be used as probes to visualize CPAF localization within live infected cells by attaching fluorescent moieties to the peptides. Because boronate peptides irreversibly bind to the catalytic hydroxyl of the CPAF active site, the probes would be covalently bound to CPAF molecules. There are discrepancies in CPAF localization determined by antibody staining in fixed cells because localization pattern is dependent upon fixation method (discussed in Chapter 2). A probe that can visualize CPAF within live cells may solve the discrepancies by circumventing the need for fixation.

Boronate peptides have been successfully used as visualization probes in other studies. Peroxysensors are a class of fluorescent probes that serve as chemosensors for hydrogen peroxide. Notably, the boronate peptide peroxyprobes were cell permeable and very sensitive to micromolar changes in hydrogen peroxide within living cells (142). A near-infrared probe consisting of a peptide conjugated to IRDye 800 CW was developed for matrix metalloproteases (143). Near-infrared dyes may be preferred in the development of a CPAF probe because they produce low auto-fluorescence in living tissues and their photons cause less damage to biological samples than fluorescent dyes (144).

There are a few potential issues that may be encountered in the development of boronate peptides as visualization probes in *Chlamydia*-infected cells. First, the probes need to be able to access CPAF. Since it is unclear whether CPAF is localized free in the host cytosol, enclosed within outer membrane vesicles, or free within the inclusion lumen, the probes would need to reach all cellular compartments. Second, the sensitivity of CPAF probes must be considered. Although the probe may bind to CPAF, low levels of protease may not be able to be detected above background signal. Finally, the fluorescent label at the C-terminus of the peptide must be stable, not cleaved or degraded by CPAF.

### **Boronate peptides as tools to determine CPAF function**

A potent and selective CPAF inhibitor would be a useful tool to investigate CPAF function. The CPAF-null mutant reveals the consequences to an infection when no CPAF is produced at any time, but it does not elucidate the timing of wildtype CPAF production, secretion, translocation, or proteolysis of substrates. Lactacystin can be used to treat infected cells and inhibit CPAF activity at a certain time, but it is difficult to work with. Lactacystin treatment from 12 to 24 hpi resulted in smaller inclusions and aberrant chlamydial forms, suggesting a role for CPAF in chlamydial growth and development (85); however, alternative treatments at different times or for different intervals were not compared because it was too difficult to ensure complete inhibition of CPAF activity. Furthermore, interpretations of any experiments utilizing lactacystin as a CPAF inhibitor are confounded by effects on the proteasome.

Boronate peptide inhibitors could be used to treat *Chlamydia*-infected cells at different times in the infection to determine when CPAF activity is important during the developmental cycle. Peptides can be synthesized in large quantities more easily than lactacystin and, if

specificity can be optimized through rational design, then off-target effects can be reduced. The data we have presented in this chapter provide evidence that boronate peptides are active CPAF inhibitors that would serve as useful tools to determine CPAF function.

## **Chapter 5**

# **Insights into the Chlamydial Developmental Cycle using Three-Dimensional Electron Microscopy**

## Contributions

The work described in this chapter was the result of a collaboration with Drs. Daniela Boassa and Mark Ellisman at the National Center for Microscopy and Imaging Research (NCMIR) at the University of California San Diego and Dr. German Enciso (University of California, Irvine). *Chlamydia*-infected monolayers were fixed and embedded for electron microscopy by Jennifer Lee and Daniela Boassa (NCMIR). Daniela Boassa acquired and processed the electron micrographs. Undergraduate students Soroush Pairawan and Chris Chander and high school students Tracy Lou and Melody Guo performed segmentation analysis of electron micrographs. German Enciso (UCI) conducted mathematical modeling simulations described in Figures 5.6, 5.8 and 5.10. Jennifer Lee designed the experiments, conducted data analysis, and prepared the figures.

## Summary

Intracellular *Chlamydia* infections have long been characterized by their unique biphasic developmental cycle, but little is known about how *Chlamydia* regulate the critical processes that govern a successful infection. Infectious elementary bodies (EBs), replication-competent reticulate bodies (RBs), and conversion intermediate bodies (IBs) are commonly observed, but experimental limitations have prevented detailed study of the progression of the chlamydial developmental cycle. We developed a novel three-dimensional electron microscopy (3D-EM) approach to study complete chlamydial inclusions including quantitative information about each developmental form. Our temporal analysis of 154 inclusions reconstructed from infected cells at 12 to 40 hpi provides comprehensive data on the identity and number of chlamydial forms, their size, and their spatial distribution. This analysis is the first quantitative study of *Chlamydia* development over time at the level of a single infected cell.

Our quantitative observations allow us to draw a number of conclusions about the chlamydial developmental cycle. By quantifying the changing content of chlamydial forms within each inclusion we observed that the *Chlamydia* infection progressed through three stages: RB replication only, asynchronous onset of RB-to-EB conversion, and EB accumulation. Notably, there was a delayed appearance of IBs and EBs until mid times in the infection (24-28 hpi), indicating that conversion was prevented in any inclusion until this point. By measuring the size of each bacterium, we made a novel discovery that RBs decrease in volume over the course of the developmental cycle. We also found that the inclusion increased in volume proportional to the number of chlamydiae rather than the total chlamydial volume.

Based on these results, we propose a new model in which RB size is a critical determinant of chlamydial development. We propose that chlamydiae divide prior to reaching

twice their original size, resulting in a progressive decrease in bacterial volume. We also postulate that an RB cannot convert into an EB until it has reached a small enough size. In this model, RB-to-EB conversion is delayed until the daughter RBs have completed several rounds of RB replication causing them to decrease to a threshold size that is permissive for conversion. Thus we propose that *Chlamydia* use RB size as a clock to control the timing of conversion so that it only occurs after a period of replication.

## Introduction

*Chlamydia* development is characterized by a biphasic life cycle, and the major developmental forms can be observed and distinguished by electron microscopy. Pioneering electron microscopy studies completed in the 1960s provided the first insights into the *Chlamydia* intracellular life cycle and established the characteristic morphology of each developmental form (145, 146). Elementary bodies (EBs) are infectious forms that are small, spherical, and electron dense. The average diameter of an EB is 250-300 nm (146). Reticulate bodies (RBs), on the other hand, are non-infectious forms that are larger, more irregular in shape, and less electron dense. The average diameter of an RB is about 500-1000 nm (146). RBs are the replicative chlamydial developmental form and can be seen in the process of binary fission within *Chlamydia*-infected cells beginning at 8-12 hpi (145, 146). RB-to-EB conversion is captured as a transition form called an intermediate body (IB). IBs are approximately 350-400 nm in diameter (146) and have a target-like appearance due to a nucleoid of electron dense material, representing condensed DNA.

The appearance of each developmental form is regulated over the course of the intracellular chlamydial infection. An infection is initiated when one or more EBs enters the host cell and establishes the membrane-bound inclusion. EBs convert into non-infectious replication-competent RBs between 3-8 hpi (41). RBs then replicate by binary fission within the chlamydial inclusion. This initial phase of expansion of the chlamydial population is characterized exclusively by bacterial replication in the absence of conversion. Thus, inclusions observed between 8-18 hpi contain only replicating RBs; no IBs or EBs are observed. Around 20-24 hpi RB-to-EB conversion begins, as indicated by the emerging appearance of IBs and EBs (37, 41, 45, 147-149). The conversion process is often described as asynchronous because not all RBs

convert into EBs at the same time. Additionally, RBs continue to replicate by binary fission even after the onset of conversion. Both replication and conversion continue through the remainder of the developmental cycle. Since RB-to-EB conversion is a terminal process, infectious EBs accumulate within late stage inclusions, although RBs and IBs can still be observed as late as 72 hpi (145).

Regulation of bacterial development is critical for *Chlamydia* growth and survival, but the control mechanisms of the two main developmental processes, replication and conversion, are unknown. *Chlamydia* must ensure that RBs replicate prior to conversion because premature conversion would deplete the RB population before it can expand, limiting the infectious yield. We do not know how *Chlamydia* regulate the onset of conversion, but the asynchronous nature of the process suggests that its signal is regulated at the level of an individual bacterium. How is premature conversion prevented? What is the signal for conversion and how is it triggered asynchronously? Can RBs sense the size of their population and detect when conversion has begun?

A type III secretion contact-dependent model has been proposed as the mechanism for regulating RB-to-EB conversion. Imaging of chlamydial inclusions by fluorescence and traditional two-dimensional electron microscopy consistently show that RBs preferentially localize adjacent to the inclusion membrane (37, 149-151). EBs, on the other hand, are observed dispersed throughout the inclusion volume (37, 41, 45, 149). Together these observations led to the hypothesis that loss of contact with the inclusion membrane is the signal that regulates RB-to-EB conversion (152). Contact is thought to be lost late in the infection because the number of surface projections per RB decreases over the developmental cycle (153), and spatial limitations due to increasing chlamydial number cause physical crowding, forcing some RBs to lose contact

(152). Although qualitative observations of chlamydial inclusions and mathematical simulations seem to support the contact-dependent model, there is little experimental evidence to show that loss of RB contact with the inclusion membrane is the signal for conversion.

Progression of the *Chlamydia* infection can be monitored by measuring the number of chlamydiae at different stages in the infectious time course. For example, genome copy analysis has been used to characterize the chlamydial growth curve, which corresponds to approximately 8-10 bacterial divisions during the intracellular infection (45, 154). This method is quantitative because it uses PCR amplification of a chlamydial gene to determine the number of bacterial organisms in a sample. However, it provides an overview of a population of *Chlamydia*-infected cells rather than an analysis of an individual infected cell. Furthermore, this method does not distinguish between different chlamydial developmental forms so it does not provide insight into processes such as RB-to-EB conversion.

Another method to track chlamydial development is by using a progeny assay, which indirectly determines the number of infectious EBs from a sample based on the inclusion forming units (IFUs) in a secondary infection. This assay has been useful for identifying alterations to an infected cell cause defects in RB-to-EB conversion (49, 69, 93, 106, 140, 155-163). Progeny assays offer information about a particular chlamydial form (infectious EBs), but do not reveal information about the other chlamydial forms. Additionally, progeny assays can only be used as relative measures of EB output; they cannot directly quantify the number of EBs because the relationship between IFUs and EBs is not fully established.

Two-dimensional electron microscopy is a useful tool for studying the developmental cycle because it clearly visualizes all developmental forms (RBs, EBs, and IBs) within an inclusion. For example, two-dimensional electron micrographs showing the location of RBs at

the inclusion membrane support the type III secretion contact-dependent model of conversion. This mode of imaging can also reveal information about replication since RBs can be observed in the process of binary fission by their characteristic dumbbell shape. However, conventional electron microscopy is not suitable for analyzing the entire inclusion because the inclusion is too large to be represented by a single two-dimensional image.

Three-dimensional electron microscopy (3D-EM) has been used by the National Center for Microscopy and Imaging research to study organization of tissues (164-166). In these studies, 3D-EM provided detailed high-resolution spatial information that allowed a more complete analysis than had previously been possible.

We predicted that this experimental technique could provide quantitative information about the entire inclusion, including visualization of all the chlamydial forms (RBs, dividing RBs, IBs, and EBs). Analysis of the changing populations of chlamydial forms over time would help characterize the progression of replication and conversion and perhaps identify potential regulators of the important processes.

In this chapter, we describe a novel three-dimensional electron microscopy approach to analyze complete chlamydial inclusions and their entire content of chlamydial forms. We conducted a time course generating three-dimensional reconstructions of chlamydial inclusions from 12 to 40 hpi and quantitatively analyzed temporal, volumetric, and spatial aspects of the inclusion and chlamydial forms. Our results provide the first quantitative study of *Chlamydia* development over time at the level of a single infected cell. Our findings from the three-dimensional time course led us to hypothesize that chlamydial size is a critical regulator of *Chlamydia* development and we propose a model to describe how changing RB volume could regulate both replication and conversion.

# Results and Discussion

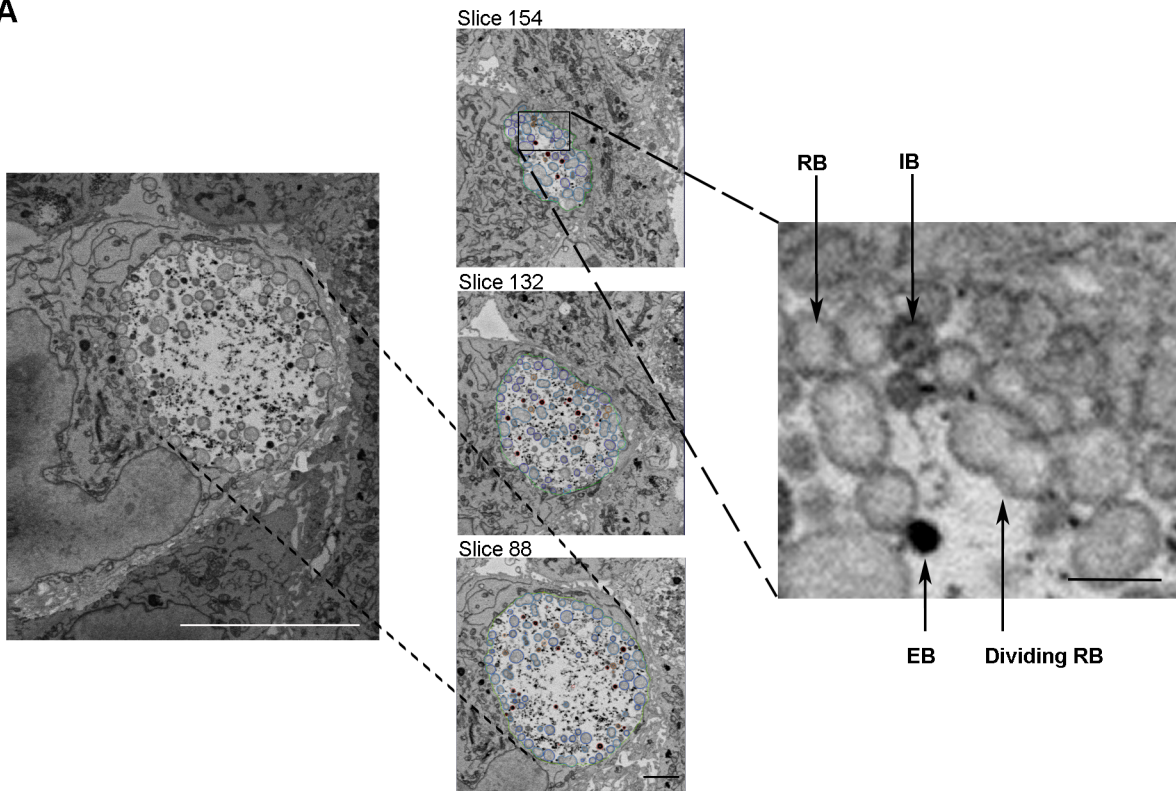
## Three-dimensional electron microscopy approach to analyze chlamydial inclusions

We developed a novel three-dimensional electron microscopy (3D-EM) approach to analyze complete chlamydial inclusions. *Chlamydia*-infected monolayers were fixed and embedded, then processed by serial block-face scanning electron microscopy. Using this automated technique, electron micrographs of a small area of the monolayer (approximately 100 square microns) were acquired every 50 nm in depth resulting in ~400-800 two-dimensional images per monolayer of infected cells. We identified infected cells from the monolayer and those with chlamydial inclusions completely contained within the 3D volume were selected for analysis (Fig. 5.1A, left panel). Each individual image was processed by segmentation, a procedure during which each *Chlamydia* form was identified and hand-marked (Fig. 5.1A, center panels). The segmentation process was time and labor intensive because each chlamydial inclusion contained 20-280 sequential micrograph images with up to 2,300 total chlamydial forms. The segmented image slices were then aligned to reconstruct three-dimensional models of complete inclusions (Fig. 5.1B and Video 5.1). In this analysis, we reconstructed 154 inclusions from different infected cells spanning 12-40 hpi. For early time points (12-16 hpi), we analyzed the inclusions within all of the infected cells we processed by electron microscopy. For later time points (20-40 hpi), however, we selected representative inclusions for analysis. We determined the volume of each inclusion within the same time point then sorted them according to size into three bins (Table 5.1). The small bin at 20 hpi, for example, contained the third of the 20 hpi inclusion population with the smallest volumes. We then used a random number generator to select at least 3 inclusions per bin per time point for analysis (Table 5.1).

**Figure 5.1. Novel three-dimensional electron microscopy approach to analyze chlamydial inclusions**

**A)** Serial block-face scanning electron microscopy was performed on a monolayer of *Chlamydia*-infected HeLa cells at 28 hpi. Electron micrographs were taken every 50 nm over a total depth of 26.55  $\mu\text{m}$  (531 slices). Left panel: single infected cell, scale bar corresponds to 10  $\mu\text{m}$ . Center panels: selected slices of the inclusion with segmentation markings for each chlamydial form, scale bar is 2000 nm. Right panel: magnified view of chlamydial forms, scale bar is 1000 nm. **B)** Three-dimensional reconstruction of complete inclusion from *Chlamydia*-infected cell at 28 hpi. Model was made by aligning 177 serial segmentation images. Position of electron micrograph slices from (A) are indicated. Scale bar corresponds to 1000 nm.

**A**



**B**

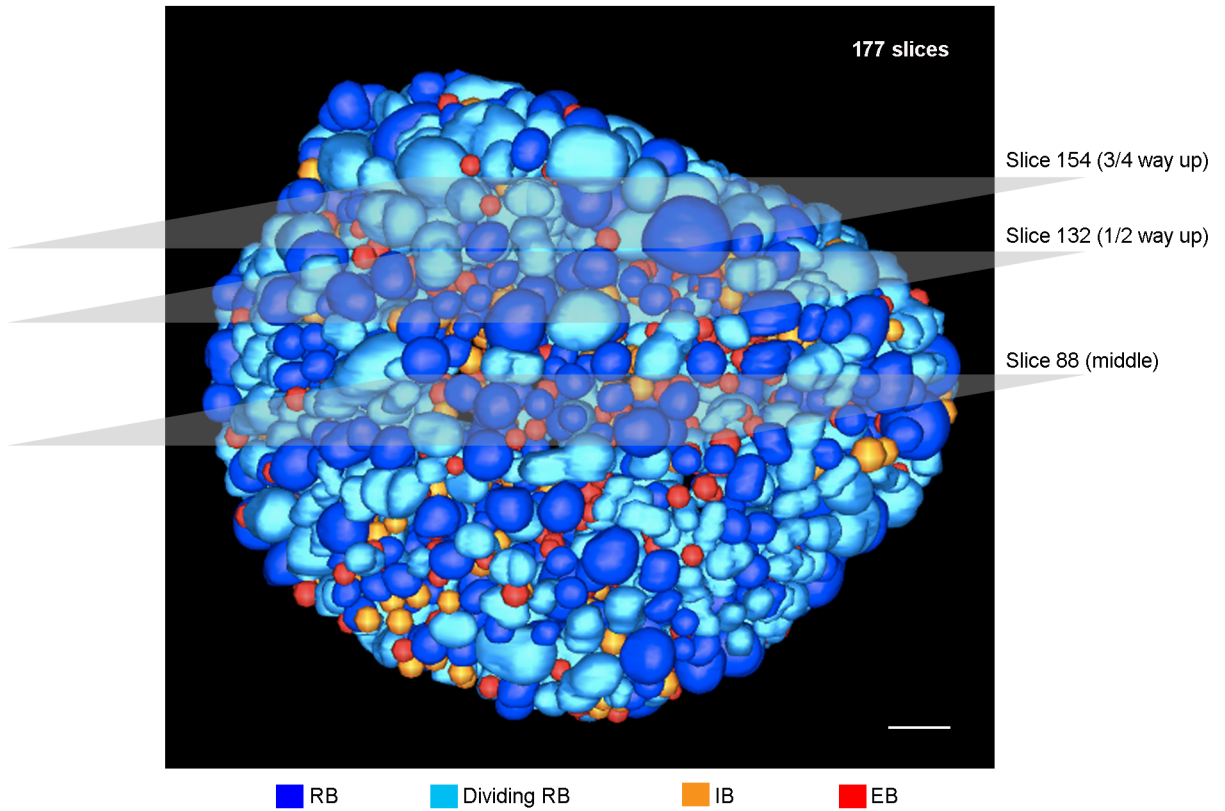


**Table 5.1. Selection of chlamydial inclusions for analysis by 3D-EM**

Inclusions marked in gray were randomly selected for segmentation and analysis.

Time point (hpi)	Size Bin	Inclusion volume ( $\mu\text{m}^3$ )
20	1	3.81
		6.88
		9.36
		18.32
		19.27
		26.91
		28.06
		28.55
		28.62
		32.90
		34.47
		34.54
		35.75
		2
	41.00	
	41.00	
	48.85	
	49.81	
	51.15	
	53.47	
	59.74	
	62.60	
	66.64	
	70.14	
	72.11	
	3	73.51
		73.90
		74.70
		76.09
		76.10
86.15		
95.02		
105.64		
107.81		
114.65		
126.77		
158.54		
189.46		
226.18		

Time point (hpi)	Size Bin	Inclusion volume ( $\mu\text{m}^3$ )	
24	1	76.86	
		83.12	
		93.99	
		95.01	
		107.38	
		107.58	
		111.96	
		120.55	
		131.54	
		132.40	
		133.25	
		2	145.06
			146.36
	147.50		
	155.88		
	158.49		
	161.40		
	163.60		
	170.22		
	183.27		
	190.90		
	191.73		
	3	193.84	
		196.37	
		203.38	
		207.15	
		268.24	
		270.47	
		280.11	
		298.20	
		317.06	
		329.19	

Time point (hpi)	Size Bin	Inclusion volume ( $\mu\text{m}^3$ )
28	1	16.44
		49.14
		63.00
		190.35
		225.48
		228.51
		239.70
		257.60
		287.62
	2	288.23
		294.30
		314.89
		322.53
		337.96
		341.77
		380.20
	3	423.89
		453.34
		754.79
		791.05
		819.90
	1474.33	
	1611.81	

Time point (hpi)	Size Bin	Inclusion volume ( $\mu\text{m}^3$ )
32	1	50.85
		151.14
		160.79
		190.12
		195.45
		262.62
		274.86
		282.70
		288.56
		296.58
		322.48
		352.48
		367.12
		369.19
		399.27
		412.72
		418.20
	424.87	
	447.88	
	470.01	
	475.89	
	514.99	
	557.72	
	584.30	
	590.53	
	591.15	
	604.14	
	616.70	
	660.31	
	697.69	
	754.25	
	784.17	
	796.53	
	865.65	
	935.59	
	1048.49	
1058.39		
1059.45		
1127.23		
1246.11		
1289.47		
1297.27		
1342.45		
1564.29		

		1626.86
		1682.98
		1737.26

Time point (hpi)	Size Bin	Inclusion volume ( $\mu\text{m}^3$ )
36	1	67.50
		81.03
		104.86
		110.92
		131.99
		151.06
		202.82
		200.72
		243.26
		244.98
		253.34
		299.65
		299.95
		313.82
		321.29
		345.89
		363.61
		375.11
		378.12
		382.24
	386.60	
	397.97	
	430.85	
	453.48	
	461.36	
	462.92	
	464.02	
	481.61	
	488.49	
	504.31	
	510.82	
	547.41	
	550.64	
	553.33	
	555.24	
	556.07	
562.86		
589.94		
601.66		
611.21		
615.60		
660.10		
669.08		
682.43		
	2	

		693.27
		763.70
	3	763.99
		868.64
		912.95
		975.63
		1005.52
		1032.44
		1069.60
		1078.86
		1105.98
		1141.24
		1145.76
		1157.24
		1175.98
		1177.25
		1180.03
		1202.05
		1239.13
		1312.94
		1357.92
		1558.06
		1648.50
		1694.19
		1718.93
1908.49		

Time point (hpi)	Size Bin	Inclusion volume ( $\mu\text{m}^3$ )
40	1	8.75
		210.15
		222.58
		222.92
		267.90
		299.21
		400.17
		418.89
		504.76
		504.99
		564.25
		617.86
	2	802.40
		804.15
		853.29
		1012.23
		1073.28
		1124.51
		1269.42
		1300.33
		1411.72
		1452.91
	3	1508.54
		1554.42
		1663.13
		1712.83
		2023.79
		2087.46
		2861.20
		3767.52

### 3D-EM validation

We quantified the number of total chlamydiae found in each inclusion from our 3D-EM analysis and compared these values to established methods for measuring chlamydial number. We prepared infected cells for genome copy analysis side-by-side with our 3D-EM samples to compare the two techniques. For the genome copy analysis, we isolated total DNA from the infected cell pellets and quantified the number of copies of chlamydial gene *euo* by qPCR to measure total number of chlamydiae in each sample. The number of infected cells in each sample was determined by calculating the total number of cells with a hemocytometer and adjusting for the efficiency of infection, which was determined by immunofluorescence staining of a representative sample. The number of chlamydiae per infected cell was determined by dividing these two calculated values. To determine the number of chlamydiae per infected cell by 3D-EM, we segmented each chlamydial form and counted the total number of forms in each cell then averaged all of the cells from each time point. We found that the total number of chlamydiae per infected cell determined by genome copy analysis and 3D-EM was similar over the developmental time course of 12-40 hpi (Fig. 5.2A). For example, at 40 hpi genome copy analysis detected an average of 1103 chlamydiae per infected cell compared to an average of 921 *Chlamydia* per infected cell determined from our 3D-EM analysis. These experiments were consistent with other genome copy studies detecting about 1000 *Chlamydia* per infected cell at 40 hpi (45). This result suggests that our segmentation procedure accurately identified and quantified the number of chlamydiae in an inclusion.

Next, we measured the infectious progeny produced from our *C. trachomatis*-infected cells. We prepared samples for progeny assays in parallel with our 3D-EM analysis samples at 24 and 36 hpi (Fig. 5.2B). At 24 hpi we detected  $1.24 \times 10^5$  IFUs/mL, which is consistent with

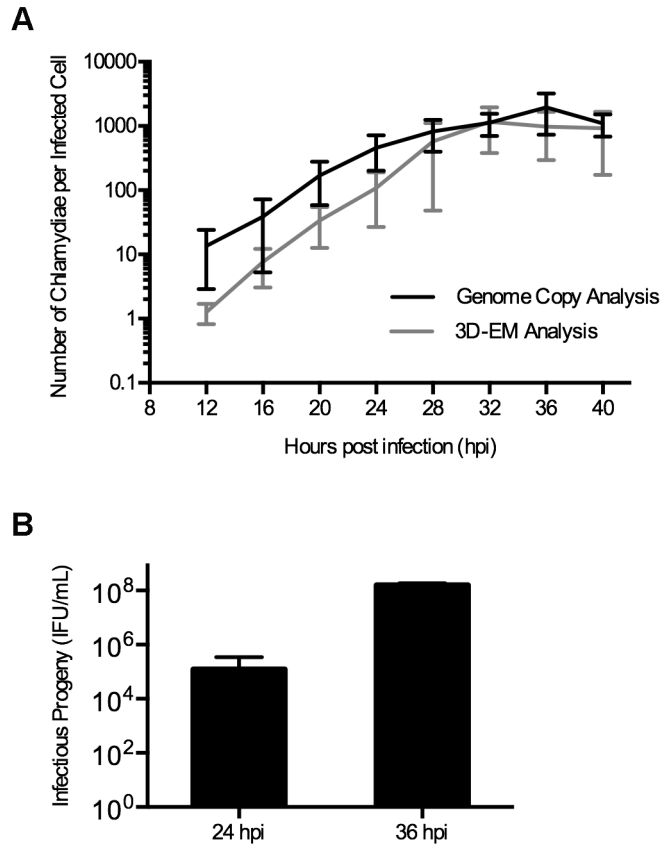


**Figure 5.2. Validation of 3D-EM approach compared to established chlamydial quantification methods**

**A)** Total number of *Chlamydia* per infected cell determined by genome copy analysis and 3D-EM. For genome copy analysis, the total number of genome copies (based on qPCR of chlamydial gene *euo*) was divided by number of infected cells as determined by hemocytometer count and immunofluorescence quantification of infection efficiency. For 3D-EM, the total number of chlamydiae was counted from each 3D reconstruction and averaged for each time point. Error bars represent standard deviation from 3 independent experiments (genome copy) or standard deviation from all inclusions analyzed by 3D-EM. **B)** Determination of infectious progeny produced at 24 and 36 hpi. Each progeny assay was performed in triplicate and results are reported as means with standard deviations marked by error bars.

published reports that typically described between  $1 \times 10^4$ - $1 \times 10^6$  IFUs/mL at the same time point (45, 49, 69, 108, 157-159). At 36 hpi we detected  $1.59 \times 10^8$  IFUs/mL, which was comparable to other published reports of  $1 \times 10^6$ - $5 \times 10^7$  IFUs/mL (22, 45, 106, 108, 140, 160). We conclude that our 3D-EM time course is representative of chlamydial cell culture infections that have been previously published.

### **3D-EM provides complete quantitative information about entire chlamydial inclusions**

3D-EM overcomes limitations of two-dimensional electron microscopy by accurately and thoroughly quantifying chlamydial forms. When imaging a single section, four chlamydial forms (RBs, dividing RBs, IBs, and EBs) can be distinguished, but only if the cross section is through the center of the chlamydial form so it has its typical appearance in shape, size, and electron density. Most chlamydiae will not be bisected, leading to difficulty discerning the type of each chlamydial form. For instance, it can be difficult to distinguish a dividing RB from two separate RBs when the plane of division is not parallel to the direction of the EM slice (Fig. 5.3A). An IB can only be identified if the EM slice bisects its center and reveals the target-like staining (Fig. 5.3B). Finally, if the single EM cross-section passes through the end of a small form like an EB, then it may be indistinguishable from background (Fig. 5.3C). 3D-EM avoids these issues by imaging every 50 nm such that even the smallest developmental forms, EBs, are visualized on six consecutive slices, and larger RBs are visualized on 15-20 consecutive slices. Therefore, classification of chlamydial developmental forms from 3D-EM provides an accurate picture of the inclusion contents because each form has been identified with high confidence.

3D-EM is also less prone to bias than two-dimensional electron microscopy because each inclusion is visualized over many images. Based on single EM images, inclusions have generally been described as densely packed with chlamydial forms (148, 149, 167), but we have found that

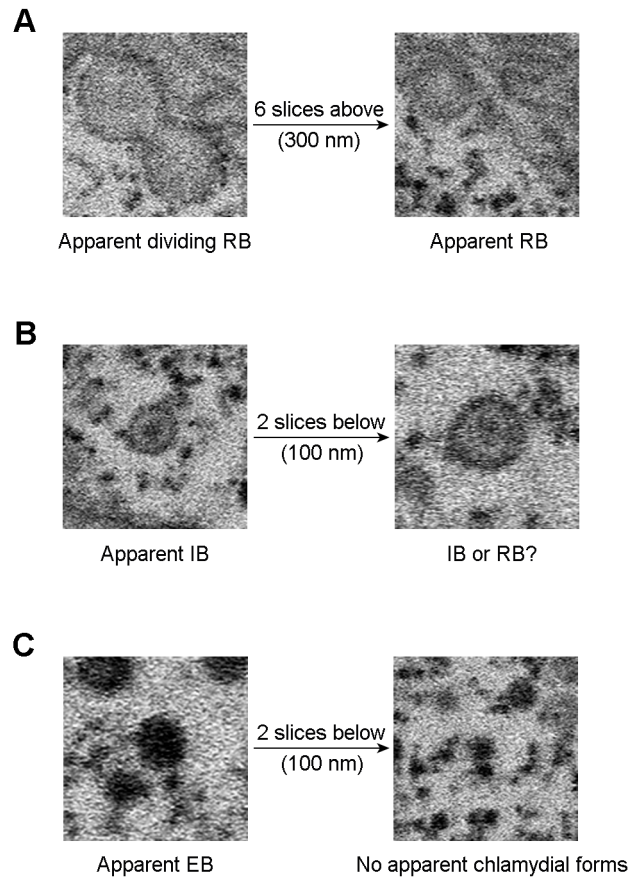


**Figure 5.3. Difficulty discerning chlamydial forms using single electron micrographs**

**A)** Left panel: An area of an electron micrograph containing an apparent chlamydial form that would be classified as a dividing RB. Right panel: same region of the *Chlamydia*-infected cell imaged 6 slices (or 300 nm) above the initial image. A portion of the dividing RB appears to be a single RB. **B)** Left panel: An electron micrograph of an apparent IB. Right panel: same section of the infected cell imaged 2 EM slices (or 100 nm) below the initial image. Chlamydial form would be difficult to classify definitively as an IB or an RB from this single image. **C)** Left panel: EM imaged area containing an EB, center. Right panel: the same region of the infected cell 2 slices (or 100 nm) below the initial image. The bottom portion of the EB is indistinguishable from background staining.

a single EM cross-section is not representative of the entire inclusion. For example, since RBs are located along the inclusion membrane, single cross-sections through the top or bottom of the inclusion will appear to have proportionally more RBs. Additionally, *Chlamydia* are not evenly distributed within the inclusion, so even a single image from the center of an inclusion cannot be extrapolated to represent the entire population of *Chlamydia* within that infected cell. Both non-representative sampling and misidentification of chlamydial forms from a single image may mislead the observer about the true distribution of chlamydial forms (Fig. 5.4).

### **Chlamydial infection is characterized by three different developmental stages**

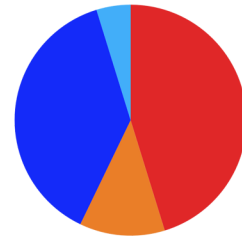
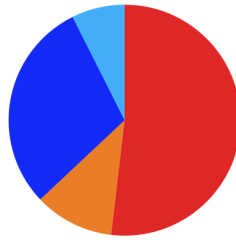
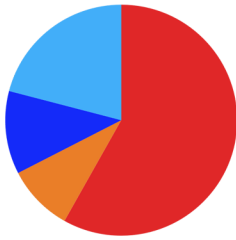
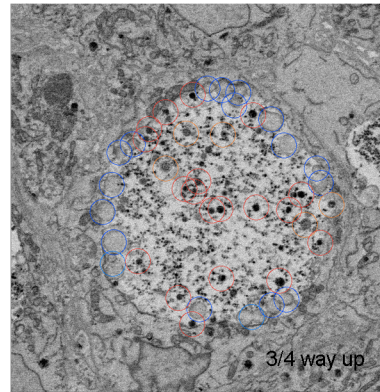
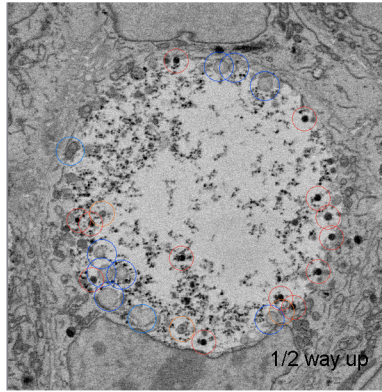
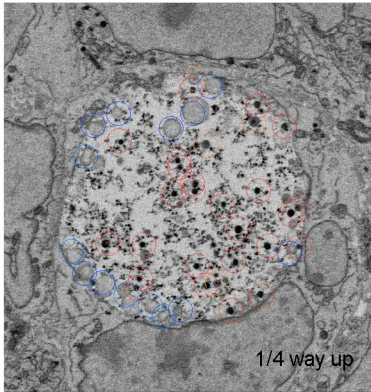
We conducted a temporal analysis of the *Chlamydia* developmental forms using our 3D-EM approach. Three-dimensional models were reconstructed for inclusions from 154 different infected cells spanning 12-40 hpi as described previously and summarized in Table 5.1 (Fig. 5.5). For each infected cell, we measured the inclusion volume and segmented each chlamydial form within the inclusion. From our segmentation analysis we were able to quantify the precise number of each developmental form (RB, dividing RB, IB, and EB), measure volumes of the inclusion and chlamydiae, and calculate distances between each bacterium and the inclusion membrane.

Over the course of the developmental cycle, we observed that chlamydial inclusions increased in size and also in total *Chlamydia* number (Fig. 5.5, Table 5.2). The average inclusion volume at 12 hpi was  $3 \mu\text{m}^3$  while the average inclusion volume at 40 hpi was  $900 \mu\text{m}^3$ , a 300-fold increase. The number of chlamydiae per inclusion also increased dramatically from one to two at 12 hpi up to an average of 921 by 40 hpi. The increase in chlamydial number exhibited exponential growth until it approached a maximal value close to 1,000 between 32-40 hpi (Fig.

**Figure 5.4. 3D-EM overcomes limitations of 2D-EM by accurately distinguishing and quantifying chlamydial forms**

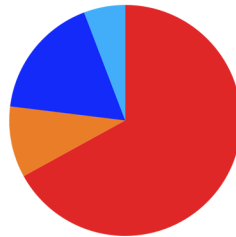
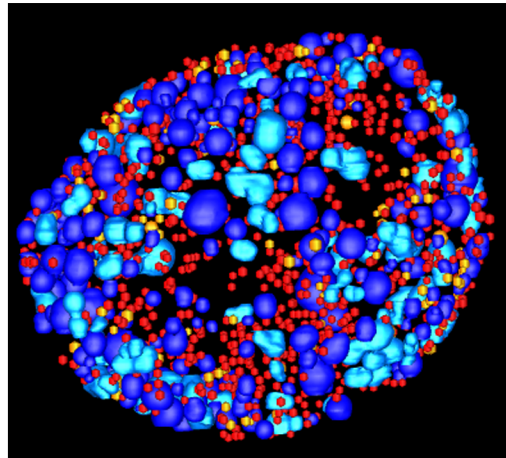
Top: Examples of varying appearance of a single chlamydial inclusion at 40 hpi based on two-dimensional electron microscope cross-sections. Chlamydial forms were identified from each single electron micrograph and the apparent distribution of chlamydial forms is reported in the pie charts below each image. Bottom: 3D-EM reconstruction of the entire 40 hpi inclusion based on 217 serial EM images. Total number of each chlamydial form was calculated from the model and shown as a distribution in the pie chart below.

## Two-Dimensional Analysis



## Three-Dimensional Analysis

- RB
- Dividing RB
- IB
- EB



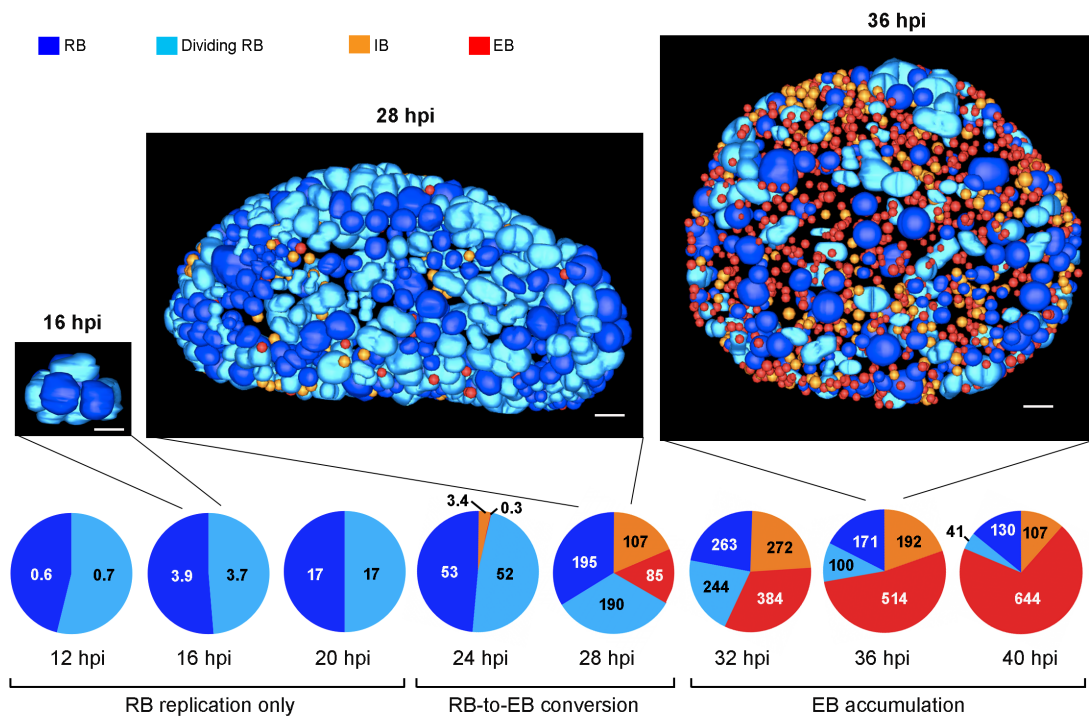


**Figure 5.5. Temporal analysis of *Chlamydia* developmental forms**

Three-dimensional reconstructions of inclusions from representative infected cells at 16, 24, and 36 hpi. Scale bars represent 1000 nm. Pie charts of the average distribution of chlamydial forms within inclusions at each timepoint indicated. n=9-50 inclusions, depending on the timepoint (See Table 5.2 for details). Pie charts are categorized into three developmental profiles: RB replication only (no IBs or EBs present), RB-to-EB conversion (IBs and EBs constitute <50% of the chlamydial forms), and EB accumulation (IBs and EBs make up >50% of the chlamydial forms).

**Table 5.2. Individual chlamydial inclusion data**

<b>Timepoint (hpi)</b>	<b>Inclusion volume (<math>\mu\text{m}^3</math>)</b>	<b>Total chlamydiae</b>	<b>RBs</b>	<b>Dividing RBs</b>	<b>IBs</b>	<b>EBs</b>
12	0.75	1	1	0	0	0
12	0.90	1	1	0	0	0
12	1.05	1	1	0	0	0
12	1.11	1	1	0	0	0
12	1.36	1	1	0	0	0
12	1.55	1	1	0	0	0
12	1.61	1	1	0	0	0
12	1.62	1	0	1	0	0
12	1.67	1	0	1	0	0
12	1.67	1	1	0	0	0
12	1.73	1	0	1	0	0
12	1.88	1	0	1	0	0
12	2.02	1	0	1	0	0
12	2.03	1	0	1	0	0
12	2.05	1	1	0	0	0
12	2.34	1	0	1	0	0
12	2.41	1	0	1	0	0
12	2.52	1	0	1	0	0
12	2.58	1	0	1	0	0
12	2.59	1	0	1	0	0
12	2.65	1	0	1	0	0
12	2.70	1	0	1	0	0
12	2.71	1	0	1	0	0
12	2.77	1	0	1	0	0
12	2.82	1	0	1	0	0
12	2.89	1	0	1	0	0
12	2.93	1	0	1	0	0
12	2.94	1	0	1	0	0
12	3.13	1	0	1	0	0
12	3.18	1	0	1	0	0
12	3.20	2	2	0	0	0
12	3.32	1	0	1	0	0
12	3.39	1	0	1	0	0
12	3.41	1	0	1	0	0
12	3.43	1	0	1	0	0
12	3.53	1	0	1	0	0
12	3.67	2	1	1	0	0
12	3.74	1	0	1	0	0
12	3.88	2	1	1	0	0
12	3.98	2	2	0	0	0

12	4.02	2	1	1	0	0
12	4.07	2	0	2	0	0
12	4.08	2	2	0	0	0
12	4.18	2	2	0	0	0
12	4.31	2	2	0	0	0
12	4.42	2	2	0	0	0
12	4.73	2	2	0	0	0
12	4.93	1	0	1	0	0
12	5.05	2	2	0	0	0
12	5.49	2	1	1	0	0
16	2.29	2	2	0	0	0
16	3.99	3	2	1	0	0
16	4.43	2	0	2	0	0
16	5.14	2	0	2	0	0
16	7.88	4	4	0	0	0
16	8.86	2	0	2	0	0
16	9.83	7	6	1	0	0
16	10.10	5	2	3	0	0
16	10.10	7	4	3	0	0
16	11.40	4	2	2	0	0
16	11.40	8	7	1	0	0
16	11.40	4	1	3	0	0
16	11.80	6	5	1	0	0
16	12.70	5	2	3	0	0
16	13.40	8	1	7	0	0
16	14.70	8	8	0	0	0
16	16.10	8	4	4	0	0
16	17.20	5	1	4	0	0
16	19.00	8	0	8	0	0
16	20.40	6	4	2	0	0
16	20.40	13	11	2	0	0
16	21.10	8	3	5	0	0
16	21.20	8	0	8	0	0
16	21.60	9	2	7	0	0
16	21.60	8	4	4	0	0
16	23.40	12	9	3	0	0
16	28.60	8	2	6	0	0
16	32.60	14	5	9	0	0
16	38.00	18	8	10	0	0
16	39.60	14	6	8	0	0
16	42.80	21	16	5	0	0
20	3.81	2	0	2	0	0
20	18.32	8	0	8	0	0
20	28.55	15	4	11	0	0
20	28.62	26	18	8	0	0

20	32.93	26	15	11	0	0
20	34.47	16	6	10	0	0
20	34.54	13	9	4	0	0
20	35.75	18	7	11	0	0
20	40.96	26	11	15	0	0
20	48.85	29	12	17	0	0
20	49.81	24	8	16	0	0
20	53.47	29	18	11	0	0
20	62.60	45	22	23	0	0
20	70.14	54	32	22	0	0
20	72.11	13	10	3	0	0
20	73.90	44	10	34	0	0
20	74.70	58	26	32	0	0
20	76.10	40	21	19	0	0
20	86.15	61	29	32	0	0
20	95.02	50	27	23	0	0
20	107.81	61	41	20	0	0
20	189.46	84	44	40	0	0
24	76.86	63	32	31	0	0
24	83.12	33	17	16	0	0
24	111.96	52	22	30	0	0
24	132.40	79	32	47	0	0
24	145.06	77	33	44	0	0
24	147.50	44	34	10	0	0
24	163.60	82	37	42	3	0
24	193.84	173	88	67	15	3
24	270.47	203	95	92	16	0
24	327.23	280	139	141	0	0
28	63.00	55	29	26	0	0
28	239.70	253	96	94	29	34
28	257.60	506	167	153	132	54
28	287.62	152	63	89	0	0
28	288.23	432	151	152	71	58
28	294.30	446	116	118	160	52
28	322.53	142	80	62	0	0
28	337.96	462	165	159	79	59
28	380.20	550	196	170	137	47
28	754.79	671	271	260	92	48
28	791.05	1272	428	372	178	294
28	819.90	551	229	273	38	11
28	1474.33	2015	550	540	477	448
32	190.12	237	98	50	52	37
32	296.58	520	98	140	148	134
32	322.48	462	200	176	58	28
32	412.72	579	150	134	129	166

32	591.15	1177	246	287	328	316
32	604.14	1275	249	253	278	495
32	754.25	1091	254	186	303	348
32	796.53	1421	361	339	308	413
32	1254.33	2214	363	438	450	963
32	1682.98	2658	614	435	669	940
36	200.72	333	44	61	91	137
36	375.11	538	123	48	103	264
36	391.55	537	99	59	162	217
36	562.86	516	138	85	118	175
36	591.45	667	103	93	151	320
36	660.10	866	182	90	195	399
36	1145.76	1415	198	112	244	861
36	1662.13	2444	379	223	491	1351
36	1694.19	1474	272	125	174	903
40	267.90	132	38	13	15	66
40	400.17	281	69	23	31	158
40	504.99	248	89	26	34	99
40	564.25	455	99	22	33	301
40	804.15	635	126	37	61	411
40	1269.42	1384	239	80	138	927
40	1300.33	845	164	39	108	534
40	1439.22	1957	128	56	364	1409
40	1706.11	958	135	55	124	644
40	2087.46	2318	212	55	165	1886

5.2A). A summary of our analysis of the inclusion volume and number of chlamydia in each of the reconstructed models can be found in Table 5.2.

In addition to a general increase in chlamydial number, the types of chlamydial forms within the inclusions changed over time as the developmental cycle progressed (Fig. 5.5). Between 12 to 20 hpi, all inclusions we analyzed contained only RBs and dividing RBs although the number of chlamydiae increased from an average of 1.3 per inclusion at 12 hpi to an average of 34 per inclusion by 20 hpi. Conversion was first detected at 24 hpi when 3 of the 10 analyzed inclusions contained IBs and EBs making up 4-10% of the chlamydial population. We concluded from this observation that conversion is gradual and does not begin coordinately across infected cells in a monolayer. After the start of conversion, EBs continued to accumulate until they made up the majority of the chlamydial forms by 36-40 hpi.

Analysis of the distribution of chlamydial forms within each inclusion revealed three developmental stages which each have a distinctive profile: RB replication only, RB-to-EB conversion, and EB accumulation. The RB replication only phase is characterized by the inclusion containing only RB and dividing RB forms with no detectable IBs or EBs and therefore no conversion. Interestingly, we noticed that the average ratio of RBs to dividing RBs was close to 1:1 at all time points within this stage (Fig. 5.5), suggesting that about 50% of the RB pool is actively dividing during this period. Next, we defined the RB-to-EB conversion stage as inclusions containing IBs and EBs which make up <50% of the *Chlamydia* within an inclusion. Most of the inclusions between 24 and 28 hpi had this RB-to-EB conversion profile. However, 24 hpi inclusions that had not yet begun conversion resembled earlier inclusions from the RB replication only phase. Even in the RB-to-EB conversion stage, the ratio of RBs to dividing RBs was maintained at 1:1 indicating that replication continued at the same rate even with the onset

of conversion. Finally, we defined EB accumulation as an inclusion in which >50% of the total chlamydial forms were IBs or EBs. At 32 hpi many inclusions displayed this profile and all of the inclusions we analyzed at 36 and 40 hpi had an EB accumulation profile. After conversion onset, EBs accumulated and made up about 70% of the chlamydiae in 40 hpi inclusions. Late in the infection, the ratio of RBs to dividing RBs increased to 3:1, consistent with decreased RB replication (Fig. 5.5).

We examined the average number of each chlamydial form over time and found that each developmental form produced a unique growth curve (Fig. 5.6B, left panel). RBs and dividing RBs increased in parallel between 12 and 32 hpi. After 32 hpi, both populations declined but the decline in dividing RBs was sharper. IBs and EBs only appeared at 24 hpi and increased in parallel until 28 hpi. After 28 hpi, EBs continued to accumulate through the end of the time course at 40 hpi while the IB population began to decline after 32 hpi.

### **New insights into the progression of chlamydial development**

Two-dimensional EM based studies have provided a qualitative description of the general chlamydial developmental cycle, but our quantitative 3D-EM analysis allows us to characterize the progression of chlamydial development with a level of detail that was not previously possible.

#### Chlamydial development within individual infected cells on a monolayer is asynchronous

Centrifugation is commonly used to synchronize *Chlamydia* binding and uptake in a population of cells on a monolayer. However, no study has examined whether this method produces a synchronized population of infected cells at later stages in the infection. Our 3D-EM technique allowed us to visualize a large population of 50 infected cells from the same monolayer at 12 hpi. Neighboring infected cells displayed different timing of the onset of

replication, indicating that the chlamydial developmental cycle within these infected cells was not completely synchronous. At 12 hpi, some inclusions contained only one RB (in a state prior to the first replication), and others contained two dividing RBs (second replication in progress) (Table 5.2). It is unclear at what point during the initial stages of the infection cells become asynchronous. It could be during the uptake process, establishment of the initial inclusion, EB differentiation into an RB, or RB growth prior to division. These results could be explained by a host cell factor that contributes to the progression of the chlamydial infection. For example, our host HeLa cells were not synchronized in the cell cycle. If uptake of EBs during a particular cell cycle stage somehow accelerates the initial steps of the chlamydial infection, then some inclusions could be expected to reach their first replication cycle sooner than others.

#### RB replication

Our 3D-EM analysis provides the first evidence of asynchronous RB replication arising at 12 hpi within the first replication cycle. Two-dimensional electron micrographs depicted mid-cycle inclusions containing a mixed population of RBs (some dividing and some not) that indicated replication was not coordinated between RBs, but our 3D-EM study reveals asynchronous replication prior to mid-cycle. We found that there is asynchrony in RB replication within a single inclusion and between separate inclusions within the same host cell. Inclusions with two chlamydiae often contained one RB and one dividing RB, indicating the completion of the first replication and the asynchronous start of a second division in one of the progeny. A few cells within our 12 hpi monolayer were infected with more than one EB, which provided an opportunity to examine separate inclusions within the same host cell environment. Comparing the inclusions within the same host cell, we observed that the onset of replication was not coordinated between them. For instance, one infected cell at 12 hpi contained 2 inclusions, one

that had not yet begun the first replication cycle and another that was beginning the second replication cycle (data not shown).

Little is known about what signals trigger the initial RB to begin binary fission. RB replication is reported to commence between 8-12 hpi (145, 146), which is corroborated by our 3D-EM data. After its initiation, RB replication continues for the duration of the infection. We cannot directly measure RB replication rate because 3D-EM does not allow us to monitor a single form over time. We can, however, determine the RB generation time, which is the amount of time it takes for the RB population to double in size. We examined the period between 12-24 hpi, when RB replication occurs in the absence of conversion, and calculated an RB generation time of 1.93 hr. RB generation time was previously reported to be 2-3 hr based on quantification of 16s rRNA (45). However, this generation time was deduced by fitting curves over the entire time course from 8-40 hpi. Our RB generation time may be shorter than previously determined because we excluded late times (28-40 hpi) when we have seen that fewer RBs replicate, which would increase the perceived average generation time.

#### RB-to-EB conversion

Asynchronous onset of RB-to-EB conversion was apparent from two-dimensional EM, but our 3D-EM analysis is quantitative and can address the specific timing and progression of conversion. We observed that asynchronous onset of RB-to-EB conversion began at 24 hpi in some of our infected cells. Previous reports have indicated conversion starts between 20-24 hpi (37, 41, 45, 147-149), and variability between studies in the precise timing of the onset of conversion is likely due to experimental conditions (MOI, chlamydial strain, host cell type). It was generally thought that delayed onset of conversion provided time for RBs to replicate and expand the pool of chlamydiae prior to terminal differentiation to the EB state which would

deplete the RB population. Our growth curves, however, indicate that the RB pool is maintained and replenished after the onset of conversion (Fig. 5.6B, left panel). Conversion begins at 24 hpi but the populations of RBs and dividing RBs continue to increase until 32 hpi. With this strategy, *Chlamydia* is able to develop a population of infectious forms to prepare for the end of infection while also continuing to increase the bacterial population. After 32 hpi, though, it seems that replication does not keep pace with conversion and the RB populations decline.

Our 3D-EM studies indicate that conversion begins slowly in a small proportion of RBs then increases over several hours. Conversion can be monitored as an index of the percentage of IBs (converting forms) in the population of all non-infectious forms (IBs, RBs, and dividing RBs) within a single inclusion. EBs are excluded from this conversion index because they represent a terminally differentiated chlamydial form that cannot participate in further replication or conversion events. At the initial onset of conversion at 24 hpi, the conversion index was only 6.8%. The conversion index increased to an average of 16.9% at 28 hpi then 32.9% by 32 hpi. The greatest conversion index was observed at 36 hpi (41.6%). At 40 hpi the conversion index decreased back down to 31.8%. Prior to these studies, it was unclear how conversion proceeded after the initial onset. Our 3D-EM time course suggests that the population of RBs participating in conversion fluctuates over time. Initially RB-to-EB conversion begins in a small proportion of RBs then reaches a peak before decreasing at late times.

Another way to monitor conversion is to measure the accumulation of EBs over time. A limitation of our 3D-EM technique is that we cannot monitor a single inclusion over time. Processing of infected cells for EM analysis requires fixation and is a terminal event. So to draw conclusions about changes in chlamydial development over time, we analyzed many inclusions to determine average numbers to compare between different time points. The number of new

EBs produced over a period of time can be found by subtracting the population of EBs detected at the previous time. For example, to find the average number of new EBs produced between 24 and 28 hpi, we can subtract the average EB population at 24 hpi (0.3) from the average EB population at 28 hpi (85). An average of 85 new EBs were produced per inclusion during this 4 hour period. Between 28 and 32 hpi, an average of 299 new EBs were added to the chlamydial population. 130 new EBs were added to the population between 32-36 hpi and 36-40 hpi. Similar to the conversion index, this data also indicates that conversion begins gradually then reaches a peak before declining at late times. The conversion index was highest at 36 hpi leading to the prediction that most new EBs would accumulate between 32-40 hpi, but we observed the greatest population of new EBs accumulate between 28-32 hpi. One reason our average EB populations could have been lower than expected at 40 hpi could be that some of the infected cells began to lyse or extrude their inclusions by this time. We did not observe host cell debris or free chlamydial inclusions indicative of these events, but our EM sample processing may not have preserved these structures.

#### Late events in chlamydial development

Late inclusions are primarily characterized by accumulation of EBs, but our 3D-EM analysis revealed there are also changes in RBs during this period. The populations of RBs and dividing RBs paralleled each other throughout the infectious time course until late times, 36-40 hpi, when the number of dividing RBs declined more sharply than RBs (Fig. 5.6B, left panel). This observation could indicate that fewer RBs replicate at late times, perhaps because conversion is favored over replication during this period. Alternatively, there may be a pool of quiescent RBs that accumulate late resulting in a perceived decrease in dividing RBs.

The population of IBs declines between 32 and 40 hpi and our calculations of conversion index and EB accumulation (discussed above) also indicate that conversion is reduced at late times. The decline in IB number parallels the decreasing population of RBs, suggesting conversion may diminish late due to the RB pool becoming depleted.

Although RBs, dividing RBs, and IBs all decreased in number after 32 hpi, no chlamydial developmental form was completely depleted in any inclusion in our study up to 40 hpi. This is consistent with previous observations that inclusions as late as 72 hpi still contain all four developmental forms (145). Thus, it seems that the populations of RBs, dividing RBs, and IBs begin to level off at later times in the developmental cycle. We would like to examine time points after 40 hpi in future 3D-EM studies to determine how the population growth dynamics of each chlamydial form change during very late times.

### **The chlamydial developmental cycle can be described with a bang-bang mathematical model**

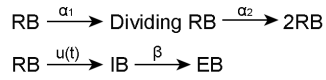
A defining feature of the chlamydial developmental cycle is a delay in the onset of RB-to-EB conversion. In our 3D-EM analysis of entire inclusions, we never observed a single IB or EB prior to 24 hpi. We hypothesized that *Chlamydia* regulate the timing of conversion as a strategy to produce a maximum yield of infectious EBs by the end of the intracellular infection. Using mathematical modeling, we approached the *Chlamydia* infection as an optimal control problem in which this intracellular bacterium must balance maximizing infectious progeny with the uncertainty of survival within its host cell intracellular niche. We modeled the chlamydial infection as a system of equations describing the populations of RBs, dividing RBs, IBs and EBs considering the rate of each transformation (Fig. 5.6A, left). For example, an RB becomes a dividing RB at a rate of  $\alpha_1$ . The rates of replication and conversion are driven by  $\alpha_1$  and  $u(t)$ ,

### **Figure 5.6. Bang-bang mathematical modeling of chlamydial development**

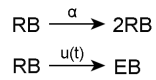
**A)** Mathematical modeling parameters used to describe chlamydial development. Infection can be represented by a series of conversion steps in which an RB transforms into an dividing RB then two RBs, or an RB converts into an IB then an EB. Each step in the transformation process is represented as having a particular rate ( $\alpha_1$ ,  $\alpha_2$ ,  $u(t)$ , or  $\beta$ ). The population of *Chlamydia* can be determined based on these rates. To treat *Chlamydia* infection as a mathematical optimization problem we simplified the description and created a function describing the population of EBs as a function of time. An optimal solution produces the maximal population of EBs after time T. **B)** Comparison of the average number of each chlamydial form within an inclusion over time based on the experimental and the modeling data. Observed data was acquired by 3D-EM analysis of n=9-50 inclusions as described in Table 5.2 and shown in Fig. 5.5. Modeled data were generated by simulating a chlamydial infection according to the parameters in (A) and applying modified bang-bang control. Parameters were adjusted to reflect onset of conversion increasing from zero to a maximal rate over an 8 hour time period. Details of parameter values are in Table 5.3.

A

Parameters of chlamydial infection



Optimization problem



Population sizes:

$$\begin{aligned}
 R' &= (\alpha - u)R, & R(0) &= R_0, & 0 &\leq u(t) \leq u_{\max}. \\
 E' &= uR, & E(0) &= E_0,
 \end{aligned}$$

Optimization of EB population at time T:

$$\max_{0 \leq u \leq u_{\max}} \left[ E(T) = \int_0^T uR dt \right]$$

B

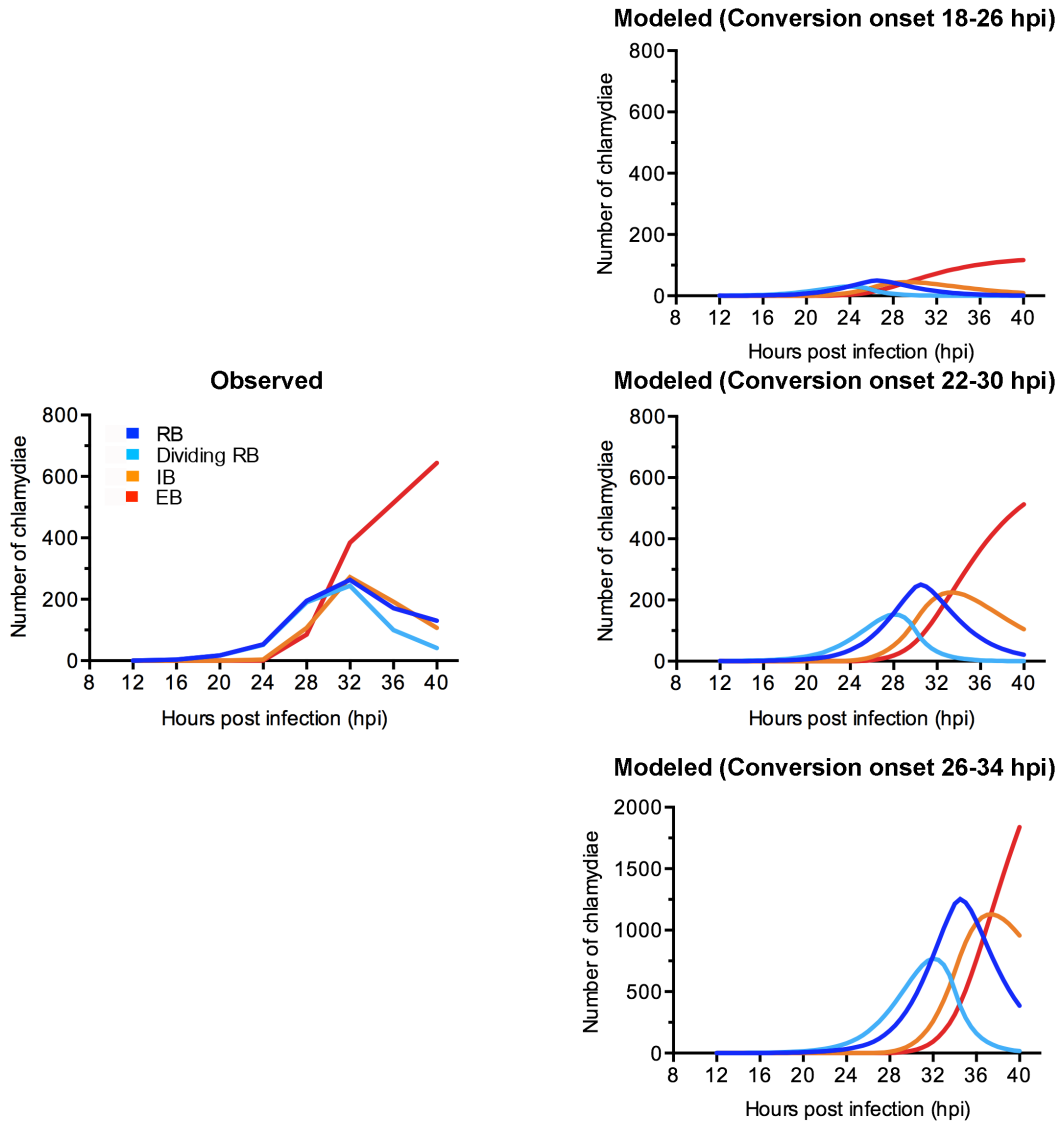


**Table 5.3. Bang-bang time course reaction parameters**

<b>Variable</b>	<b>Value (hr<sup>-1</sup>)</b>	<b>Description</b>
$\alpha1\_min$	0	Minimum rate of reaction RB→dividing RB
$\alpha1\_max$	2.3	Maximum rate of reaction RB→dividing RB
$\alpha2$	0.57	Rate of reaction dividing RB→2RB
$u\_min$	0	Minimum rate of reaction RB→IB
$u\_max$	0.35	Maximum rate of reaction RB→IB
$\beta2$	0.25	Rate of reaction IB→EB

respectively, thus we simplified this system of equations for the optimal control problem (Fig. 5.6A, right). The solution to the optimization problem represents the strategy that produces a maximum population of EBs at the time of host cell death  $T$  (Fig. 5.6A, right). We first set a specific time for the end of the intracellular infection and found that the optimal solution was complete bang-bang control (168). Bang-bang control refers to switching abruptly between two different states (on-off), which in the chlamydial infection model was a switch from an RB-to-EB conversion rate of zero to a maximum rate at the switch time  $t_s$ . In a second approach, we allowed the length of the intracellular infection to be variable by expressing the timing of host cell death as a probability density function. Again, the solution was bang-bang control (168). Thus in our mathematical model of the *Chlamydia* infection, the best regulation strategy for RB-to-EB conversion is bang-bang control in which there is initially no conversion followed by a switch to a maximum conversion rate at some time  $t_s$ .

We then attempted to fit the bang-bang model to our 3D-EM experimental data to see whether there is evidence *Chlamydia* use the mathematically optimal strategy *in vivo*. We simulated a chlamydial time course according to a system of ordinary differential equations representing the transformation between developmental forms (Fig. 5.6A, left). We found that if we used a discrete switch time ( $t_s$ ), the bang-bang mathematical model did not fit with our observed chlamydial growth patterns, but adjusting the parameter slightly to allow a switch time window ( $\Delta t_s$ ) was sufficient for bang-bang modeling to produce a pattern of chlamydial growth similar to what we observed (Fig. 5.6B, right). This modeling data suggests that *Chlamydia* do not abruptly switch from a conversion rate of zero to the maximal rate, but rather increase conversion rate over a period of time from zero to maximal. We found that the  $\Delta t_s$  that best fit our experimental data was 8 hours, meaning that once conversion switched on it increased to its

maximal rate over an 8 hour period. From our experimental data, we knew that the start of interval  $\Delta t_s$  must be at a time slightly before 24 hpi, when we saw the first evidence of conversion. The remaining parameter values were set by systematically changing them to fit the experimentally measured data (Table 5.3). A bang-bang control model using a time interval of 22-30 hpi produced chlamydial growth curves similar to what were observed in our 3D-EM time course, with 512 EBs by 40 hpi in the model compared to 644 EBs by our 3D-EM analysis (Fig. 5.6B, compare left and right middle). In contrast, when the time interval was shifted earlier or later the growth curves were not comparable to our observed data (Fig. 5.6B, right top and bottom). Specifically, an earlier conversion switch window of 18-26 hpi produced only 117 EBs at 40 hpi while a later window of 26-34 hpi predicted 1838 EBs. This data suggests that a relatively simple bang-bang control mechanism in which RB-to-EB conversion is switched on between 22-30 hpi is sufficient to describe the complex growth behavior of four chlamydial forms over the developmental time course.

### **Bang-bang model provides a rationale for delayed conversion**

Delayed onset of conversion is a characteristic feature of chlamydial development, but here we provide mathematical support for the benefits of this strategy. Two-dimensional EM of early inclusions (prior to 20 hpi) were consistently devoid of IBs or EBs (37, 41, 45, 147-149), indicating that conversion was prevented at early times. It seems logical for *Chlamydia* to first go through several rounds of RB replication in order to expand the pool of chlamydiae prior to conversion; however, there was no clear reason why conversion should be turned on at one specific time versus another. Additionally, it was unclear how conversion proceeded after it began – Was its rate adjusted over time? Did it turn off at any point in the infection? Our bang-bang control model of chlamydial development provides mathematical evidence that delayed

conversion is an optimal strategy for infectious progeny production and provides clues about why *Chlamydia* delay conversion with specific timing.

The mathematically optimal strategy to produce the highest infectious yield would be for *Chlamydia* to utilize a strict bang-bang control system to regulate RB-to-EB conversion. In such a regulatory system, RBs would first solely replicate to expand the bacterial population then all RBs would convert at once, just prior to the end of the infection. From a biological perspective, there are a few reasons why the mathematically optimal strategy may not be physiologically realistic. First of all, biological signaling events involve changes in gene expression and protein production, which are not instantaneous. Secondly, the optimal strategy is high risk because if the host cell lyses before expected, a chlamydial infection could potentially produce no infectious progeny.

Our mathematical modeling data suggests that *Chlamydia* utilize a modified version of bang-bang control in the *in vivo* intracellular infection. This modified bang-bang control, in which conversion is switched on gradually, can be seen as a “bet-hedging” strategy that *Chlamydia* use in the face of unknown timing of host cell death. It is imperative for RBs to begin conversion with ample time before host cell lysis, but if they convert too early then they limit the infectious yield of the infection. We saw that setting the switch time earlier (18-26 hpi in our simulated infection) reduced the EB yield (Fig. 5.6B). On the other hand, delaying conversion further (26-34 hpi in our simulated infection) produced a higher infectious yield (Fig. 5.6B), but there is a risk of the host cell lysing prior to completing the conversion process. A conversion switch time of 22-30 hpi best fit our experimental data. Considering replication begins between 8-12 hpi and takes about 2 hours (45, 145), this strategy allows 5-7 replication cycles producing 32-128 RBs prior to starting conversion. Therefore it seems that *Chlamydia* ensure there is some

expansion of the RB pool prior to the onset of conversion, but they regulate the onset to maintain a low risk of the host cell lysing prior to completing the process. What is not clear from the bang-bang model, however, is the mechanism of onset of RB-to-EB conversion.

### **Inclusion growth correlates with chlamydial number not chlamydial volume**

Our 3D-EM temporal analysis revealed that the inclusion volume changed drastically over the course of the chlamydial infection (Fig. 5.7A). Growth of inclusion size during the chlamydial developmental time course was previously noted, but this is the first report quantifying precise inclusion volumes for *Chlamydia*-infected cells. Considering the volume of a HeLa cell to be  $2,425 \mu\text{m}^3$  (169), the average inclusion starts out occupying less than 0.03% of the cell volume then grows to occupy 37% of the total cell volume by 40 hpi.

One possible explanation for such pronounced expansion is that the inclusion volume must increase to accommodate the growing volume of *Chlamydia* housed within the vacuole.

However, we found that the total chlamydial volume did not correlate with inclusion volume over the complete developmental cycle (Fig. 5.7B). Between 12-24 hpi chlamydial volume and inclusion volume increased proportionately, but after 24 hpi, inclusion volume continued to increase at a rapid rate while chlamydial volume peaked then decreased due to the onset of RB-to-EB conversion that replaced RBs with smaller EBs. Thus, expansion of the inclusion far exceeded the space requirements for the bacteria within it. At 12 hpi inclusions were approximately 60% occupied by chlamydial forms, but inclusions became increasingly empty of chlamydial forms over the developmental time course and by 40 hpi occupied less than 10% of the inclusion volume (Fig. 5.7B).

Although inclusion volume did not correlate with total chlamydial volume, there was a direct relationship between the inclusion volume and the total number of chlamydial forms (Fig.

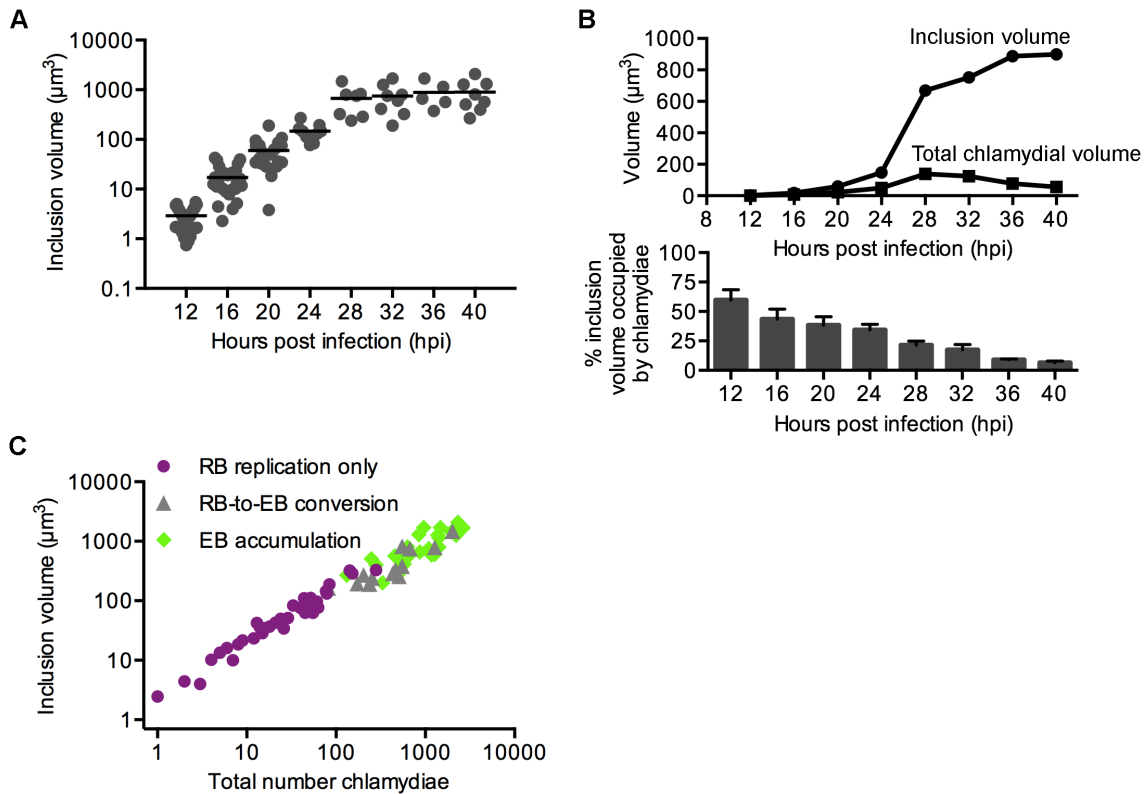


**Figure 5.7. Temporal analysis of the chlamydial inclusion**

**A)** Individual inclusion volume was determined from three-dimensional reconstructions. Each point represents a single inclusion and black lines indicate mean inclusion volume at each time point.  $n=9-50$  inclusions, depending on the time point. **B)** Average inclusion volume and total chlamydial volume were quantified from three-dimensional reconstructions of inclusions over the developmental time course. Top: Comparison of average inclusion volume and average total chlamydial volume over time. Bottom: Total chlamydial volume presented as a percentage of inclusion volume over time. **C)** Plot of individual inclusion volume as a function of total number of chlamydiae contained within that inclusion. Each point represents a single inclusion and points are distinguished by their developmental profile (see Figure 5.5).

5.7C). We noticed that this direct relationship was independent of time point in the infection - inclusions from different time points with similar volumes contained similar numbers of total chlamydial forms. For instance, a 20 hpi inclusion with a volume of  $70 \mu\text{m}^3$  contained 54 total chlamydiae and a 24 hpi inclusion with a similar volume ( $77 \mu\text{m}^3$ ) contained 63 total chlamydiae.

We observed that as inclusion volume increased, there was a progression of the inclusions through the three developmental stages (Fig. 5.7C). Inclusions grouped together by their developmental profiles showing a progression from RB replication only profiles (smallest inclusions with the lowest number of chlamydial forms) to RB-to-EB conversion and EB accumulation profiles (larger inclusions with greater numbers of chlamydial forms). Examining this graph, there appeared to be a shift representing the onset of RB-to-EB conversion occurring at a specific chlamydial number and inclusion volume (approximately 100 chlamydial forms and  $200 \mu\text{m}^3$  inclusion volume). We hypothesized that either of these parameters could act as a regulatory signal to trigger conversion. For example, conversion could begin once the chlamydial population surpasses a threshold value. To identify whether there appeared to be a threshold population of *Chlamydia* above which RB-to-EB conversion was turned on, we examined our individual inclusion 3D-EM data (Table 5.2). The inclusion that had begun conversion with the smallest chlamydial population contained 82 total chlamydiae, but another inclusion had 280 chlamydiae and still no detectable IBs or EBs. Thus there was not an apparent threshold chlamydial population that triggered the onset of RB-to-EB conversion. We also examined whether there was a threshold inclusion volume above which RB-to-EB conversion commenced. The smallest inclusion that had begun conversion was  $164 \mu\text{m}^3$ , but an inclusion with a volume of  $327 \mu\text{m}^3$  was also observed that had not yet begun conversion. Together, our analysis indicates

that inclusion volume growth correlates with chlamydial number rather than chlamydial volume, but that neither of these parameters correlates strongly with the onset of conversion.

### **Heterogeneity between infected cells from the same time point**

Our 3D-EM analysis at a single-cell level revealed heterogeneity between infected cells on the same monolayer that had not been previously characterized. Infected cells at the same time point in infection exhibited considerable variability in inclusion size and total number of chlamydiae. For example, at 12 hpi inclusion volume ranged from 0.75-5.49  $\mu\text{m}^3$ , which represents a 7.3-fold range (Fig. 5.7A). Despite this variable range in inclusion size, all inclusions at 12 hpi contained 1-2 chlamydiae (Table 5.2). Heterogeneity in inclusion volume was maintained throughout the developmental time course. At 40 hpi, inclusion volume ranged from 267.9-2087.46  $\mu\text{m}^3$ , a 7.8-fold range which is similar to that observed at 12 hpi (Fig. 5.7A). Variability in chlamydial number increased over time. The number of chlamydiae within 40 hpi inclusions was anywhere between 132 and 2318, a 17.6-fold range (Table 5.2). Our analysis indicates that monolayers of infected cells do not represent a homogenous population, and that averaging of large populations of infected cells obscures differences at the single cell level.

Heterogeneity between infected cells at the same time point in the chlamydial infection was previously uncharacterized because studies were based on large populations of infected cells. For example, genome copy analysis and progeny assays are based on measurements from  $10^5$ - $10^6$  cells. Our 3D-EM analysis of single infected cells indicates there is measurable heterogeneity between infected cells at the same time point, even from the same monolayer. It is unclear whether there is an experimental source of this heterogeneity or whether it is simply a feature of the chlamydial infection. Asynchrony in the phase of the host cell cycle, early events of infection, or in the onset of RB-to-EB conversion could contribute to variability observed

between chlamydial inclusions. These findings suggest that the progression through the developmental cycle is not strictly regulated by absolute numbers or timing in the intracellular infection.

### **Spatial analysis of developmental forms within the inclusion**

Our 3D-EM analysis showed that RBs are localized within close proximity of the inclusion membrane. For example, in an inclusion from 40 hpi, 80% of RBs were within 200 nm (1/5 of RB diameter) of the inclusion membrane (Fig. 5.8B, left panel). In contrast, EBs were more evenly distributed throughout the inclusion and only 35% were within 200 nm of the inclusion membrane (Fig. 5.8B, left panel).

Our data provides experimental support for a critical assumption in the contact-dependent model that RBs are closely associated with the inclusion membrane (152). The contact-dependent model postulates that RB contact with the inclusion membrane promotes replication and that detachment from the membrane is the signal for conversion (152). RB proximity with the inclusion membrane has been observed in two-dimensional EM micrographs, which provide snapshots of the inclusion, but our 3D-EM approach provides a comprehensive analysis of all RBs in the entire inclusion.

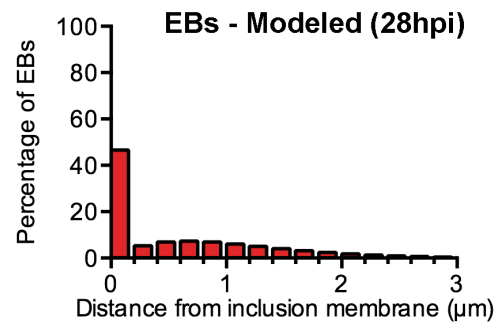
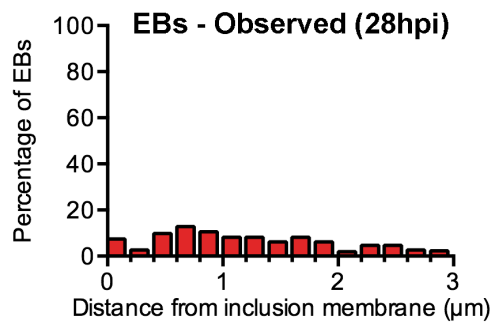
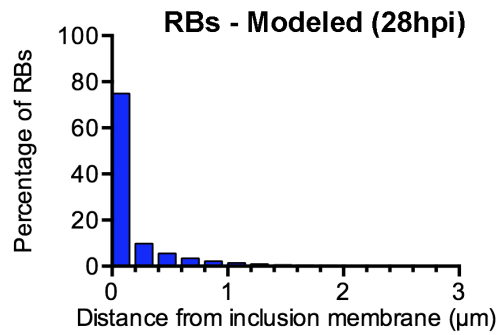
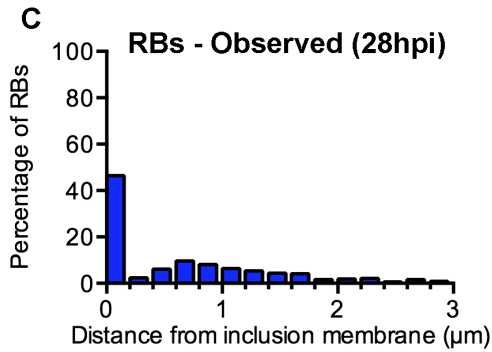
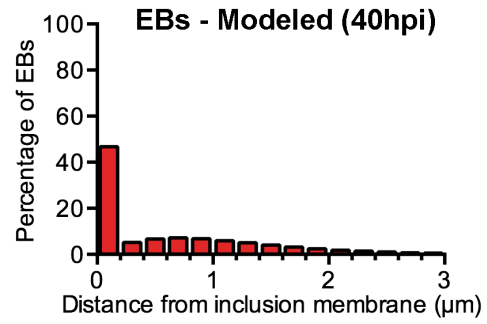
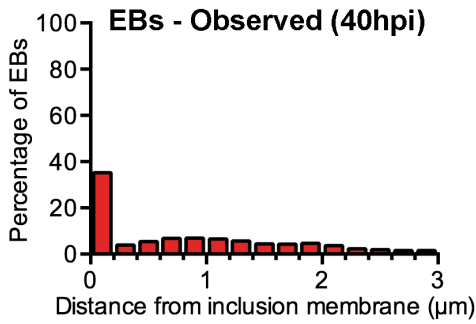
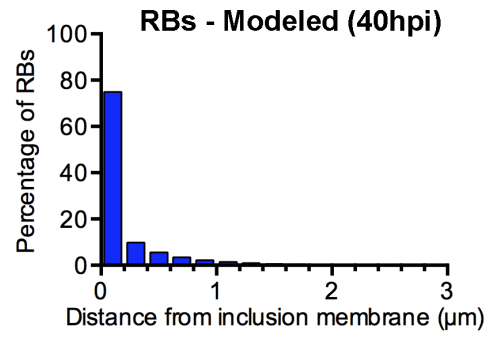
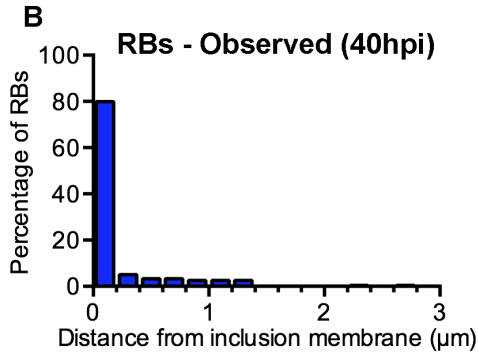
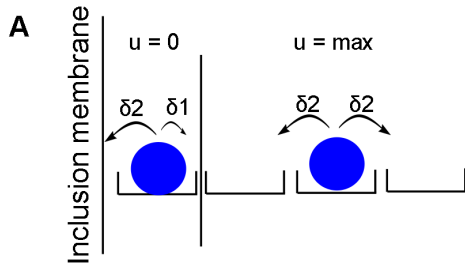
Using a mathematical modeling approach, we tested whether we could model the localization pattern of RBs and EBs by altering just a few parameters according to the contact-dependent hypothesis. We modeled the inclusion as a spherical compartment divided into 25 concentric bins then introduced parameters to describe the diffusion rate between bins and the RB-to-EB conversion rate (Fig. 5.8A). To represent preferential RB localization at the inclusion membrane, we decreased RB diffusion rate from the outermost bin to the next bin. Using our insights from the bang-bang model, we set the conversion parameter so that RBs in the outermost

**Figure 5.8. Spatial analysis of developmental forms within the inclusion**

**A)** Summary diagram of mathematical scheme used to describe the contact-dependent model.

Inclusion was divided into 25 spherical concentric bins. RBs in the first bin were represented as being in contact with the inclusion by the rate of diffusion toward the inclusion membrane ( $\delta_2$ ) being larger than the rate of diffusion away from the inclusion membrane ( $\delta_1$ ). RBs outside of the first bin were modeled to have an equal diffusion rate toward any adjacent bin. Within the first bin the conversion rate was zero. Outside of the first bin the conversion rate was maximal.

**B)** Observed: The shortest distance from the outer surface of each RB or EB to the inner surface of the inclusion membrane was determined from a three-dimensional reconstruction of an inclusion at 40 hpi. The distribution of RB or EB distances in relation to the inclusion membrane was plotted by histogram. Modeled: histogram of the expected distribution of RB distances from the inclusion membrane at 40 hpi applying the mathematical contact-dependent model outlined in (A) **C)** Observed: The shortest distance from the outer surface of each RB or EB to the inner surface of the inclusion membrane was determined from a three-dimensional reconstruction of an inclusion at 28 hpi. The distribution of RB distances in relation to the inclusion membrane was plotted by histogram. Modeled: histogram of the expected distribution of RB or EB distances from the inclusion membrane at 28 hpi applying the mathematical contact-dependent model outlined in (A).



bin had a conversion rate of zero and RBs outside of this bin had a maximal conversion rate (Fig. 5.8A). A mathematical model incorporating these simple parameters was sufficient to produce spatial distributions of RBs and EBs that closely resembled the experimental data at 40 hpi (Fig. 5.8B, right panels). The mathematical model designed based on the contact-dependent hypothesis predicted 75% of the RB population would be within 200 nm of the inclusion membrane at 40 hpi which is very similar to the 80% that we observed in our 3D-EM analysis (Fig. 5.8B, compare left and right panels). The model also predicted that only 47% of EBs would be located within the same distance of the inclusion membrane, which was similar to our experimental results showing 35% of the EB population within the first bin. We have also conducted this analysis at 28 hpi and obtained similar results (Fig. 5.8C).

### **Insights into the contact-dependent model**

Experimental support for the contact-dependent model has been restricted due to technical limitations, and 3D-EM is the first technique that can provide a complete picture of an inclusion and all its contents while preserving location information. We have shown here that 3D-EM analysis was able to quantify distances between chlamydial forms and the inclusion membrane that support the hypothesis that RBs maintain close association with the inclusion membrane throughout chlamydial development. Our observations lend support to the idea that proximity to the inclusion membrane promotes RB maintenance. Since our analysis only examined contact, it is unclear whether type III secretion (T3S) projections are responsible for mediating RB contact with the inclusion membrane as has been proposed in the contact-dependent model (152).

Our 3D-EM observations raise new questions about the dynamics of RB contact with the inclusion membrane and the signal that promotes RBs to retain their RB identity. The contact-

dependent model proposed that detachment of the RB from the inclusion membrane signaled the RB to convert into an EB (152). Our experimental observations, however, suggest that RBs may exhibit a dynamic relationship with the inclusion membrane in which they can lose contact with the inclusion membrane then regain contact without converting. We observed that many RBs were very close to the inclusion membrane (less than 100 nm away), but did not appear to be directly in contact. This was true at all time points that we examined in the infectious time course, including 20 hpi which is a time prior to the onset of conversion. Thus, our observations suggest that loss of contact from the inclusion membrane does not immediately trigger RB-to-EB conversion. Perhaps RBs must be detached for some period of time before conversion programming is activated.

Spatial constraints at the inclusion membrane were proposed to be the mechanism for RB detachment during the onset of conversion; however we do not see evidence of physical crowding in our 3D-EM analysis. The contact-dependent model proposed that as the RB population expanded, physical crowding at the inclusion membrane would force some RBs to lose contact and trigger conversion (152). Our 3D-EM observations, though, do not suggest a link between crowding and RB detachment because RBs were visualized within the inclusion lumen even when there was free space at the inclusion membrane. However, our observations do not exclude the possibility that local crowding resulted in RBs being physically displaced from the inclusion membrane. Physical crowding also cannot explain why we continue to see conversion at late times. At 40 hpi, RBs were spread out along the inclusion membrane showing no signs of physical crowding yet we continued to observe a large population of IBs at this time (average of 107 per inclusion), indicating conversion was still actively taking place.

### **Size of chlamydial forms changes over time**

In our analysis of 154 inclusions, we noted that average RB size decreased over the course of the developmental cycle. The average RB size was  $1.01 \mu\text{m}^3$  at 12 hpi and decreased about 4-fold over the developmental time course to  $0.25 \mu\text{m}^3$  at 40 hpi (Fig. 5.9A). A similar 4.8-fold decrease in size was observed for dividing RBs (Fig. 5.9A). To compare these size changes, we calculated the ratio of the average sizes of dividing RBs and RBs each time. We found that the ratio remained relatively constant over the developmental time course, suggesting that decreases in chlamydial size were occurring coordinately in these two chlamydial forms (Fig. 5.9B). IBs and EBs also decreased in volume over time, but only by 1.6 fold between 28 and 40 hpi (Fig. 5.9C). This progressive decrease in chlamydial size is a novel finding that was made possible by our comprehensive and quantitative size analysis of all the chlamydiae within multiple inclusions.

To examine the heterogeneity in chlamydial size we measured the volume of every RB within an inclusion. We examined a single inclusion at 24 hpi and a single inclusion at 40 hpi to represent average mid and late cycle inclusions, respectively. At both 24 and 40 hpi we observed a range of RB sizes, but RBs became clustered at a smaller sizes by 40 hpi (Fig. 5.10A, left panels). The average size of the 40 RBs in the single 24 hpi inclusion was  $0.37 \mu\text{m}^3$  (Fig. 5.10A), which was within the range of the average RB size determined from a population of inclusions at 24 hpi ( $0.55 \pm 0.23 \mu\text{m}^3$ ) (Fig. 5.9A). Similarly, the average size of the 240 RBs in the single 40 hpi inclusion was  $0.21 \mu\text{m}^3$  (Fig. 5.10A), comparable to the average RB size determined from a population of inclusions at 40 hpi ( $0.25 \pm 0.07 \mu\text{m}^3$ ) (Fig. 5.9A). The histogram data illustrates that while the average RB size decreased over the developmental cycle, the population remained heterogeneous, exhibiting a wide range of sizes throughout the infectious time course. Overall,

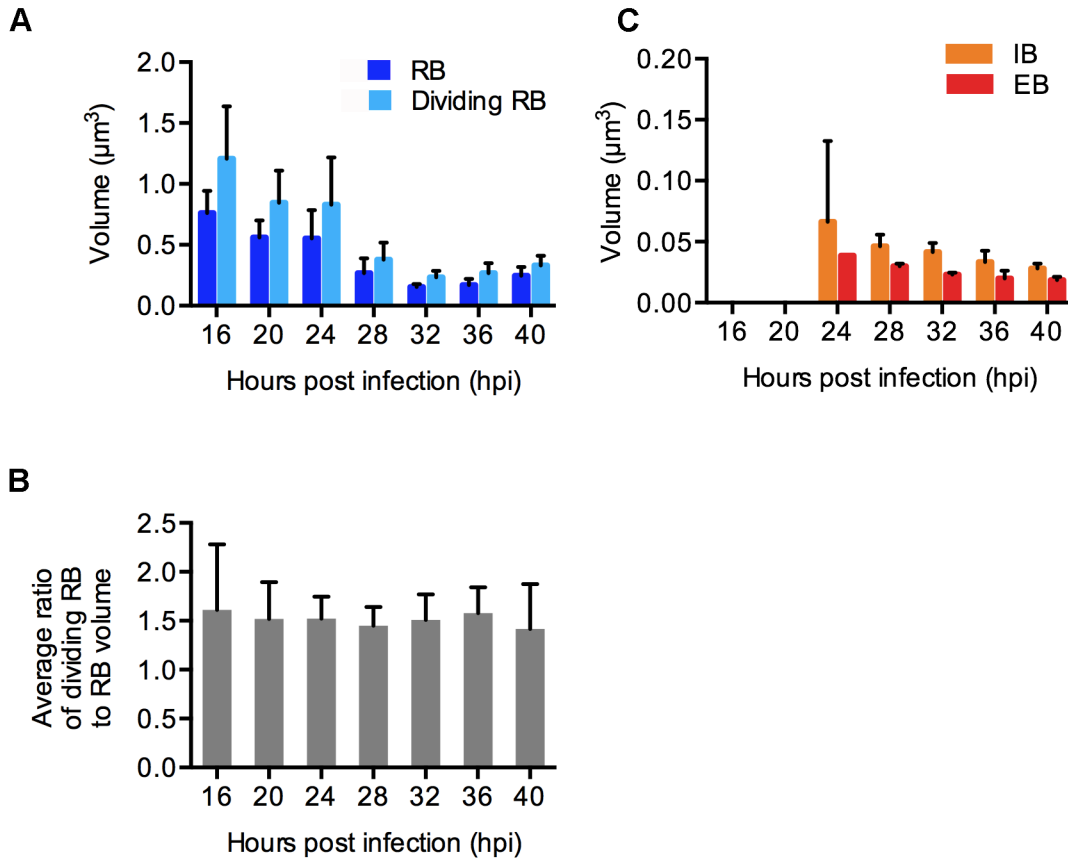
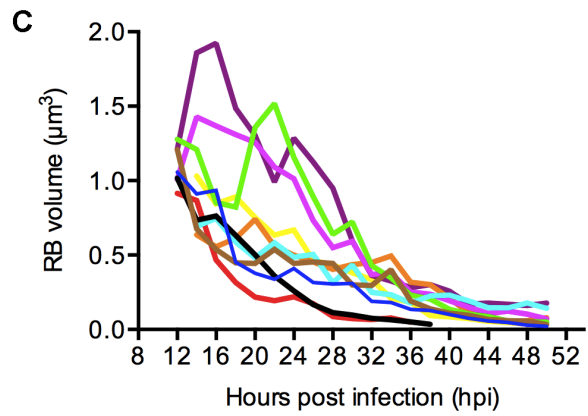
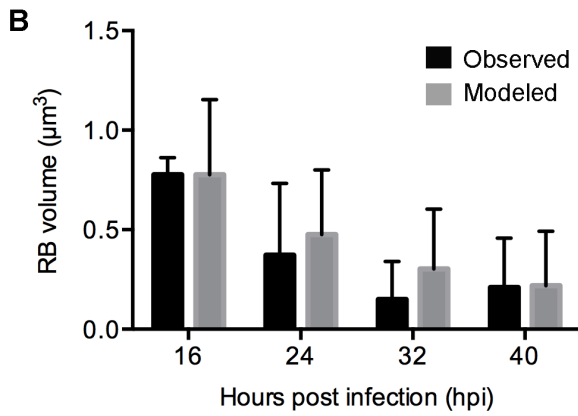
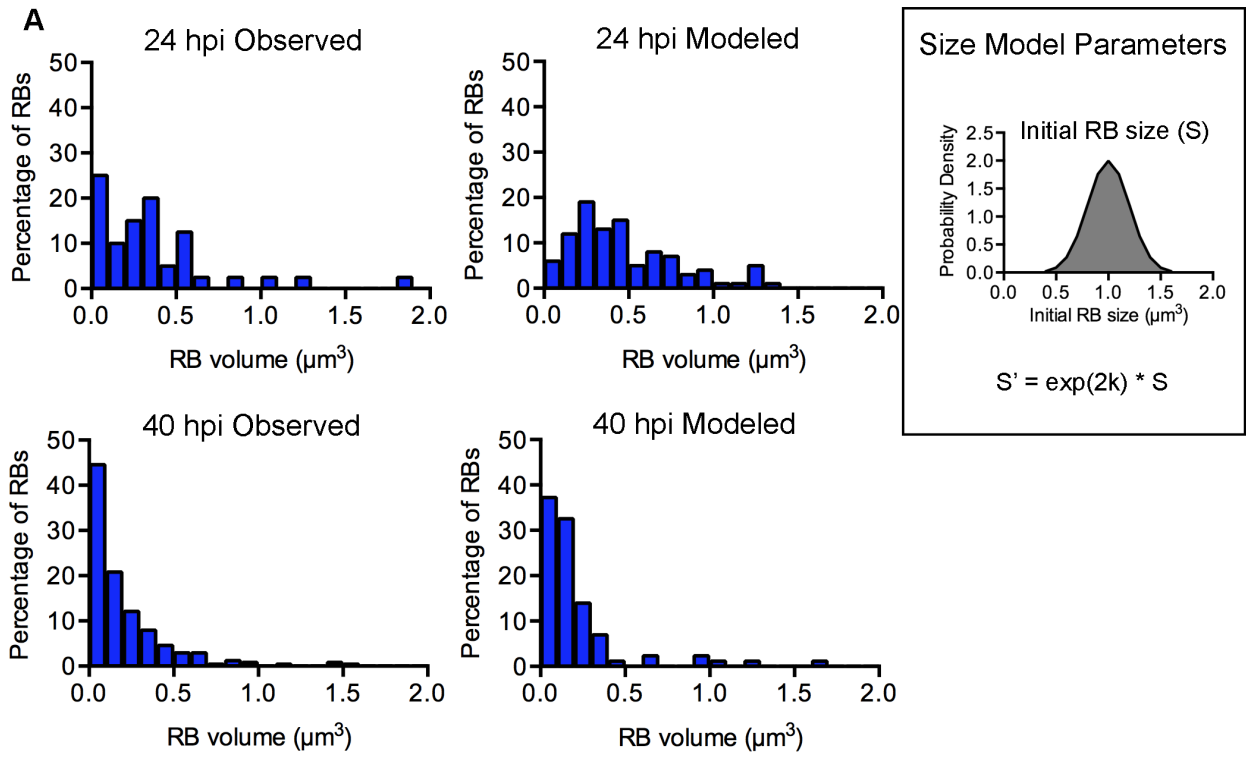


**Figure 5.9. Size of chlamydial forms changes over time**

**A)** The average RB or dividing RB volume was determined from all of the forms within one inclusion. These values were then averaged to determine overall average size of each chlamydial form at each time point.  $n=9-31$  inclusions. Error bars indicate the standard deviation. **B)** The ratio between the average dividing RB volume and average RB volume within each inclusion was determined, then these ratios were averaged to determine the overall average ratio.  $n=9-31$  inclusions. Error bars show the standard deviation. **C)** The average IB or EB volume was determined from all of the forms within one inclusion, then these values were averaged to determine overall average size of each chlamydial form at each time point.  $n=3-9$  inclusions. Error bars indicate the standard deviation.

**Figure 5.10. Stochastic division prior to doubling can account for RB heterogeneity**

**A)** Individual RB volume was determined for every RB within a single inclusion at 24 hpi (n=40) and a single inclusion at 48 hpi (n=240). The distributions of RB volumes in each inclusion are presented in the histograms on the left (“observed”). Distribution of RB volume was modeled using a simulated chlamydial infection in which bacterial division occurred with the greatest likelihood when RBs reached 1.7X their previous size. This replication parameter was adjusted to permit bacterial division outside of this range at reduced frequency. The resultant RB volumes generated at 24 hpi and 40 hpi are plotted as histograms. **Box:** Summary of mathematical parameters used to describe size-dependent regulation of RB division. We assumed initial RB size ( $S$ ) was variable with a normal distribution around the average size determined from 3D-EM at 12 hpi,  $1 \mu\text{m}^3$ . Assuming continuous growth  $k$ , also with a normal probability distribution, the size of the daughter RB ( $S'$ ) can be calculated. Therefore, each division occurred stochastically with a variable probability **B)** Individual RB volume was determined for every RB within a single inclusion at 16, 24, 32, and 40 hpi then the volumes were averaged to produce the bar graph (black bars). The distribution of individual RB volumes was also modeled at these times and the results averaged to produce the bar graph (gray bars). Black lines indicate standard deviation in RB volume under each condition. **C)** Stochastic timecourse following individual modeled RBs as they change in volume over successive replicative binary fission events. Note that some RBs are lost over time (for example the black line terminates at 38 hpi), which represents RB-to-EB conversion in our proposed RB size control model of chlamydial development (See Fig. 5.11).



our observations of decreasing RB size and striking heterogeneity suggest that chlamydial replication may be regulated differently from other bacteria, which tend to maintain cell size homeostasis over time (170).

Our ability to measure the volume of individual chlamydiae with 3D-EM allowed us to make the novel discovery that chlamydial size decreases over time. This phenomenon was not detected earlier because of the limitations of 2D-EM for studying chlamydial size. RBs of different sizes had been observed in electron micrographs, but some heterogeneity could be explained by the two-dimensional analysis of the approximately spherical RBs: if the RB was transected closer to its pole it would appear smaller than if it were bisected in the middle. Thus, previous characterizations of RB size only described a general range for diameter between 500-1000 nm (146). Our 3D-EM technique allowed us to measure the exact size of individual RBs and showed that the actual range in RB diameter was much broader than originally reported. We observed that RB diameter ranged from 133-1807 nm.

### **Chlamydial division prior to doubling in size**

The progressive decrease in RB size in conjunction with increasing RB population can be explained by division before doubling in size. For normal cell size homeostasis, division occurs when a cell reaches twice its original size; however, in order to decrease in size RBs would need to divide at <2X their original size. We performed mathematical modeling to simulate size-dependent regulation of RB replication at factors <2X. In the model, we simplified RB replication by assuming synchronous cell division every two hours. We set the initial cell size, based on our experimental data at 12 hpi, to be  $1.0 \mu\text{m}^3 \pm 0.2$ , using a normal distribution (Fig. 5.10A, box). Between bacterial divisions we assumed a continuous growth rate  $k$ , also with a normal distribution (Fig. 5.10A, box). Setting  $k$  to a growth rate reflecting an average increase in

bacterial size of 1.7X between divisions best fit our experimental results. Using these parameters, we compared our observed distribution of RB sizes within single inclusions at 24 and 40 hpi to modeled predictions of the size distributions (Fig. 5.10A). We found that the predicted RB size profiles based on modeling were similar to our experimental observations with 3D-EM analysis. At 24 hpi we observed 75% of RBs below  $0.5\mu\text{m}^3$  compared to the model, which predicted 65% of the RB population would reach this size by 24 hpi. At 40 hpi we observed 90% of RBs below  $0.5\mu\text{m}^3$  compared to the model, which predicted 92% of RBs in this range. We used the same parameters to compute the RB sizes expected at additional time points and these models also produced data comparable to our experimental results (Fig. 5.10B).

At all time points we noted a wide range of RB sizes in both the experimental and modeled data (Fig. 5.10B). We modeled the size of an individual RB over successive divisions to examine the source of this variability. In our model, each RB division occurs at 1.7X its original size with a certain probability exhibiting a normal distribution (50% of divisions occurring between 1.46X and 2.02X). RB sizes are variable because each division is an independent stochastic event that can produce differently sized daughter RBs. To visualize how a heterogeneous population of RBs could emerge after several replication cycles, we modeled RB replication over time with our 1.7X parameter following the size of a single RB over time (Fig. 5.10C). We simulated replication for hundreds of RBs (10 are shown on the graph) and observed a progressive decrease in size for each individual RB, although the rate of the size decrease was different for each chlamydiae due to the stochastic nature of division. The earliest any RB reached  $0.20\mu\text{m}^3$  (the average RB size during active conversion, 28-40 hpi) was after 4 divisions, but some RBs required 14 divisions before reaching this size. Differences in initial RB size and variation in the size of an RB upon each division results in overall RB size variability.

The initial RB can have a range of sizes ( $1 \pm 0.2 \mu\text{m}^3$ ) prior to beginning replication, resulting in a different starting RB size in each inclusion. As successive divisions occur, RB size variability increases because each division is permitted within a range of sizes. From comparing our experimental and modeling data we conclude that RB division occurring with size-dependent probability at a size less than 2X original size provides an explanation for the range and distribution of RB sizes we observed.

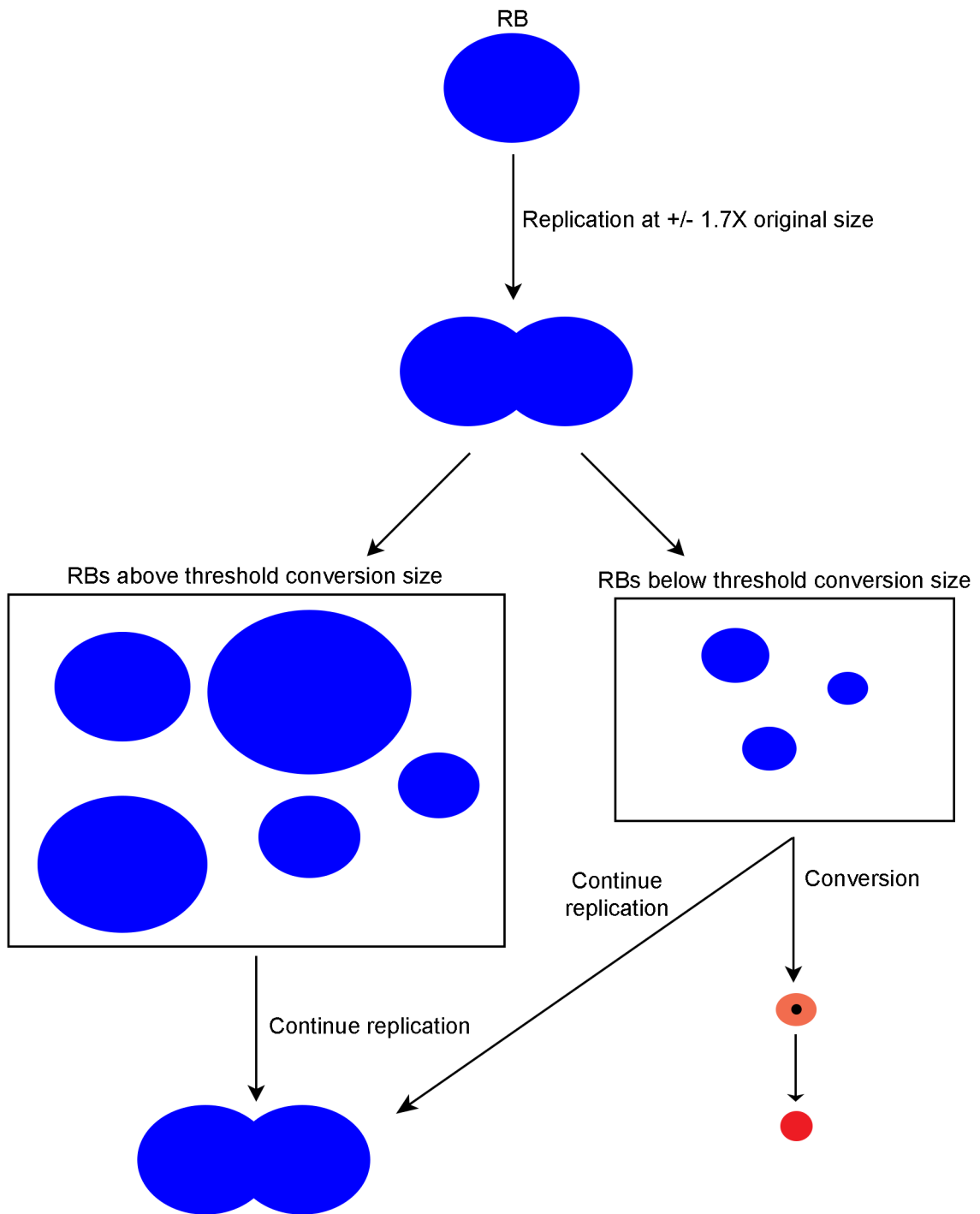
This progressive decrease in RB size should not be sustainable. Indeed, our 3D-EM analysis showed that average RB size leveled off between 32-40 hpi., and we did not detect an accumulation of small RBs below  $0.05 \mu\text{m}^3$ . It is possible that at this size threshold RBs revert back to canonical division only upon doubling in size or that they stop growing and dividing. However, a more elegant explanation could be that small RBs disappear from the pool by converting into EBs. In the next section we propose a new model of *Chlamydia* development in which RB size acts as a critical regulator of both replication and conversion.

### **Proposed model: RB size as a critical regulator of chlamydial development**

Based on our 3D-EM analysis we propose a model in which RB size is a critical regulator of chlamydial development (Fig. 5.11). We propose that this single factor can account for observed chlamydial behavior during two major developmental events, RB replication and RB-to-EB conversion. In our model, RB replication is regulated to occur with size-dependent probability prior to doubling, resulting in RB size gradually decreasing over successive replication cycles. When RB size is above a certain threshold, conversion is prohibited. Several replication cycles are required for an RB to reach a critical small threshold size and become licensed for conversion. Consequently, RBs expand the bacterial population prior to converting. Once an RB converts into an EB it is removed from the RB population, thus preventing any RB

**Figure 5.11. Proposed model of RB size regulation of chlamydial development.**

An initial RB begins at a large volume and replication occurs stochastically with size-dependent probability around 1.7X the original RB size. This produces a heterogeneous population of RBs with variable sizes. RBs with sizes above the threshold conversion size continue replicating. RBs below the conversion threshold size may convert or continue replicating. If they convert they transform into an IB then an EB and are removed from the RB population. Alternatively, if they replicate they produce two RB progeny and continue expanding the RB population.



from becoming indefinitely smaller. In our model, regulation of RB size can account for the delayed onset and asynchrony of RB-to-EB conversion – two characteristic features of chlamydial development.

In our model, regulation of RB replication prior to doubling creates progressively smaller RBs that act as a clock to delay the onset of RB-to-EB conversion. We observed that at 12 hpi RBs started at a large size, which would not be permissive for conversion. If RB division is most likely to occur upon reaching 1.7X original size, this sets an average rate for the decrease in size of an RB. It is highly unlikely, for example, that an RB would perform successive divisions at 1.2X its original size to get smaller more quickly and reach the threshold size for conversion. Specifically, taking the average initial RB to be  $1.00 \mu\text{m}^3$  and assuming replication occurs when the RB achieves 1.7X its original size, it would take 10 replication cycles to reach 20% of its original size ( $0.20 \mu\text{m}^3$ ), the average RB size during active conversion between 28 and 40 hpi (Table 5.4). Taking each replication cycle to be 2 hours in an RB (45), we can deduce that it would take 20 hours for an RB to go from  $1.00$  to  $0.20 \mu\text{m}^3$  in this model. Since we did not observe RBs beginning replication until around 12 hours, we could expect an RB to reach a size of  $0.20 \mu\text{m}^3$  by 32 hpi (Table 5.4). Our 3D-EM data showed that the average RB size at 32 hpi was  $0.16 \pm 0.02 \mu\text{m}^3$  (Fig. 5.9A), which is comparable to the prediction of the model.

This chlamydial developmental strategy is advantageous to the bacteria because it ensures that RBs will first replicate to expand the *Chlamydia* population prior to converting into EBs. We observed conversion was delayed in our inclusions until 24 hpi. If we consider replication begins between 8-12 hpi and takes 2 hours, we expect that 6-8 replication cycles were completed prior to the onset of conversion at 24 hpi. That means we could expect a pool of 64-256 RBs accumulated prior to conversion. From our 3D-EM analysis of inclusions at 24 hpi we

**Table 5.4. Expected RB size over time assuming division at 1.7X original size**

<b>Replication cycle</b>	<b>RB size (<math>\mu\text{m}^3</math>)</b>	<b>Time point (hpi)</b>
0	1.00	12
1	0.85	14
2	0.72	16
3	0.61	18
4	0.52	20
5	0.44	22
6	0.38	24
7	0.32	26
8	0.27	28
9	0.23	30
10	0.20	32

determined an average RB population size of 105 forms (including RBs and dividing RBs), which falls into the mathematically predicted range lending support to our model.

Our model of RB size as a regulator of chlamydial development accounts for asynchrony in conversion events by relating them to heterogeneity in RB size. We identified several events during chlamydial development that lead to variability in RB size. First, our 3D-EM analyses at 12 hpi showed that RBs grew to different sizes prior to starting replication. Second, RBs exhibited unsynchronized replication cycles. Additionally, our model of RB replication describes division as a stochastic event that is not regulated tightly by size but occurs with size-dependent probability around 1.7X. Thus, with each replication cycle a range of different sized progeny RBs can be produced. Although all RBs show a general pattern of decreasing size, each would reach the conversion threshold at a different time. Since only a proportion of RBs at a particular time would be expected to be licensed to convert, this could account for the asynchronous nature of conversion that we observe.

To determine what the threshold size for conversion might be, we looked at the size of IBs. The first IBs that were observed at 24 hpi had an average size of  $0.06\mu\text{m}^3$  (Fig. 5.9C). We examined our RB populations to see whether there appeared to be a cut-off around  $0.06\mu\text{m}^3$  below which no RBs were detected. An individual inclusion at 24 hpi containing 40 RBs contained 4 RBs with sizes less than  $0.06\mu\text{m}^3$ ; however analysis of 240 RBs in a 40 hpi inclusion revealed that 66 were less than  $0.06\mu\text{m}^3$  (Fig. 5.10A). Therefore, it does not seem like  $0.06\mu\text{m}^3$  is a strict threshold size for conversion. Instead, our data suggest that a minimum size threshold might act as a permissive signal for conversion. We propose a mechanism, where upon reaching a minimal threshold size for conversion, an RB becomes licensed to convert. After licensing,

conversion occurs with a certain probability producing a mixed population of RBs – some that convert and are removed from the replicating pool and others that remain small RBs (Fig. 5.11).

### **Testing RB size as a critical regulator of chlamydial development**

#### Alter initial RB size

Our model requires that the first RB must grow to some large size prior to beginning replication, otherwise RBs would reach a permissive size for conversion too early in the developmental time course and prematurely convert to EBs. One approach to test whether RB size affects conversion is to experimentally manipulate the size of RBs early in infection and measure effects on the timing of RB-to-EB conversion. Penicillin is an antibiotic which has been shown to produce large, aberrant RBs within *Chlamydia*-infected cells, and upon removal of penicillin from the culture, productive chlamydial development resumes (171). Based on our model, we predict that enlarging the initial RB size will result in more replication cycles to achieve a threshold size for conversion and thus a longer delay in the onset of conversion compared to the normal infection (24 hpi). Alternatively, we predict that decreasing the initial RB size would result in premature onset of conversion.

#### Modulate RB contact with the inclusion membrane

RB size and RB contact with the inclusion membrane may act coordinately to regulate RB-to-EB conversion. Our 3D-EM analysis of distance between RBs and the inclusion membrane show that RBs preferentially localize near the inclusion surface. RB size could mediate attachment to the inclusion membrane by modulating the number of T3S projections or other surface adhesins. Scanning EM of *Chlamydia* revealed rosettes on the chlamydial surface, morphological markers of surface projections (153). The number of rosettes per RB was maximal at 10 hpi (30-60 per chlamydiae) and decreased by 20 hpi (10-30 per chlamydiae).

Interestingly, EBs showed a further reduction in number of surface projections (10-20 per chlamydiae) (153). Combining these observations with our data, decreasing RB size is correlated with a downregulation in the production of surface projections and conversion into an EB. We were unable to visualize whether projections mediated contact between RBs and the inclusion membrane, but previous studies using cryo-EM have demonstrated the importance of T3S-mediated contact with the inclusion membrane during early infection events. T3S projections are polarized on the EB surface and EBs orient with their T3S-face toward target cells, allowing the T3S projections to directly contact the host cell plasma membrane (172).

By altering type III secretion, we can investigate whether a functional T3S system plays a role in mediating RB contact with the inclusion membrane and regulating conversion. Previous studies have reported that *Yersenia* T3S inhibitors disrupt the normal progression of chlamydial development. Treatment with *Yersenia* T3S inhibitor C1 caused a dose-dependent reduction in inclusion size and inhibited production of EBs, as measured by immunofluorescence and progeny assay respectively (157). Another *Yersenia* T3S inhibitor, INP0400, also demonstrated that T3S inhibition produced smaller inclusions with fewer RBs, and inhibition of T3S after 24 hpi resulted in RB detachment from the inclusion membrane and reduced infectious progeny yield (173). From these studies we can conclude that T3S plays a role in regulating chlamydial development at the level of replication and conversion, but with 3D-EM we would be able to quantitatively examine the specific defects in response to these inhibitor treatments. For instance, inhibitor treatment appeared to reduce RB contact with the inclusion membrane by immunofluorescence staining, but we could use 3D-EM to quantify RB distances and define how far T3S is able to mediate contact. Furthermore, we could assess the roles of RB size and inclusion membrane contact in mediating RB-to-EB conversion. If T3S is the main regulator of

conversion, we would expect inhibition of T3S to result in detachment that promotes premature conversion producing a limited pool of EBs. However, if the size of an RB is also important, we would predict that detachment of an RB is not sufficient for conversion. We would expect to see an accumulation of RBs detached from the inclusion membrane that do not immediately convert. Since inhibition of T3S also reduces RB replication (173), only some of the detached RB population are likely to replicate enough times to achieve a threshold size for conversion; therefore, we would expect that many RBs at the end of infection do not successfully convert, reducing infectious yield.

# **Chapter 6**

## **Conclusions**

The work described in this dissertation illustrates two exciting but different paths to scientific discovery about the intracellular *Chlamydia* infection: the first was a journey of challenging and correcting a commonly accepted model in *Chlamydia* biology while the other was an exploration of new frontiers using novel technology. Our studies of the chlamydial protease CPAF challenged over 20 years of published research from multiple research groups. We found that the reported proteolysis of multiple host proteins by CPAF was an *in vitro* phenomenon. We demonstrated that experimental manipulations such as cell detachment and ineffective enzymatic inhibition promoted CPAF activity in infected cell lysates, which caused *in vitro* proteolysis of several host protein substrates during lysate preparation. Our findings warranted a major reassessment of CPAF's intracellular substrates and called into question the role of this protease as a major chlamydial virulence factor that mediates host-pathogen interactions.

Our novel 3D-EM approach to investigate the intracellular *Chlamydia* infection provided the first quantitative analysis of entire inclusions over the chlamydial developmental time course. The method we developed allowed us to categorize and quantify chlamydial developmental forms precisely and accurately, as well as measure volume and location of individual chlamydiae. Analysis of the quantitative data led us to propose a new model of chlamydial development in which chlamydial size regulates bacterial replication and conversion. Our model postulates that RBs divide prior to doubling resulting in a progressive decrease in size over successive replications. Upon reaching a lower size threshold, RBs convert into EBs. Since several replication cycles are required for RBs to decrease to a threshold size for conversion, RB size regulates the timing of the onset of RB-to-EB conversion. Our data raise exciting new questions about how *Chlamydia* regulate their cell size and the signal that mediates conversion.

The 3D-EM technique will be useful for addressing these new hypotheses and for studying many other aspects of the intracellular infection in a quantitative manner.

# Challenging accepted views about CPAF

## How researchers were misled about CPAF function

Up to 2012, there was accumulating published data supporting a role for the chlamydial protease CPAF as a major virulence factor in *Chlamydia*. CPAF had been reported to cleave or degrade multiple host proteins, thereby altering their function and causing effects such as Golgi reorganization or inhibition of apoptosis in the infected host cell. The discovery of each new CPAF substrate bolstered the importance of this protease to the intracellular infection. We experienced first-hand the thrill of identifying novel CPAF substrates when we examined centrosomal proteins as part of a potential mechanism of *Chlamydia*-induced centrosome amplification.

Early reports of the first CPAF substrates provided an experimental road map that was followed by subsequent studies that demonstrated CPAF-mediated proteolysis and its role in *Chlamydia*-induced phenotypes. Analysis of infected cell lysates by immunoblot was regularly used to demonstrate CPAF-mediated cleavage or degradation of specific host proteins (52, 68-70, 79, 86, 87), but alternative corroborating methods were not employed except in a single study that used immunofluorescence analysis to examine whether proteolysis occurred in intact infected cells (87). The effect of proteolysis was then extrapolated from each protein's known function in an uninfected cell without direct evidence that CPAF mediated the phenotypes in an infected cell. Technical limitations contributed to the lack of direct experimental proof for the role of CPAF within an infected cell. At the time of these studies, no genetic knockout method was developed to be able to show whether CPAF was necessary for the observed proteolysis and host-pathogen interactions. Accumulating reports using similar experimental strategies led to

mis-characterization of CPAF as a major chlamydial virulence factor, and this idea became a central belief in *Chlamydia* biology.

### **Reaction from the field**

It was intimidating to publish a study that contradicted findings in multiple published reports and which challenged the dogma of CPAF function. However, we were able to make a convincing case by showing that we could reproduce the published cleavage or degradation of CPAF substrates but prevent this proteolysis solely by inhibiting CPAF activity during lysate preparation (75). Additionally, we confirmed that intracellular proteolysis did not just occur with altered timing because we were unable to detect any proteolysis of the reported substrates up to 48 hpi (or in some cases as late at 60 hpi), which is much later than the proteins were reported to be cleaved or degraded (75).

The *Chlamydia* field has to a large part recognized that previous reports of CPAF-mediated proteolysis are an *in vitro* phenomenon, but the published studies have not been corrected. A number of reviews on the topic have been published (174-176), but the previous literature has been left mostly uncorrected with no retractions to date. This presents a problem for new scientists entering the chlamydial field. They will be bombarded by 20 years of publications espousing CPAF's role as a major chlamydial virulence factor and only a handful of recent works that counter those findings.

A few remain skeptical that proteolysis of previously reported CPAF substrates is entirely an *in vitro* artifact (177, 178). Some contend that immunoblot assays are not sensitive enough to detect *in vivo* proteolysis. We do not deny that a small amount of intracellular proteolysis may occur below the level of detection of immunoblots, but if this is the case it would be hard to explain how such a minimal level of proteolysis can produce major chlamydial phenotypes such

as inhibition of apoptosis. Thus the meaning of such proteolysis would require future study and may still result in a re-characterization of CPAF function.

Few attempts have been made to verify whether published CPAF substrates that we did not test are bona fide or artifactual intracellular substrates. The Valdivia group recently reported that vimentin and LAP-1 are host proteins that are cleaved by CPAF late in the chlamydial infection (74). In our own experiments, we could not verify intracellular cleavage of vimentin even by examining cells at 60 hpi, which is much later than the reported proteolysis at 48 hpi (74). Snavelly *et al.* also used a fluorescence-based assay to demonstrate proteolysis of EGFP-tagged vimentin in live cells. GFP signal was lost upon inclusion rupture in wildtype *Chlamydia*-infected cells and retained in CPAF-null mutants, suggesting a role for CPAF in cleaving vimentin during late effects in the infection (74). However, CPAF-null mutant inclusions had abnormal phenotypes and did not appear to rupture in the same way as wildtype infected cells. Thus, it is unclear whether loss of GFP signal could be attributed to another mechanism besides CPAF-mediated proteolysis. The identity of LAP-1 as an intracellular CPAF substrates remains to be tested by other groups since its publication.

## **Implications of *in vitro* CPAF activity**

### **Studies of *Chlamydia*-infected cells**

Our findings demonstrate that proteins in a cell lysate from *Chlamydia* infected cells are susceptible to *in vitro* CPAF-mediated proteolysis. Thus, any protein analysis requires precautions to completely inhibit CPAF enzymatic activity at the time of lysate preparation. In addition, it is important to verify that CPAF activity in each lysate has been completely inhibited because no method for inhibiting CPAF activity is 100% reliable. In Chapter 3, we described an *in vitro* CPAF activity assay for testing lysates.

This concern about artifactual proteolysis extends beyond studies of CPAF. Approaches such as immunoblot analysis, mass spectrometry, protein affinity chromatography, and biochemical studies all utilize infected cell lysates that may contain CPAF activity. Artifactual proteolysis affects host proteins (75, 109) as well as chlamydial proteins (Hanson and Tan, unpublished) and will lead to a misrepresentation of the *in vivo* protein contents of an infected cell. Importantly, it is not sufficient to add a CPAF inhibitor at the time of cell lysis because experimental methods that detach cells from a monolayer artifactually activate CPAF (109).

### **Enzymatic studies**

There is precedent for *in vitro* findings to mislead researchers about the identity of biologically relevant substrates in studies of other proteases like caspases and calpains. Caspases are a family of cysteine proteases with roles in apoptotic cell death. Caspase substrates contain a relatively common consensus sequence, and consequently hundreds of potential substrates have been identified (179). Evidence for caspase-mediated cleavage of these substrates was provided *in vitro*, but few studies established *in vivo* relevance. In many cases, the functional consequences of cleavage were simply inferred from the protein's normal function (180). Without direct evidence of intracellular proteolysis, it is unclear how many of the hundreds of previously identified caspase substrates are purely *in vitro* substrates (179). Additionally, many of the substrates that are cleaved *in vivo* are thought to be cleaved as bystanders because their proteolysis does not appear to serve any biologically relevant purpose (180). Calpains are calcium-dependent cysteine proteases whose substrates have also been identified using *in vitro* methods. Many calpain-1 substrates were identified *in vitro* with roles in platelet aggregation, but it was later determined that several of the identified substrates were not cleaved *in vivo* (181).

Our studies on CPAF have general implications for the analysis of any modification enzymes (kinases, phosphatases, proteases) that retain activity under standard cell processing conditions. Our findings underscore the importance of inhibiting the relevant enzymatic activity during cell processing and verifying that this activity has been blocked.

### **Artifactual CPAF activation**

Artifactual induction of CPAF activity in response to cell detachment appears to be an unusual phenomenon. The principal molecules that mediate cell-cell and cell-matrix interactions are cell adhesion molecules (CAMs). CAMs are cell surface proteins that can respond to and induce changes in attachment via ligand/receptor interactions that transduce a signal into the cell interior. Although CAMs respond to changes in cell attachment, activation of downstream effectors is not instantaneous (182). There is no precedent for cell detachment to quickly (within <10 minutes) promote proteolytic activity of an intracellular enzyme, as appears to be the case with CPAF.

We speculate that the mechanical stress of cell detachment is sufficient to release active CPAF in the cytosol. CPAF was originally believed to be translocated into the host cell cytosol based on immunofluorescence studies (63, 67, 68, 91, 103-106); however our data shows that this localization pattern is dependent upon fixation method. Additionally, our findings that many host protein substrates are not cleaved or degraded intracellularly (75) suggest active CPAF is actually sequestered from the host cytosol. The Valdivia group proposed that active CPAF resides within the inclusion lumen until very late in infection when the cell is preparing for lysis (74), and some of our immunofluorescence experiments also suggested CPAF resided within the inclusion (Chapter 2). Upon chemical or mechanical detachment of infected cells from the monolayer, the inclusion membrane could be compromised releasing active CPAF to access host

proteins. Attempts to isolate chlamydial inclusions have provided evidence that the inclusion membrane is fragile and relatively unstable (183), suggesting it may be sensitive to physical manipulations of the host cell. Alternatively, it has also been suggested that CPAF may be secreted in outer membrane vesicles (63). It is possible that detachment of cells causes disruption of the vesicles releasing active CPAF to its host protein substrates. A final possibility is that CPAF is free in the host cell cytosol but bound by an inhibitor to prevent proteolysis of host protein substrates. In this scenario, detachment from the monolayer could disrupt of an inhibitor-CPAF complex to release active CPAF.

## **Future directions for CPAF**

### **Identification of intracellular substrates**

To understand the function of CPAF, it will be important to identify its *in vivo* substrates. An attempt has been made to identify CPAF substrates from a proteomic screen, but expression of active CPAF in uninfected cells yielded 3000 cleavage events (178), a number that seems impossibly high to represent intracellular proteolysis unless it mediates a terminal event like host cell lysis. Overexpression of CPAF in uninfected cells has been utilized in previous studies of CPAF-mediated proteolysis (69, 79, 86), but it does not seem to be a biologically relevant representation of CPAF during a chlamydial infection. Expression of active CPAF does not recapitulate the processes of secretion and translocation that occur in a *Chlamydia*-infected cell, nor does it account for the possibility that CPAF is sequestered within the inclusion lumen or in vesicles. Furthermore, lysates from cells overexpressing CPAF are subject to *in vitro* CPAF activity artifacts, and without proper inhibition during the protein extraction process *in vitro* CPAF activity could lead to an artifactual proteomic profile.

Determination of CPAF's localization within a *Chlamydia*-infected cell would aid in the identification of potential CPAF substrates. Since CPAF localization in immunofluorescence studies is dependent on fixation method, other approaches must be used to determine where active protease resides in an infected cell. One approach that does not rely on fixation would be to directly visualize CPAF using a fluorescent tag. Chlamydial genetics now allows expression of exogenous proteins in chlamydial organisms using a plasmid shuttle vector (184, 185). Bauler and Hackstadt successfully infected cells with *Chlamydia* expressing flag-tagged CPAF, but had to fix cells in order to visualize CPAF localization (108); thus, these experiments were still subject to possible fixation artifacts. Perhaps localization could be determined by infecting cells with *Chlamydia* expressing a fluorescently tagged form of CPAF and visualizing the protease in live cells. A benefit to this method is that changing CPAF localization could be monitored over time. One caveat to consider with this experiment, though, is that the placement of the tag could affect CPAF secretion and translocation, resulting in a different localization pattern than would be observed for wildtype protease. An alternative approach that does not require genetic modifications to CPAF itself, would be to label CPAF indirectly using a secondary probe. For example, labeled antibodies and click-chemistry probes have been used to determine localization of other proteins in *Chlamydia*-infected cells (108, 151). We discussed how tagged boronate peptides could be used as CPAF probes to determine localization (Chapter 4).

Our studies of CPAF's active site may be helpful to identify features of CPAF substrates. In the case of another serine protease, the HTRA1 enzyme, interactions of an inhibitor with the active site revealed selectivity pockets in the HTRA1 enzyme that helped identify features that would be present in putative substrates (137). We have performed molecular modeling of boronate peptide inhibitors within the CPAF active site, but we unfortunately did not identify

specific residues or sequences that we could use to identify putative substrates. The vast panel of *in vitro* CPAF substrates suggests that CPAF is a promiscuous protease without a strong substrate binding specificity. Indeed, previous attempts to identify a CPAF consensus sequence have been unsuccessful. Cleavage sites were identified for keratin-8 and vimentin, but the actual CPAF recognition site could not be determined (52, 80). Interestingly, mutations at the cleavage site of vimentin revealed alternative cleavage sites, suggesting CPAF has broad substrate recognition (52). CPAF may demonstrate wide-ranging substrate recognition, but it must exhibit some specificity as not all host proteins are proteolytically processed by CPAF. Perhaps molecular modeling of *in vitro* CPAF substrates within the CPAF active site could reveal further information about CPAF substrate binding specificity.

A few proteins continued to be cleaved or degraded when precautions were taken to inhibit CPAF activity during lysate preparation, and these substrates may be targeted intracellularly. As we discussed above, vimentin and LAP-1 may be CPAF substrates during late times in the chlamydial developmental cycle. However, these substrates need to be re-evaluated including controls that show CPAF activity was blocked in the lysates where proteolysis was detected (74). Besides CPAF itself, one other chlamydial protein, OmcB, appears to be an intracellular CPAF substrate. OmcB was reported to be cleaved when precautions were taken to inhibit *in vitro* CPAF activity (186). We examined OmcB cleavage in our lysates prepared in 8M urea and confirmed the detection of OmcB C-terminal fragments (data not shown).

### **What is the role of CPAF?**

The CPAF-null mutant demonstrates that CPAF is not necessary for a successful chlamydial infection in cell culture. These results suggest that the role of CPAF is either minor or redundant with other mechanisms to support the intracellular *Chlamydia* infection. It is

possible, however, that CPAF plays an important role in the context of a physiological infection that cannot be detected from cell culture experiments. Future experiments in which mouse models are infected with CPAF-null mutant *Chlamydia* will help elucidate the role of CPAF in an animal infection.

CPAF's putative intracellular substrates indicate a potential function for this chlamydial protease in mediating bacterial exit. Cleavage of vimentin and LAP-1 by CPAF during inclusion rupture is proposed to play a role host cell lysis (74). However, CPAF-null mutant *Chlamydia* were still able to facilitate host cell lysis in the absence of proteolysis of vimentin or LAP-1 (74), which suggests that CPAF-mediated proteolysis is not necessary for bacterial release. CPAF, therefore, may help facilitate the events leading up to host cell lysis, but it does not appear to be an essential regulator. CPAF's broad specificity and potent enzymatic activity could logically aid bacterial exit by degrading host cell proteins to promote lysis and the spread of new progeny, but further investigation is necessary to characterize the role of CPAF in this process. One approach to characterize bacterial exit in CPAF-null mutant *Chlamydia* would be to use a fluorescence label to monitor lysis and extrusion in live cells, as has been done in other studies (42). GFP expressed in the host cytosol is excluded from the inclusion, and lysis is distinguishable from extrusion because it results in rupture of the inclusion membrane. These experiments could help determine whether host cell lysis is altered in function or timing compared to wildtype chlamydia, and additionally would reveal whether CPAF plays a role in the other bacterial exit strategy, extrusion.

CPAF's putative chlamydial substrate, OmcB, is a chlamydial outer membrane complex protein that may function as an adhesin for chlamydial invasion (187, 188) and is important for cell wall stability in EBs (189). OmcB was observed to be cleaved at mid to late times during the

infection which suggests that cleavage could be important for preparing EBs for the next round of infection (186). OmcB has also been implicated as an important protein for the conversion of RBs to EBs (189, 190), which could implicate CPAF as a regulator of conversion. However, the Valdivia group's experiments with the CPAF-null mutant indicate that loss of this protease does not greatly affect infectious progeny (74). CPAF-null mutants experienced a threefold reduction in progeny, which only suggests a minor role for CPAF in producing infectious EBs (74). The importance of CPAF-mediated cleavage of OmcB has not been tested directly in intact infected cells. Zhong *et al.* have proposed a role for the product of OmcB cleavage in host organism immunity. The OmcB C-terminal fragment accesses the host cytosol and is immunogenic in humans (105). Although modulation of immune response may be a functional consequence of OmcB cleavage in humans, it seems unlikely that it is the main role of CPAF since CPAF is conserved in chlamydial species that infect lower organisms.

CPAF homology to other enzymes suggests it may function as a general degradation protease. CPAF's only structural homolog is the C-terminal processing protease D1P (66). D1P is an essential plant serine protease involved in photosynthesis. D1P recognizes its substrate, D1 polypeptide, via a PDZ binding domain that interacts with the C-terminal sequence of the polypeptide (191). Unlike D1P, CPAF does not appear to have very selective substrate specificity. CPAF's active site resembles tricorn protease encoded by the archaeon *Thermoplasma acidophilum* (66). Tricorn is part of a multisubunit proteolytic complex with multicatalytic activities that resembles the proteasome (192). CPAF's active site also seems to share features with the proteasome and two other serine proteases, cathepsin A and tripeptidyl peptidase II, because all of these enzymes are inhibited by lactacystin. Cathepsin A is a lysosomal serine carboxypeptidase that plays a role in degrading proteins in the lysosome (193,

194). Tripeptidyl peptidase II is a cytosolic enzyme postulated to participate in extralysosomal polypeptide degradation that may be able to substitute for the proteasome function in some cases (195). If CPAF serves a function similar to its homologs, then it may play a role as a general proteasome-like degradation machinery to recycle amino acids for use during the chlamydial infection.

Our studies on CPAF have led to a shift in *Chlamydia* biology both in the understanding of this chlamydial protease and in the experimental methods used to analyze *Chlamydia*-infected cells. Our findings will be helpful for guiding future studies to identify CPAF substrates and function, but also have general implications in the experimental handling of *Chlamydia*-infected cells.

## Exploring new frontiers in *Chlamydia* visualization

Our 3D-EM studies of *Chlamydia*-infected cells began as a qualitative approach to visualize entire inclusions, but developed into a valuable quantitative technique that provided us with several novel insights into chlamydial development and its regulation. We originally became interested in 3D-EM as a visualization method to provide an image of an entire *Chlamydia*-infected cell for a book cover (28). After processing the first sample, however, it became clear that 3D-EM provides more than just a visually impressive image. We realized the potential of this technique to provide precise quantitative data about *Chlamydia* and the inclusion.

We had to develop several tools and protocols to be able to extract quantitative data from our 3D reconstructions of *Chlamydia* inclusions. For instance, we established segmentation protocols to accurately and consistently mark each chlamydial form. Since several different people were completing the segmentation, we spent many hours comparing our analyses to ensure we were consistent about the definition of each chlamydial form and how we marked it. We made several attempts to automate the segmentation procedure using machine learning, but found that automated segmentation still required time-intensive manual correction for chlamydial forms that were missed or incorrectly categorized. Future 3D-EM studies will focus more on the development of these automated techniques because they will be helpful for analyzing larger populations of cells efficiently. Another challenge we faced was determining the best way to analyze the 3D-EM data. We experimented with different methods to measure certain parameters, for instance chlamydial volume, which resulted in back and forth analyzing and re-analyzing the same inclusion in different ways. Now that we have established 3D-EM for *Chlamydia*-infected cells, future studies will remain work-intensive, but a lot more streamlined.

Our 3D-EM time course study represents the first complete quantitative analysis of entire inclusions and their contents. We were able to precisely measure the number, volume, and spatial location of each chlamydial form and how each of these factors changed over time. These data do not simply provide numbers, but can be related to each other to determine important relationships that govern the developmental cycle. For example, we related the average populations of RBs to dividing RBs at each time point and observed that the ratio was maintained at 1:1 until 36 hpi, suggesting that RB replication rate is constant for most of the developmental cycle. One limitation of 3D-EM is that we cannot track a single cell over time, but population averages and relationships between numbers in one inclusion can still provide information about the dynamics of chlamydial development.

Another advantage of 3D-EM is that analysis is on the level of a single infected cell. We found that there is heterogeneity between cells on the same infected monolayer which was previously uncharacterized. Other methods to measure the progression of chlamydial development, like genome copy analysis and progeny assays, are based on large populations of cells, which masks variability between infected cells.

Our 3D-EM studies have demonstrated how powerful a visualization technique is for making new observations and deriving new hypotheses. Advances in technology have forged the way for studies of chlamydial development that address new hypotheses (such as the RB size model of chlamydial development that we propose here). Older studies can also be revisited with the 3D-EM method to provide new insights into previously described effects on chlamydial development that may have been limited based on existing experimental methods.

## Future directions with 3D-EM

### Address new hypotheses

#### Is asynchrony in chlamydial development intrinsic to the intracellular infection?

We observed asynchronous chlamydial development between infected cells on the same monolayer beginning at 12 hpi. Our infection protocol utilized centrifugation to synchronize binding of *Chlamydia* to the HeLa cell surface in an attempt to coordinate chlamydial development in the population of infected cells. Another commonly used method to synchronize an infection on a monolayer of cells is to perform the centrifugation of EBs at 4°C followed by a shift to 37°C to coordinate uptake of EBs (93). A 3D-EM analysis comparing these two infection protocols could elucidate whether either experimental technique reduces asynchrony in chlamydial development or whether this asynchrony is intrinsic to the infection.

Another experimental source of asynchrony could be the host cells. We did not synchronize our HeLa cells in the cell cycle, which could have led to another source of asynchrony in bacterial attachment or uptake. A future 3D-EM investigation comparing early infection events in synchronized and unsynchronized HeLa cells would reveal whether the host cell cycle stage affects the level of asynchrony in chlamydial development.

#### How does chlamydial development proceed in other *Chlamydia* species?

We would like to conduct time course studies of infections with other species of *Chlamydia* by 3D-EM to compare development to *C. trachomatis*. All chlamydial species proceed through a conserved biphasic development (24), but there are some timing and phenotypic variations between chlamydial infections that could be quantitatively assessed by 3D-EM. For example, the *C. pneumoniae* infectious cycle lasts longer than that of *C. trachomatis*, so it would be interesting to compare the timing of critical events like RB-to-EB conversion

between these species. *C. psittaci* has an invaginated rather than a spherical inclusion like *C. trachomatis*. Thus, it would be interesting to compare the localization of chlamydial forms in this altered intracellular environment to see if they exhibit enhanced contact with the inclusion membrane due to its increased surface area. According to the contact-dependent model, we would also predict that enhanced contact of *C. psittaci* RBs with the inclusion membrane would lead to delayed conversion timing compared to *C. trachomatis*.

#### Does the size of the host cell affect chlamydial development?

We observed by 3D-EM that *C. trachomatis* inclusions expanded to take up a large proportion of host cell volume by 40 hpi and our analysis by light microscope indicates that inclusions can continue to grow until 60 hpi. In contrast, mouse L929 fibroblasts infected with the same strain of *C. trachomatis* begin to lyse around 48 hpi by light microscope. HeLa cells are larger than mouse fibroblasts, which led us to question whether host cell size affects the length and progression of the chlamydial developmental cycle. *C. trachomatis* can infect many human cells in culture including epithelial cells, fibroblasts, and macrophages (196, 197). Using 3D-EM, we could examine the progression of *C. trachomatis* in each of these cell types quantifying total host cell volume and inclusion growth, as well as counting chlamydial forms to monitor progression and timing of RB-to-EB conversion.

In Chapter 5, we discussed how we could conduct experiments using the 3D-EM method that would provide further experimental support for our proposed model of size-dependent regulation of chlamydial development. According to our model, it is important for RBs to regulate their size so that they continually decrease in volume approaching a permissive size for conversion. The mechanism by which RBs regulate their size, however, is unknown. Once RBs achieve a permissive size, it is unclear what factors influence their decision to convert. In the

next two sections we look to other biological systems to identify possible mechanisms to regulate RB size and RB-to-EB conversion.

## Cell size regulation

In many biological systems, cells impose regulatory systems to maintain an average cell size (198, 199). We have observed that *Chlamydia* RBs are an anomaly in that their average size gradually decreases over the developmental cycle. By examining the mechanisms by which other cells achieve cell size homeostasis, we may be able to postulate how *Chlamydia* could produce a decrease in size over time.

### Sizers

Cells under the control of a sizer actively monitor their size and trigger conversion at a particular critical size. Yeast *Schizosaccharomyces pombe* use a sizer mechanism that relies on a spatial gradient to sense cell length. A mitotic activator is localized to the middle of the cell while an inhibitor of the activator exists in a gradient from the cell poles. As the cell elongates, the amount of inhibitor interacting with the activator decreases and drives mitosis (198). In bacterial cells, the conserved Min system proteins create a spatial gradient in a similar manner to regulate location of septal formation. MinC and MinD proteins are distributed in a concentration gradient from the poles of rod-shaped cells, inhibiting septal formation at the cell poles (200). *Chlamydia* encode a protein with homology to *E. coli* MinD, but do not encode homologs to any other Min system proteins (201). MinD could establish a spatial gradient for RBs to sense cell size, but since RBs are generally spherical, the gradient would need to be established along the spherical surface. To account for a decrease in RB size over successive cell divisions, we would expect that the expression level of MinD protein in RBs decreases over time to allow the spatial gradient to be modulated over the developmental time course. The MinD protein expression and

localization pattern in *Chlamydia* has not been characterized, but this type of sizer mechanism could theoretically be modified to produce decreasing RB size over time.

Yeast *Saccharomyces cerevisiae* utilize a protein synthesis rate-based sensor to detect cell size. A division-promoting sizer protein is synthesized at a rate proportional to overall protein synthesis and once the protein reaches a threshold level the cell divides (198). Bacteria such as *E. coli* and *B. subtilis* have been shown to use the division protein FtsZ as a sizer in a protein synthesis sensor mechanism. FtsZ is the major protein organizer of bacterial division and its amount is proportional to cell size. Once FtsZ reaches a threshold level the cell divides (199). Although FtsZ is a common sizer in other bacteria, *Chlamydia* do not encode a homolog of FtsZ (47, 202). MreB, an actin homolog, has been proposed to substitute for FtsZ function in *Chlamydia* to coordinate the division process (201). MreB is recruited to the division septum by interacting with another protein, RodZ (201). Either MreB or RodZ may be candidate proteins to act as chlamydial sizers to regulate division. However, it is difficult to reconcile how a protein synthesis rate-based sensor could facilitate decreasing RB size over successive divisions. If a threshold level of MreB, for example, is required to coordinate bacterial division, then a small RB with less MreB would be incapable of division. Thus, using this sizer mechanism it is difficult to see how RB cell size could decrease over time.

*Mycobacterium smegmatis* cells appear to utilize a “sloppy” sizer. Rather than trigger division at a particular size, cells become licensed to divide upon reaching a minimal size. From that point, division is a random process with a size-dependent probability (203). “Sloppy” sizer control tolerates division at a wider range of cell sizes and leads to a more heterogeneous population of cells. We observed that RB populations were heterogeneous in size, and a model incorporating size-dependent probability of division reproduced the observed ranges in RB size

and convergence toward a minimal average size that we saw in our experimental data. The “sloppy” sizer can be tuned to produce cells that get smaller over successive divisions when the probability distribution of division is shifted to favor division at smaller sizes. In this way, cells will converge towards a smaller RB size after several replications instead of maintaining homeostasis. Cells that use “sloppy” sizer mechanisms still require a signal to know their size; thus, “sloppy” sizer control could potentially be combined with a protein sizer spatial gradient to regulate decreasing RB size in *Chlamydia*.

### **Timers**

Cells under the control of a timer grow for a specific amount of time prior to division. In yeast, cell cycle time is controlled coordinately with cell sizers. In *S. pombe*, extended cell cycle times produce larger cells while shorter cell cycle times produce smaller cells (204). A timer acts to control the period between S phase and the start of nuclear division such that division occurs only after a minimum amount of time, preventing formation of daughter cells that are too small (205). *S. cerevisiae* cells regulate the length of G1 to control the size of the cell prior to division (206).

Little is known about chlamydial regulation of RB cell cycle time. Using population based measurements of chlamydial genome copies over time, RB doubling time has been calculated to be 2-3 hours (45, 154). Our 3D-EM analysis comparing RB population growth over 4 hour increments suggests a doubling time of 1.93 hours between 12 and 24 hpi. However, neither genome copy analysis nor 3D-EM is able to measure the length of a single RB cell cycle. Genome copy analysis averages gene expression from a large population of cells, and 3D-EM only captures snapshots of the chlamydial developmental cycle and cannot track a single form over time. The obligate intracellular lifestyle of *Chlamydia* makes it hard to study individual

RBs. If RBs could be grown in axenic media, we may be able to track single chlamydiae using live-cell microscopy or flow cytometry as has been done for other single cell studies of yeast and bacteria (198, 199). Flow cytometric analysis of lymphocytes effectively monitored cell proliferation over 8-10 discrete replication cycles by serial halving of a fluorescent vital dye (CFSE) (207). If RBs could be successfully isolated and induced to replicate outside of a host cell, we could determine precise RB replication time by transforming *Chlamydia* with a plasmid encoding a fluorescent protein that is evenly partitioned between daughter cells then tracking RB divisions by flow cytometry. It seems, though, that even if axenic replication of RBs is possible, it may not be representative of the situation in a *Chlamydia*-infected cell. RBs have been shown to be metabolically active in a formula of axenic media, but their transcription profiles were not the same as during an *in vivo* intracellular infection (208). In order to achieve a decrease in RB size over the infectious cycle using a timer mechanism, replication cycles would need to become increasingly shorter. We need an experimental technique to be able to measure individual RB replication cycle time in order to determine what the time is and whether it stays constant or changes over the developmental time course. Until we can profile the cell cycle of an RB, it will be difficult to determine whether a timer plays a role in regulating RB size.

### **Constant size extension**

The constant size extension model, or adder principle, was recently proposed as an alternative mechanism to regulate cell size. In this model, cells increase their size by a set amount prior to division. The amount that a cell grows between divisions is dependent on growth conditions and can vary between individual cells (170, 209).

Constant size extension could be modulated by *Chlamydia* to produce cells that decrease in size over time. If RBs start out at an initial large size and only grow by a small amount

between divisions, progeny RBs would decrease in size over successive divisions. However, if the constant size extension were the mechanism of size regulation in *Chlamydia*, we would expect more homogeneity in RB sizes. For example, an infection beginning with a single RB should have two daughter RBs of same size after the first division. We have visualized inclusions with two RBs (after the first division) and observed that they are quite variable in size (about 20% difference). Additionally, with a constant size extension mechanism we would expect all RBs to consistently decrease in size, never remain the same or increase in size. Our analysis of individual RB size at 40 hpi indicated that some RBs were the same size or larger than those observed at 12 hpi. Thus, our 3D-EM observations do not seem to support constant size extension as the mechanism of size regulation in *Chlamydia*.

## **Regulators of cell fate in other systems**

The decision of an RB to convert into an EB can be viewed as a cell fate decision. According to our model of chlamydial development, once an RB achieves a permissive size for conversion it decides whether or not to actually convert into an EB. Other biological systems are faced with similar decisions and are often guided by environmental factors to make a determination of the path to follow. In this section we will discuss four mechanisms that govern cell fate decision in response to nutrient availability, population size, cell stress, and niche. In looking to other systems, we may gain insights into the factors that could possibly trigger RB-to-EB conversion.

### ***Coxiella burnetii* LCV to SCV conversion**

Development of *Chlamydia* is most similar to that of another intracellular pathogen, *Coxiella burnetii*. *Coxiella* is an intracellular bacterial pathogen morphologically similar to *Rickettsia*. It resides in a parasitophorous vacuole similar to the chlamydial inclusion and has a

similar developmental cycle (210). *Coxiella* has distinct morphological forms that are analogous to chlamydial EBs and RBs. Small cell variants (SCVs) are small and infectious, like EBs, while large cell variants (LCVs) are larger and replicate by binary fission, similar to RBs (210). The *Coxiella* developmental cycle proceeds very similarly to the *Chlamydia* developmental cycle. First, an SCV converts into an LCV during an initial differentiation phase. LCVs then undergo replication prior to re-differentiation back into SCVs at the end of infection. The nutritional status of the host cell (as detected by metabolites like amino acids) is proposed to regulate LCV to SCV conversion (211).

*Chlamydia* could potentially use levels of host cell metabolites as a signal for RB-to-EB conversion, similarly to *Coxiella*. Tying the regulation of RB-to-EB conversion to host cell resources is a smart strategy because then the bacteria ensure the timing of the production of infectious forms coordinates with the viability of their intracellular niche. *Chlamydia* rely on many metabolites from the host cell to support the intracellular infection and encode transporters for amino acids, ATP, and inorganic chemicals (magnesium, phosphate, nitrate, and sulfate) (47). Differences in local concentrations of nutrients within the inclusion could also explain the asynchrony we observe in RB-to-EB conversion. Depending on their location, some RBs may receive more of a metabolite and continue replicating while other RBs receive less and are signaled to convert to EBs.

### ***Bacillus subtilis* sporulation**

*B. subtilis* are rod-shaped bacteria that can undergo two types of division. During normal division, the bacteria double in length then divide centrally to yield two identical daughter cells. Sporulation, on the other hand, is an asymmetric division yielding one environmentally stable endospore packaged into a resistant coat (212). The decision to sporulate is based on

environmental factors including nutritional signals and population density. *B. subtilis* monitor carbon, nitrogen, and phosphorus availability to assess their environment. When these critical nutrients are in low supply sporulation is triggered. *B. subtilis* also sense their population size using an extracellular peptide that acts as a sporulation stimulating factor. Only dense populations of bacteria can be induced to sporulate efficiently (213).

Onset of RB-to-EB conversion in *Chlamydia* only occurs after a period of RB replication, so it is possible that population density plays a role in regulating the conversion process. Similarly to *B. subtilis*, RBs could secrete a peptide or other molecule into the inclusion. As the population of RBs grows the signal would reach a threshold level, triggering conversion. However, if a secreted signal stimulated RB-to-EB conversion we would expect a more coordinated response. Instead, we observe asynchrony of RB-to-EB conversion resulting in some RBs that convert at 24 hpi and others that convert at 40 hpi. No obvious quorum sensing system has been detected thus far within the chlamydial inclusion.

### **Bacteriophage $\lambda$ lytic/lysogenic decision**

Upon entry into a host *E. coli* cell, the bacteriophage  $\lambda$  must decide whether to pursue lytic or lysogenic development. Lytic growth is a productive cycle in which progeny phage particles are released through bacterial lysis. The lysogenic cycle is a latent or dormant state in which  $\lambda$  DNA incorporates into the host genome and is replicated with the bacterial host chromosome. Phage later exit the lysogenic phase and switch to a lytic cycle to produce progeny (214). Regulatory factor CII acts as a gene regulation switch and dictates whether the phage will go through lytic or lysogenic development. Low levels of CII promote lytic development and high levels of CII activate a lysogenic transcriptional profile to coordinate a lysogenic cycle (215). Environmental factors like multiplicity of infection and nutrient status influence the levels

of CII and regulate the lytic/lysogenic switch. Each viral particle produces CII, so MOI is sensed based on population density. Nutrient status is thought to be detected through cyclic AMP levels (215).

Lysogenic phage  $\lambda$  must make an additional fate decision about when to transition to a lytic cycle. The transition generally occurs in response to a bacterial SOS stress response in unfavorable environments. An SOS response can be elicited in the host *E. coli* cell by several environmental factors including UV damage, drug or antibiotic treatment, hydrogen peroxide exposure, or starvation (216).

Similar to phage  $\lambda$ , *Chlamydia* invade a host cell and are dependent upon the host to provide an intracellular niche. If *Chlamydia* could sense host cell status, it could ensure its own survival by regulating conversion to switch on prior to host cell death. *Chlamydia* appear to dampen host protective pathways by decreasing ROS production early and inhibiting apoptosis during mid-cycle (76, 217). Since *Chlamydia* are modulating these host stress signaling pathways, it seems unlikely they would use them as a sensor to monitor the host cell condition.

### **Stem Cell Fate**

Stem cells have the capacity to self-renew or generate differentiated progeny. Environmental features of the stem cell niche are important regulators of cell fate in *C. elegans*. In the *C. elegans* germline, distal tip cells produce a ligand that promotes stem cell divisions. As the stem cell pool expands, some cells are displaced and forced further away from the ligand source causing them to differentiate (218). In this system, differentiation is repressed by a maintenance signal that promotes stem cell division.

The type III secretion dependent contact-dependent model proposes *Chlamydia* RB and EB regulation occurs similarly to *C. elegans* stem cell fate regulation. For *Chlamydia* RBs, the

niche that promotes RB fate is the inclusion membrane. In the model, RB contact with the inclusion membrane provides a signal for RBs to continue replicating while detachment removes the signal and results in conversion. There is experimental evidence that inhibition of type III secretion (T3S) results in decreased RB replication (157, 173), suggesting T3S signaling is either directly or indirectly important for RB division. However, it is unclear whether the signal that promotes *Chlamydia* to remain an RB is a T3S effector or another molecule located at the inclusion membrane surface. Unlike in the *C. elegans* germline, our 3D-EM observations of chlamydial inclusions do not reveal any correlation between physical crowding and loss of RB contact with the inclusion membrane. Thus, *Chlamydia* appear to regulate RB contact with the inclusion membrane through another mechanism. We have proposed that RB size could be the regulator that causes chlamydiae to lose their RB signal and trigger conversion.

Overall, these comparisons lead us to hypothesize that regulation of decreasing RB size over the developmental cycle is coordinated by a protein spatial gradient that operates based on a “sloppy” sizer principle. We also hypothesize that proximity to the inclusion membrane promotes RB maintenance while inhibiting RB-to-EB conversion. The signal that promotes RB identity may be located within the inclusion membrane, secreted through the T3S projection, or be a diffusible factor that accumulates at the inclusion membrane border.

## **Summary**

The work described in this thesis makes significant contributions to two major fields of study in *Chlamydia* biology: CPAF and the developmental cycle. Our CPAF studies challenged previously held beliefs about the role of this chlamydial protease, and provoked a major re-assessment of CPAF substrates, protease function, and importance to the chlamydial infection.

We developed recommendations for how to handle *Chlamydia*-infected cells to prevent *in vitro* CPAF activity and avoid artifactual proteolysis, which will be useful to guide future studies of proteins within *Chlamydia*-infected cells. Our 3D-EM studies of the intracellular *Chlamydia* infection provided the first quantitative analysis of entire inclusions over the chlamydial developmental time course. We were able to provide detailed reports of the number and type of each developmental form, as well as accurately quantify volume and distances. Through our 3D-EM observations we described novel aspects of chlamydial development, including decreasing RB size over time and heterogeneity of RB size within a single inclusion. Based on our 3D-EM analysis, we proposed a new model of the regulation of chlamydial development based on RB size. We propose that RBs grow to an initial large size prior to beginning replication. Successive replication cycles produce RBs of decreasing average size because replication is regulated to occur prior to the RB doubling in size. Over time, RBs approach a small threshold size that licenses them for conversion.

Our model accounts for several characteristic features of chlamydial development including decreasing RB size, RB heterogeneity, delayed onset of RB-to-EB conversion, and asynchrony of conversion events. The 3D-EM technique represents a significant technological advance in the chlamydial field that will be essential to address questions about the regulation of chlamydial development and allow quantitative analysis in any future studies of the intracellular *Chlamydia* infection.

## References

1. **Nunes A, Gomes JP.** 2014. Evolution, phylogeny, and molecular epidemiology of Chlamydia. *Infect Genet Evol* **23**:49–64.
2. **Van Droogenbroeck C, Van Risseghem M, Braeckman L, Vanrompay D.** 2009. Evaluation of bioaerosol sampling techniques for the detection of *Chlamydochlamydia psittaci* in contaminated air. *Vet Microbiol* **135**:31–37.
3. **Rowley J, Toskin I, Ndowa F.** 2012. Global incidence and prevalence of selected curable sexually transmitted infections, 2008.
4. **Grayston JT, Campbell LA, Kuo C-C, Mordhorst CH, Saikku P, Thorn DH, Wang S-P.** 1990. A New Respiratory Tract Pathogen: *Chlamydia pneumoniae* Strain TWAR. *Journal of Infectious Diseases* **161**:618–625.
5. **Hahn DL, Dodge RW, Golubjatnikov R.** 1991. Association of *Chlamydia pneumoniae* (Strain Twar) Infection with Wheezing, Asthmatic Bronchitis, and Adult-Onset Asthma. *JAMA* **266**:225–230.
6. **O'Connor S, Taylor C, Campbell LA, Epstein S, Libby P.** 2001. Potential infectious etiologies of atherosclerosis: A multifactorial perspective. *Emerging Infect Dis* **7**:780–788.
7. **Thomson NR, Holden MTG, Carder C, Lennard N, Lockey SJ, Marsh P, Skipp P, O'Connor CD, Goodhead I, Norbertzcak H, Harris B, Ormond D, Rance R, Quail MA, Parkhill J, Stephens RS, Clarke IN.** 2007. *Chlamydia trachomatis*: Genome sequence analysis of lymphogranuloma venereum isolates. *Genome Research* **18**:161–171.
8. **Wright HR, Turner A, Taylor HR.** 2008. Trachoma. *Lancet* **371**:1945–1954.
9. **Burton MJ, Mabey DCW.** 2009. The Global Burden of Trachoma: A Review. *PLoS Negl Trop Dis* **3**:e460.
10. **Burton MJ.** 2007. Trachoma: an overview. *Br Med Bull* **84**:99–116.
11. **US Department of Health and Human Services, Centers for Disease Control and Prevention.** 2015. Sexually Transmitted Disease Surveillance 2014.
12. **Fehlner-Gardiner C, Roshick C, Carlson JH, Hughes S, Belland RJ, Caldwell HD, McClarty G.** 2002. Molecular basis defining human *Chlamydia trachomatis* tissue tropism. A possible role for tryptophan synthase. *J Biol Chem* **277**:26893–26903.

13. **Naucler P, Chen H-C, Persson K, You S-L, Hsieh C-Y, Sun C-A, Dillner J, Chen C-J.** 2007. Seroprevalence of human papillomaviruses and Chlamydia trachomatis and cervical cancer risk: nested case-control study. *J Gen Virol* **88**:814–822.
14. **Smith JSJ, Bosetti CC, Muñoz NN, Herrero RR, Bosch FFX, Eluf-Neto JJ, Meijer CJLMC, Van Den Brule AJCA, Franceschi SS, Peeling RWR.** 2004. Chlamydia trachomatis and invasive cervical cancer: a pooled analysis of the IARC multicentric case-control study. *Int J Cancer* **111**:431–439.
15. **da Silva Barros NK, Costa MC, Alves RRF, Villa LL, Derchain SFM, Zeferino LC, Santos Carneiro Dos MA, Rabelo-Santos SH.** 2012. Association of HPV infection and Chlamydia trachomatis seropositivity in cases of cervical neoplasia in Midwest Brazil. *J Med Virol* **84**:1143–1150.
16. **Arnheim Dahlström L, Andersson K, Luostarinen T, Thoresen S, Ögmundsdóttir H, Tryggvadóttir L, Wiklund F, Skare GB, Eklund C, Sjölin K, Jellum E, Koskela P, Wadell G, Lehtinen M, Dillner J.** 2011. Prospective seroepidemiologic study of human papillomavirus and other risk factors in cervical cancer. *Cancer Epidemiol Biomarkers Prev* **20**:2541–2550.
17. **Walboomers JM, Jacobs MV, Manos MM, Bosch FX, Kummer JA, Shah KV, Snijders PJ, Peto J, Meijer CJ, Muñoz N.** 1999. Human papillomavirus is a necessary cause of invasive cervical cancer worldwide. *J Pathol* **189**:12–19.
18. **Koskela PP, Anttila TT, Bjørge TT, Brunsvig AA, Dillner JJ, Hakama MM, Hakulinen TT, Jellum EE, Lehtinen MM, Lenner PP, Luostarinen TT, Pukkala EE, Saikku PP, Thoresen SS, Youngman LL, Paavonen JJ.** 2000. Chlamydia trachomatis infection as a risk factor for invasive cervical cancer. *Int J Cancer* **85**:35–39.
19. **Anttila TT, Saikku PP, Koskela PP, Bloigu AA, Dillner JJ, Ikäheimo II, Jellum EE, Lehtinen MM, Lenner PP, Hakulinen TT, Närvänen AA, Pukkala EE, Thoresen SS, Youngman LL, Paavonen JJ.** 2001. Serotypes of Chlamydia trachomatis and risk for development of cervical squamous cell carcinoma. *JAMA* **285**:47–51.
20. **Knowlton AE, Fowler LJ, Patel RK, Wallet SM, Grieshaber SS.** 2013. Chlamydia induces anchorage independence in 3T3 cells and detrimental cytological defects in an infection model. *PLoS ONE* **8**:e54022–e54022.
21. **Grieshaber SS, Grieshaber NA, Miller N, Hackstadt T.** 2006. Chlamydia trachomatis causes centrosomal defects resulting in chromosomal segregation abnormalities. *Traffic* **7**:940–949.
22. **Johnson KA, Tan M, Sütterlin C.** 2009. Centrosome abnormalities during a Chlamydia trachomatis infection are caused by dysregulation of the normal duplication pathway. *Cell Microbiol* **11**:1064–1073.

23. **Anderhub SJ, Krämer A, Maier B.** 2012. Centrosome amplification in tumorigenesis. *Cancer Lett* **322**:8–17.
24. **Abdelrahman YM, Belland RJ.** 2005. The chlamydial developmental cycle. *FEMS Microbiol Rev* **29**:949–959.
25. **Matsumoto A, Bessho H, Uehira K, Suda T.** 1991. Morphological studies of the association of mitochondria with chlamydial inclusions and the fusion of chlamydial inclusions. *J Electron Microsc (Tokyo)* **40**:356–363.
26. **Hatch TP.** 1996. Disulfide cross-linked envelope proteins: The functional equivalent of peptidoglycan in chlamydiae? *J Bacteriol* **178**:1–5.
27. **Zhang JP, Stephens RS.** 1992. Mechanism of C-Trachomatis Attachment to Eukaryotic Host-Cells. *Cell* **69**:861–869.
28. **Tan M, Bavoil P.** 2012. *Intracellular Pathogens I.* American Society for Microbiology Press.
29. **Puolakkainen M, Kuo CC, Campbell LA.** 2005. Chlamydia pneumoniae Uses the Mannose 6-Phosphate/Insulin-Like Growth Factor 2 Receptor for Infection of Endothelial Cells. *Infect Immun* **73**:4620–4625.
30. **Abromaitis S, Stephens RS.** 2009. Attachment and Entry of Chlamydia Have Distinct Requirements for Host Protein Disulfide Isomerase. *PLoS Pathog* **5**:e1000357.
31. **Ward ME, Murray A.** 1984. Control Mechanisms Governing the Infectivity of Chlamydia-Trachomatis for Hela-Cells - Mechanisms of Endocytosis. *J Gen Microbiol* **130**:1765–1780.
32. **Dautry-Varsat A, Balañá ME, Wyplosz B.** 2004. Chlamydia- Host Cell Interactions: Recent Advances on Bacterial Entry and Intracellular Development. *Traffic* **5**:561–570.
33. **Boleti H, Benmerah A, Ojcius DM, Cerf-Bensussan N, Dautry-Varsat A.** 1999. Chlamydia infection of epithelial cells expressing dynamin and Eps15 mutants: clathrin-independent entry into cells and dynamin-dependent productive growth. *J Cell Sci* **112 (10)**:1487–1496.
34. **Carabeo RA, Grieshaber SS, Fischer E, Hackstadt T.** 2002. Chlamydia trachomatis Induces Remodeling of the Actin Cytoskeleton during Attachment and Entry into HeLa Cells. *Infect Immun* **70**:3793–3803.
35. **Hackstadt T, Carlson MS.** 1999. The Chlamydia trachomatis IncA protein is required for homotypic vesicle fusion. *Microbiology* **1**:119–130.

36. **Lutter EI, Martens C, Hackstadt T.** 2012. Evolution and Conservation of Predicted Inclusion Membrane Proteins in Chlamydiae. *Comp Funct Genomics* **2012**:1-13.
37. **Hackstadt T, Fischer ER, Scidmore MA, Rockey DD, Heinzen RA.** 1997. Origins and functions of the chlamydial inclusion. *Trends Microbiol* **5**:288–293.
38. **Fields KA, Hackstadt T.** 2002. The Chlamydial Inclusion: Escape from the Endocytic Pathway. *Annu Rev Cell Dev Biol* **18**:221–245.
39. **Carabeo RA, Mead DJ, Hackstadt T.** 2003. Golgi-dependent transport of cholesterol to the Chlamydia trachomatis inclusion. *PNAS* **100**:6771–6776.
40. **Taraska T, Ward DM, Ajioka RS, Wyrick PB.** 1996. The late chlamydial inclusion membrane is not derived from the endocytic pathway and is relatively deficient in host proteins. *Infection and ...*
41. **Belland RJ, Zhong G, Crane DD, Hogan D, Sturdevant D, Sharma J, Beatty WL, Caldwell HD.** 2003. Genomic transcriptional profiling of the developmental cycle of Chlamydia trachomatis. *PNAS* **100**:8478–8483.
42. **Hybiske K, Stephens RS.** 2007. Mechanisms of Chlamydia trachomatis entry into nonphagocytic cells. *Infect Immun* **75**:3925–3934.
43. **Hybiske KK, Stephens RSR.** 2007. Mechanisms of host cell exit by the intracellular bacterium Chlamydia. *PNAS* **104**:11430–11435.
44. **Chin E, Kirker K, Zuck M, James G, Hybiske K.** 2012. Actin Recruitment to the Chlamydia Inclusion Is Spatiotemporally Regulated by a Mechanism That Requires Host and Bacterial Factors. *PLoS ONE* **7**:e46949.
45. **Shaw EI, Dooley CA, Fischer ER, Scidmore MA, Fields KA, Hackstadt T.** 2000. Three temporal classes of gene expression during the Chlamydia trachomatis developmental cycle. *Molecular Microbiology* **37**:913–925.
46. **Scidmore MA, Fischer ER, Hackstadt T.** 2003. Restricted Fusion of Chlamydia trachomatis Vesicles with Endocytic Compartments during the Initial Stages of Infection. *Infect Immun* **71**:973–984.
47. **Stephens RS, Kalman S, Lammel C, Fan J, Marathe R, Aravind L, Mitchell W, Olinger L, Tatusov RL, Zhao Q, Koonin EV, Davis RW.** 1998. Genome sequence of an obligate intracellular pathogen of humans: Chlamydia trachomatis. *Science (New York, NY)* **282**:754–759.
48. **Saka HA, Valdivia RH.** 2010. Acquisition of nutrients by Chlamydiae: unique challenges of living in an intracellular compartment. *Current Opinion in Microbiology* **13**:4–10.

49. **Heuer D, Lipinski AR, Machuy N, Karlas A, Wehrens A, Siedler F, Brinkmann V, Meyer TF.** 2009. Chlamydia causes fragmentation of the Golgi compartment to ensure reproduction. *Nature* **457**:731–735.
50. **Hackstadt T, Rockey DD, Heinzen RA, Scidmore MA.** 1996. Chlamydia trachomatis interrupts an exocytic pathway to acquire endogenously synthesized sphingomyelin in transit from the Golgi apparatus to the plasma membrane. *EMBO J* **15**:964–977.
51. **Derré I, Swiss R, Agaisse H.** 2011. The Lipid Transfer Protein CERT Interacts with the Chlamydia Inclusion Protein IncD and Participates to ER-Chlamydia Inclusion Membrane Contact Sites. *PLoS Pathog* **7**:e1002092.
52. **Kumar Y, Valdivia RH.** 2008. Actin and intermediate filaments stabilize the Chlamydia trachomatis vacuole by forming dynamic structural scaffolds. *Cell Host Microbe* **4**:159–169.
53. **Fan T, Lu H, Hu H, Shi L, McClarty GA, Nance DM, Greenberg AH, Zhong G.** 1998. Inhibition of apoptosis in chlamydia-infected cells: blockade of mitochondrial cytochrome c release and caspase activation.
54. **Betts HJ, Wolf K, Fields KA.** 2009. Effector protein modulation of host cells: examples in the Chlamydia spp. arsenal. *Current Opinion in Microbiology* **12**:81–87.
55. **Karyagina AS, Alexeevsky AV, Spirin SA, Zigangirova NA, Gintsburg AL.** 2009. Effector proteins of chlamydiae. *Mol Biol* **43**:897–916.
56. **Cocchiario JL, Valdivia RH.** 2009. New insights into Chlamydia intracellular survival mechanisms. *Cell Microbiol* **11**:1571–1578.
57. **Subtil A, Blocker A.** 2000. Type III secretion system in Chlamydia species: identified members and candidates. *Microbes and Infection* **2**:367–369.
58. **Cornelis GR.** 2006. The type III secretion injectisome. *Nat Rev Microbiol* **4**:811–825.
59. **Peters J, Wilson DP, Myers G, Timms P, Bavoil PM.** 2007. Type III secretion à la Chlamydia. *Trends Microbiol* **15**:241–251.
60. **Fields KA, Hackstadt T.** 2000. Evidence for the secretion of Chlamydia trachomatis CopN by a type III secretion mechanism. *Molecular Microbiology* **38**:1048–1060.
61. **Fields KA, Mead DJ, Dooley CA, Hackstadt T.** 2003. Chlamydia trachomatis type III secretion: evidence for a functional apparatus during early-cycle development. *Mol Microbio* **48**:671–683.

62. **Cianciotto NP.** 2005. Type II secretion: a protein secretion system for all seasons. *Trends Microbiol* **13**:581–588.
63. **Chen D, Lei L, Lu C, Flores R, DeLisa MP, Roberts TC, Romesberg FE, Zhong G.** 2010. Secretion of the chlamydial virulence factor CPAF requires the Sec-dependent pathway. *Microbiology* **156**:3031–3040.
64. **Zhong G.** 2009. Killing me softly: chlamydial use of proteolysis for evading host defenses. *Trends Microbiol* **17**:467–474.
65. **Dong F, Zhong Y, Arulanandam B, Zhong G.** 2005. Production of a proteolytically active protein, chlamydial protease/proteasome-like activity factor, by five different *Chlamydia* species. *Infect Immun* **73**:1868–1872.
66. **Huang Z, Feng Y, Chen D, Wu X, Huang S, Wang X, Xiao X, Li W, Huang N, Gu L, Zhong G, Chai J.** 2008. Structural basis for activation and inhibition of the secreted chlamydia protease CPAF. *Cell Host Microbe* **4**:529–542.
67. **Chen D, Lei L, Flores R, Huang Z, Wu Z, Chai J, Zhong G.** 2010. Autoprocessing and self-activation of the secreted protease CPAF in *Chlamydia*-infected cells. *Microbial Pathogenesis* **49**:164–173.
68. **Zhong G, Fan P, Ji H, Dong F, Huang Y.** 2001. Identification of a chlamydial protease-like activity factor responsible for the degradation of host transcription factors. *J Exp Med* **193**:935–942.
69. **Christian JG, Heymann J, Paschen SA, Vier J, Schauenburg L, Rupp J, Meyer TF, Häcker G, Heuer D.** 2011. Targeting of a chlamydial protease impedes intracellular bacterial growth. *PLoS Pathog* **7**:e1002283.
70. **Pirbhai M, Dong F, Zhong Y, Pan KZ, Zhong G.** 2006. The secreted protease factor CPAF is responsible for degrading pro-apoptotic BH3-only proteins in *Chlamydia trachomatis*-infected cells. *J Biol Chem* **281**:31495–31501.
71. **Dong F, Pirbhai M, Xiao YM, Zhong YM, Wu YM, Zhong GM.** 2005. Degradation of the proapoptotic proteins Bik, Puma, and Bim with Bcl-2 domain 3 homology in *Chlamydia trachomatis*-infected cells. *Infect Immun* **73**:1861–1864.
72. **Zhong G, Fan T, Liu L.** 1999. *Chlamydia* inhibits interferon gamma-inducible major histocompatibility complex class II expression by degradation of upstream stimulatory factor 1. *J Exp Med* **189**:1931–1938.
73. **Zhong G, Liu L, Fan T, Fan P, Ji H.** 2000. Degradation of transcription factor RFX5 during the inhibition of both constitutive and interferon gamma-inducible major histocompatibility complex class I expression in *chlamydia*-infected cells. *J Exp Med* **191**:1525–1534.

74. **Snaveley EA, Kokes M, Dunn JD, Saka HA, Nguyen BD, Bastidas RJ, McCafferty DG, Valdivia RH.** 2014. Reassessing the role of the secreted protease CPAF in Chlamydia trachomatis infection through genetic approaches. *Pathog Dis* **0**:1-16.
75. **Chen AL, Johnson KA, Lee JK, Sütterlin C, Tan M.** 2012. CPAF: A Chlamydial Protease in Search of an Authentic Substrate. *PLoS Pathog* **8**:e1002842.
76. **Fischer SF, Vier J, Kirschnek S, Klos A, Hess S, Ying S, Häcker G.** 2004. Chlamydia inhibit host cell apoptosis by degradation of proapoptotic BH3-only proteins. *J Exp Med* **200**:905–916.
77. **Doxsey S.** 2001. Re-evaluating centrosome function. *Nat Rev Mol Cell Biol* **2**:688–698.
78. **Strnad P, Gönczy P.** 2008. Mechanisms of procentriole formation. *Trends Cell Biol* **18**:389–396.
79. **Paschen SA, Christian JG, Vier J, Schmidt F, Walch A, Ojcius DM, Häcker G.** 2008. Cytopathicity of Chlamydia is largely reproduced by expression of a single chlamydial protease. *J Cell Biol* **182**:117–127.
80. **Dong F, Su H, Huang Y, Zhong Y, Zhong G.** 2004. Cleavage of host keratin 8 by a Chlamydia-secreted protease. *Infect Immun* **72**:3863–3868.
81. **Mayor T, Stierhof YD, Tanaka K, Fry AM, Nigg EA.** 2000. The centrosomal protein C-Nap1 is required for cell cycle-regulated centrosome cohesion. *J Cell Biol* **151**:837–846.
82. **Kohlmaier G, LonCarek J, Meng X, McEwen BF, Mogensen MM, Spektor A, Dynlacht BD, Khodjakov A, Gönczy P.** 2009. Overly Long Centrioles and Defective Cell Division upon Excess of the SAS-4-Related Protein CPAP. *Current Biology* **19**:1012–1018.
83. **Yang J, Adamian M, Li TS.** 2006. Rootletin interacts with C-Nap1 and may function as a physical linker between the pair of centrioles/basal bodies in cells. *Mol Biol Cell* **17**:1033–1040.
84. **Leidel S, Delattre M, Cerutti L, Baumer K, Gönczy P.** 2005. SAS-6 defines a protein family required for centrosome duplication in *C. elegans* and in human cells. *Nat Cell Biol* **7**:115–125.
85. **Johnson KA.** 2012. Characterization of Host Centrosome Amplification During Infection with Chlamydia Trachomatis. *Dissertations & Theses* © University of California.

86. **Christian J, Vier J, Paschen SA, Häcker G.** 2010. Cleavage of the NF- $\kappa$ B family protein p65/RelA by the chlamydial protease-like activity factor (CPAF) impairs proinflammatory signaling in cells infected with Chlamydiae. *J Biol Chem* **285**:41320–41327.
87. **Sun J, Schoborg RV.** 2009. The host adherens junction molecule nectin-1 is degraded by chlamydial protease-like activity factor (CPAF) in Chlamydia trachomatis-infected genital epithelial cells. *Microbes Infect* **11**:12–19.
88. **Balsara ZR, Misaghi S, Lafave JN, Starnbach MN.** 2006. Chlamydia trachomatis infection induces cleavage of the mitotic cyclin B1. *Infect Immun* **74**:5602–5608.
89. **Dong F, Sharma J, Xiao Y, Zhong Y, Zhong G.** 2004. Intramolecular dimerization is required for the chlamydia-secreted protease CPAF to degrade host transcriptional factors. *Infect Immun* **72**:3869–3875.
90. **Chen D, Chai J, Hart PJ, Zhong G.** 2009. Identifying catalytic residues in CPAF, a Chlamydia-secreted protease. *Arch Biochem Biophys* **485**:16–23.
91. **Shaw AC, Vandahl BB, Larsen MR, Roepstorff P, Gevaert K, Vandekerckhove J, Christiansen G, Birkelund S.** 2002. Characterization of a secreted Chlamydia protease. *Cell Microbiol* **4**:411–424.
92. **Yu H, Schwarzer K, Förster M, Kniemeyer O, Forsbach-Birk V, Straube E, Rödel J.** 2010. Role of high-mobility group box 1 protein and poly(ADP-ribose) polymerase 1 degradation in Chlamydia trachomatis-induced cytopathicity. *Infect Immun* **78**:3288–3297.
93. **Jorgensen I, Bednar MM, Amin V, Davis BK, Ting JPY, McCafferty DG, Valdivia RH.** 2011. The Chlamydia protease CPAF regulates host and bacterial proteins to maintain pathogen vacuole integrity and promote virulence. *Cell Host Microbe* **10**:21–32.
94. **Holden P, Horton WA.** 2009. Crude subcellular fractionation of cultured mammalian cell lines. *BMC Res Notes* **2**:243.
95. **Pesin JA, Orr-Weaver TL.** 2008. Regulation of APC/C Activators in Mitosis and Meiosis. *Annu Rev Cell Dev Biol* **24**:475–499.
96. **Strnad P, Leidel S, Vinogradova T, Euteneuer U, Khodjakov A, Gönczy P.** 2007. Regulated HsSAS-6 Levels Ensure Formation of a Single Procentriole per Centriole during the Centrosome Duplication Cycle. *Developmental Cell* **13**:203–213.
97. **Rzomp KA, Scholtes LD, Briggs BJ, Whittaker GR, Scidmore MA.** 2003. Rab GTPases Are Recruited to Chlamydial Inclusions in Both a Species-Dependent and Species-Independent Manner. *Infect Immun* **71**:5855–5870.

98. **Rzomp KA, Moorhead AR, Scidmore MA.** 2006. The GTPase Rab4 Interacts with Chlamydia trachomatis Inclusion Membrane Protein CT229. *Infect Immun* **74**:5362–5373.
99. **Rejman Lipinski A, Heymann J, Meissner C, Karlas A, Brinkmann V, Meyer TF, Heuer D.** 2009. Rab6 and Rab11 Regulate Chlamydia trachomatis Development and Golgin-84-Dependent Golgi Fragmentation. *PLoS Pathog* **5**:e1000615.
100. **Burguete AS, Fenn TD, Brunger AT, Pfeffer SR.** 2008. Rab and Arl GTPase Family Members Cooperate in the Localization of the Golgin GCC185. *Cell* **132**:286–298.
101. **Rajalingam K, Sharma M, Paland N, Hurwitz R, Thieck O, Oswald M, Machuy N, Rudel T.** 2006. IAP-IAP Complexes Required for Apoptosis Resistance of C. trachomatis–Infected Cells. *PLoS Pathog* **2**:e114.
102. **Walker ME, Hjort EE, Smith SS, Tripathi A, Hornick JE, Hinchcliffe EH, Archer W, Hager KM.** 2008. Toxoplasma gondii actively remodels the microtubule network in host cells. *Microbes and Infection* **10**:1440–1449.
103. **Kawana K, Quayle AJ, Ficarra M, Ibana JA, Shen L, Kawana Y, Yang H, Marrero L, Yavagal S, Greene SJ, Zhang Y-X, Pyles RB, Blumberg RS, Schust DJ.** 2007. CD1d degradation in Chlamydia trachomatis-infected epithelial cells is the result of both cellular and chlamydial proteasomal activity. *J Biol Chem* **282**:7368–7375.
104. **Gong S, Lei L, Chang X, Belland R, Zhong G.** 2011. Chlamydia trachomatis secretion of hypothetical protein CT622 into host cell cytoplasm via a secretion pathway that can be inhibited by the type III secretion system inhibitor compound 1. *Microbiology* **157**:1134–1144.
105. **Qi MM, Gong SS, Lei LL, Liu QQ, Zhong GG.** 2011. A Chlamydia trachomatis OmcB C-terminal fragment is released into the host cell cytoplasm and is immunogenic in humans. *Infect Immun* **79**:2193–2203.
106. **Wang J, Frohlich KM, Buckner L, Quayle AJ, Luo M, Feng X, Beatty W, Hua Z, Rao X, Lewis ME, Sorrells K, Santiago K, Zhong G, Shen L.** 2011. Altered protein secretion of Chlamydia trachomatis in persistently infected human endocervical epithelial cells. *Microbiology* **157**:2759–2771.
107. **Schnell U, Dijk F, Sjollem KA, Giepmans BNG.** 2012. Immunolabeling artifacts and the need for live-cell imaging. *Nat Methods* **9**:152–158.
108. **Bauler LD, Hackstadt T.** 2014. Expression and targeting of secreted proteins from Chlamydia trachomatis. *J Bacteriol* **196**:1325–1334.

109. **Johnson KA, Lee JK, Chen AL, Tan M, Sütterlin C.** 2015. Induction and inhibition of CPAF activity during analysis of Chlamydia-infected cells. *Pathog Dis* **73**:1–8.
110. **Ekici OD, Paetzel M, Dalbey RE.** 2008. Unconventional serine proteases: variations on the catalytic Ser/His/Asp triad configuration. *Protein Sci* **17**:2023–2037.
111. **Tan M, Sütterlin C.** 2014. The Chlamydiaprotease CPAF: Caution, Precautions And Function. *Pathog Dis* **72**:7-9.
112. **Lad SP, Li J, da Silva Correia J, Pan Q, Gadwal S, Ulevitch RJ, Li E.** 2007. Cleavage of p65/RelA of the NF-kappaB pathway by Chlamydia. *PNAS* **104**:2933–2938.
113. **Fenteany G, Standaert RF, Lane WS, Choi S, Corey EJ, Schreiber SL.** 1995. Inhibition of proteasome activities and subunit-specific amino-terminal threonine modification by lactacystin. *Science* **268**:726–731.
114. **Dick LR, Cruikshank AA, Grenier L, Melandri FD, Nunes SL, Stein RL.** 1996. Mechanistic studies on the inactivation of the proteasome by lactacystin: a central role for clasto-lactacystin beta-lactone. *J Biol Chem* **271**:7273–7276.
115. **Manam RR, McArthur KA, Chao T-H, Weiss J, Ali JA, Palombella VJ, Groll M, Lloyd GK, Palladino MA, Neuteboom STC, Macherla VR, Potts BCM.** 2008. Leaving Groups Prolong the Duration of 20S Proteasome Inhibition and Enhance the Potency of Salinosporamides. *J Med Chem* **51**:6711–6724.
116. **Walker J, Hambly FJ.** 1895. Transformation of ammonium cyanate into urea. *J Chem Soc, Trans* **67**:746–767.
117. **Marier JR, Rose D.** 1964. Determination Of Cyanate, and a Study of its Accumulation in Aqueous Solutions of Urea. *Anal Biochem* **7**:304–314.
118. **Jung K, Hampel G, Scholz M, Henke W.** 1995. Culture of human kidney proximal tubular cells–The effect of various detachment procedures on viability and degree of cell detachment. *Cell Physiol Biochem* **5**:353-360.
119. **Canavan HE, Cheng X, Graham DJ, Ratner BD, Castner DG.** 2005. Cell sheet detachment affects the extracellular matrix: A surface science study comparing thermal liftoff, enzymatic, and mechanical methods. *J Biomed Mater Res* **75**:1–13.
120. **Fujioka N, Morimoto Y, Takeuchi K, Yoshioka M, Kikuchi M.** 2003. Difference in infrared spectra from cultured cells dependent on cell-harvesting method. *Appl Spectrosc* **57**:241–243.

121. **Hwang J, Yi M, Zhang X, Xu Y, Jung JH, Kim D-K.** 2013. Cytochalasin B induces apoptosis through the mitochondrial apoptotic pathway in HeLa human cervical carcinoma cells. *Oncol Rep* **30**:1929-1935.
122. **Domnina LV, Ivanova OY, Cherniak BV.** 2002. Effects of the inhibitors of dynamics of cytoskeletal structures on the development of apoptosis induced by the tumor necrosis factor. *Biochemistry* **68**:890-900.
123. **Hedstrom L.** 2002. Serine Protease Mechanism and Specificity. *Chem Rev* **102**:4501–4524.
124. **Kisselev AF, Goldberg AL.** 2001. Proteasome inhibitors: from research tools to drug candidates. *Chem Biol* **8**:739–758.
125. **Garcia-Calvo M, Peterson EP, Leiting B, Ruel R, Nicholson DW, Thornberry NA.** 1998. Inhibition of human caspases by peptide-based and macromolecular inhibitors. *J Biol Chem* **273**:32608–32613.
126. **Bednar MM, Jorgensen I, Valdivia RH, McCafferty DG.** 2011. Chlamydia protease-like activity factor (CPAF): characterization of proteolysis activity in vitro and development of a nanomolar affinity CPAF zymogen-derived inhibitor. *Biochemistry* **50**:7441–7443.
127. **Ring CS, Sun E, McKerrow JH, Lee GK, Rosenthal PJ, Kuntz ID, Cohen FE.** 1993. Structure-based inhibitor design by using protein models for the development of antiparasitic agents. *PNAS* **90**:3583–3587.
128. **Ding K, Lu Y, Nikolovska-Coleska Z, Wang G, Qiu S, Shangary S, Gao W, Qin D, Stuckey J, Krajewski K, Roller PP, Wang S.** 2006. Structure-Based Design of Spiro-oxindoles as Potent, Specific Small-Molecule Inhibitors of the MDM2–p53 Interaction. *J Med Chem* **49**:3432–3435.
129. **Wang D-F, Helquist P, Wiech NL, Wiest O.** 2005. Toward Selective Histone Deacetylase Inhibitor Design: Homology Modeling, Docking Studies, and Molecular Dynamics Simulations of Human Class I Histone Deacetylases. *J Med Chem* **48**:6936–6947.
130. **Koehler KA, Lienhard GE.** 1971. 2-phenylethaneboronic acid, a possible transition-state analog for chymotrypsin. *Biochemistry* **10**:2477–2483.
131. **Kettner CA, Shenvi AB.** 1984. Inhibition of the serine proteases leukocyte elastase, pancreatic elastase, cathepsin G, and chymotrypsin by peptide boronic acids. *J Biol Chem* **259**:15106–15114.
132. **Walker B, Lynas JF.** 2001. Strategies for the inhibition of serine proteases. *Cell Mol Life Sci* **58**:596–624.

133. **Kettner C, Mersinger L, Knabb R.** 1990. The selective inhibition of thrombin by peptides of boroarginine. *J Biol Chem* **265**:18289–18297.
134. **Teicher BA, Ara G, Herbst R, Palombella VJ, Adams J.** 1999. The proteasome inhibitor PS-341 in cancer therapy. *Clin Cancer Res* **5**:2638–2645.
135. **Soskel NT, Watanabe S, Hardie R.** 1986. A New Peptide Boronic Acid Inhibitor of Elastase-Induced Lung Injury in Hamsters 1–4. *Am Rev Respir Dis* **133**:639-642.
136. **Kinder DH, Elstad CA, Meadows GG, Ames MM.** 1992. Antimetastatic activity of boro-amino acid analog protease inhibitors against B16BL6 melanoma in vivo. *Invasion Metastasis* **12**:309–319.
137. **Truebestein L, Tennstaedt A, Mönig T, Krojer T, Canellas F, Kaiser M, Clausen T, Ehrmann M.** 2011. Substrate-induced remodeling of the active site regulates human HTRA1 activity. *Nature Struct Biol* **18**:386–388.
138. **Groll M, Berkers CR, Ploegh HL, Ovaa H.** 2006. Crystal Structure of the Boronic Acid-Based Proteasome Inhibitor Bortezomib in Complex with the Yeast 20S Proteasome. *Structure* **14**:451–456.
139. **Futaki S.** 2005. Membrane-permeable arginine-rich peptides and the translocation mechanisms. *Advanced Drug Delivery Reviews* **57**:547–558.
140. **Park N, Yamanaka K, Tran D, Chandrangsu P, Akers JC, de Leon JC, Morrisette NS, Selsted ME, Tan M.** 2009. The cell-penetrating peptide, Pep-1, has activity against intracellular chlamydial growth but not extracellular forms of *Chlamydia trachomatis*. *Journal of Antimicrobial Chemotherapy* **63**:115–123.
141. **Morris MC, Depollier J, Mery J, Heitz F, Divita G.** 2001. A peptide carrier for the delivery of biologically active proteins into mammalian cells **19**:1173–1176.
142. **Miller EW, Albers AE, Pralle A, Isacoff EY, Chang CJ.** 2005. Boronate-based fluorescent probes for imaging cellular hydrogen peroxide. *J Am Chem Soc* **127**:16652–16659.
143. **Linder KE, Metcalfe E, Nanjappan P, Arunachalam T, Ramos K, Skedzielewski TM, Marinelli ER, Tweedle MF, Nunn AD, Swenson RE.** 2011. Synthesis, In Vitro Evaluation, and In Vivo Metabolism of Fluor/Quencher Compounds Containing IRDye 800CW and Black Hole Quencher-3 (BHQ-3). *Bioconjugate Chem* **22**:1287-1297.
144. **Guo Z, Park S, Yoon J, Shin I.** 2014. Recent progress in the development of near-infrared fluorescent probes for bioimaging applications. *Chem Soc Rev* **43**:16–29.
145. **Armstrong JA, Valentine RC.** 1963. Structure and replication of the trachoma agent in cell cultures, as shown by electron microscopy. *J Gen Microbiol* **30**:59-73.

146. **Higashi N.** 1965. Electron microscopic studies on the mode of reproduction of trachoma virus and psittacosis virus in cell cultures. *Experimental and Molecular Pathology* **4**:24-39.
147. **Matsumoto A, Manire GP.** 1970. Electron microscopic observations on the effects of penicillin on the morphology of *Chlamydia psittaci*. *J Bacteriol* **101**:278–285.
148. **Ward M.** 1988. The Chlamydial Developmental Cycle. *Chlamydiales* 1–13.
149. **Rockey D, Fischer E, Hackstadt T.** 1996. Temporal analysis of the developing *Chlamydia psittaci* inclusion by use of fluorescence and electron microscopy. *Infect Immun* **64**:4269–4278.
150. **Kintner J, Lajoie D, Hall J, Whittimore J, Schoborg RV.** 2014. Commonly prescribed  $\beta$ -lactam antibiotics induce *C. trachomatis* persistence/stress in culture at physiologically relevant concentrations. *Front Cell Infect Microbiol* **4**:44.
151. **Liechti GW, Kuru E, Hall E, Kalinda A, Brun YV, VanNieuwenhze M, Maurelli AT.** 2014. A new metabolic cell-wall labelling method reveals peptidoglycan in *Chlamydia trachomatis*. *Nature* **506**:507–510.
152. **Wilson DP, Timms P, Mcelwain DLS, Bavoil PM.** 2006. Type III secretion, contact-dependent model for the intracellular development of chlamydia. *Bull Math Biol* **68**:161–178.
153. **Matsumoto A.** 1982. Electron microscopic observations of surface projections on *Chlamydia psittaci* reticulate bodies. *J Bacteriol* **150**:358–364.
154. **Mathews SA, Volp KM, Timms P.** 1999. Development of a quantitative gene expression assay for *Chlamydia trachomatis* identified temporal expression of sigma factors. *FEBS Lett* **458**:354–358.
155. **Al-Younes HM, Brinkmann V, Meyer TF.** 2004. Interaction of *Chlamydia trachomatis* serovar L2 with the host autophagic pathway. *Infect Immun* **72**:4751–4762.
156. **Al-Younes HM, Gussmann J, Braun PR, Brinkmann V, Meyer TF.** 2006. Naturally occurring amino acids differentially influence the development of *Chlamydia trachomatis* and *Chlamydia (Chlamydophila) pneumoniae*. *J Med Microbiol* **55**:879–886.
157. **Wolf K, Betts HJ, Chellas-Géry B, Hower S, Linton CN, Fields KA.** 2006. Treatment of *Chlamydia trachomatis* with a small molecule inhibitor of the *Yersinia* type III secretion system disrupts progression of the chlamydial developmental cycle. *Molecular Microbiology* **61**:1543–1555.

158. **Ouellette SP, Hatch TP, Abdelrahman YM, Rose LA, Belland RJ, Byrne GI.** 2006. Global transcriptional upregulation in the absence of increased translation in Chlamydia during IFN $\gamma$ -mediated host cell tryptophan starvation. *Molecular Microbiology* **62**:1387–1401.
159. **Chellas-Géry BB, Linton CNC, Fields KAK.** 2007. Human GCIP interacts with CT847, a novel Chlamydia trachomatis type III secretion substrate, and is degraded in a tissue-culture infection model. *Cell Microbiol* **9**:2417–2430.
160. **Robertson DK, Gu L, Rowe RK, Beatty WL.** 2009. Inclusion Biogenesis and Reactivation of Persistent Chlamydia trachomatis Requires Host Cell Sphingolipid Biosynthesis. *PLoS Pathog* **5**:e1000664–e1000664.
161. **Nguyen BD, Valdivia RH.** 2012. Virulence determinants in the obligate intracellular pathogen Chlamydia trachomatis revealed by forward genetic approaches. *PNAS* **109**:1263–1268.
162. **Olive AJ, Haff MG, Emanuele MJ, Sack LM, Barker JR, Elledge SJ, Starnbach MN.** 2014. Chlamydia trachomatis-Induced Alterations in the Host Cell Proteome Are Required for Intracellular Growth. *Cell Host Microbe* **15**:113–124.
163. **Engström P, Krishnan KS, Ngyuen BD, Chorell E, Normark J, Silver J, Bastidas RJ, Welch MD, Hultgren SJ, Wolf-Watz H, Valdivia RH, Almqvist F, Bergström S.** 2015. A 2-pyridone-amide inhibitor targets the glucose metabolism pathway of Chlamydia trachomatis. *MBio* **6**:e02304–14.
164. **Capani F, Martone ME, Deerinck TJ, Ellisman MH.** 2001. Selective localization of high concentrations of F-actin in subpopulations of dendritic spines in rat central nervous system: a three-dimensional electron microscopic study. *J Comp Neurol* **435**:156–170.
165. **West JB, Fu Z, Deerinck TJ, Mackey MR, Obayashi JT, Ellisman MH.** 2010. Structure–function studies of blood and air capillaries in chicken lung using 3D electron microscopy. *Respiratory Physiology & Neurobiology* **170**:202–209.
166. **Shu X, Lev-Ram V, Deerinck TJ, Qi Y, Ramko EB, Davidson MW, Jin Y, Ellisman MH, Tsien RY.** 2011. A Genetically Encoded Tag for Correlated Light and Electron Microscopy of Intact Cells, Tissues, and Organisms. *PLoS Biol* **9**:e1001041.
167. **Peterson EM, la Maza de LM.** 1988. Chlamydia parasitism: ultrastructural characterization of the interaction between the chlamydial cell envelope and the host cell. *J Bacteriol* **170**:1389–1392.
168. **Enciso G, Wan FYM.** 2015. Chlamydia Trachomatis. Unpublished 1–35.

169. **Zhao L, Kroenke CD, Song J, Piwnica-Worms D, Ackerman JJH, Neil JJ.** 2008. Intracellular water-specific MR of microbead-adherent cells: the HeLa cell intracellular water exchange lifetime. *NMR Biomed* **21**:159–164.
170. **Taheri-Araghi S, Bradde S, Sauls JT, Hill NS, Levin PA, Paulsson J, Vergassola M, Jun S.** 2015. Cell-size control and homeostasis in bacteria. *Curr Biol* **25**:385–391.
171. **Hogan RJ, Mathews SA, Mukhopadhyay S, Summersgill JT, Timms P.** 2004. Chlamydial persistence: beyond the biphasic paradigm. *Infect Immun* **72**:1843–1855.
172. **Nans A, Saibil HR, Hayward RD.** 2014. Pathogen-host reorganisation during Chlamydia invasion revealed by cryo-electron tomography. *Cell Microbiol.*
173. **Muschiol S, Bailey L, Gylfe A, Sundin C, Hultenby K, Bergström S, Elofsson M, Wolf-Watz H, Normark S, Henriques-Normark B.** 2006. A small-molecule inhibitor of type III secretion inhibits different stages of the infectious cycle of *Chlamydia trachomatis*. *PNAS* **103**:14566–14571.
174. **Conrad TA, Yang Z, Ojcius D, Zhong G.** 2013. A path forward for the chlamydial virulence factor CPAF. *Microbes and Infection* **15**:1026–1032.
175. **Bavoil PM, Byrne GI.** 2014. Analysis of CPAF mutants: new functions, new questions (The ins and outs of a chlamydial protease). *Pathog Dis* **71**:287-291.
176. **Grieshaber SS, Grieshaber NA.** 2014. The role of the chlamydial effector CPAF in the induction of genomic instability. *Pathog Dis* **72**:5-6.
177. **Häcker G, Heuer D, Ojcius DM.** 2014. Is the hoopla over CPAF justified? *Pathog Dis* **72**:1–2.
178. **Häcker G.** 2014. The chlamydial protease CPAF: important or not, important for what? *Microbes and Infection* **16**:367-370.
179. **Timmer JC, Salvesen GS.** 2006. Caspase substrates. *Cell Death Differ* **14**:66–72.
180. **Fischer U, Jänicke RU, Schulze-Osthoff K.** 2003. Many cuts to ruin: a comprehensive update of caspase substrates. *Cell Death Differ* **10**:76–100.
181. **Tsujinaka T, Kajiwara Y, Kambayashi J, Sakon M, Higuchi N, Tanaka T, Mori T.** 1988. Synthesis of a new cell penetrating calpain inhibitor (calpeptin). *Biochem Biophys Res Commun* **153**:1201–1208.
182. **Katz AM, Rosenthal D, Sauder DN.** 1991. Cell adhesion molecules. Structure, function, and implication in a variety of cutaneous and other pathologic conditions. *Int J Dermatol* **30**:153–160.

183. **Matsumoto A.** 1981. Isolation and electron microscopic observations of intracytoplasmic inclusions containing *Chlamydia psittaci*. *J Bacteriol* **145**:605–612.
184. **Wang Y, Kahane S, Cutcliffe LT, Skilton RJ, Lambden PR, Clarke IN.** 2011. Development of a Transformation System for *Chlamydia trachomatis*: Restoration of Glycogen Biosynthesis by Acquisition of a Plasmid Shuttle Vector. *PLoS Pathog* **7**:e1002258.
185. **Wickstrum J, Sammons LR, Restivo KN, Hefty PS.** 2013. Conditional Gene Expression in *Chlamydia trachomatis* Using the Tet System. *PLoS ONE* **8**:e76743.
186. **Hou S, Lei L, Yang Z, Qi M, Liu Q, Zhong G.** 2012. The *Chlamydia trachomatis* outer membrane complex protein B (OmcB) is processed by the protease CPAF. *J Bacteriol* –.
187. **Fadel S, Eley A.** 2007. *Chlamydia trachomatis* OmcB protein is a surface-exposed glycosaminoglycan-dependent adhesin. *J Med Microbiol* **56**:15–22.
188. **Fadel S, Eley A.** 2008. Differential glycosaminoglycan binding of *Chlamydia trachomatis* OmcB protein from serovars E and LGV. *J Med Microbiol* **57**:1058–1061.
189. **Newhall WJ.** 1987. Biosynthesis and disulfide cross-linking of outer membrane components during the growth cycle of *Chlamydia trachomatis*. *Infect Immun* **55**:162-168.
190. **Mygind P, Christiansen G, Birkelund S.** 1998. Topological analysis of *Chlamydia trachomatis* L2 outer membrane protein 2. *J Bacteriol* **180**:5784–5787.
191. **Liao DI, Qian J, Chisholm DA, Jordan DB, Diner BA.** 2000. Crystal structures of the photosystem II D1 C-terminal processing protease. *Nat Struct Biol* **7**:749–753.
192. **Tamura NN, Lottspeich FF, Baumeister WW, Tamura TT.** 1998. The role of tricorn protease and its aminopeptidase-interacting factors in cellular protein degradation. *Cell* **95**:637–648.
193. **Ostrowska HEA.** 1997. Lactacystin, a Specific Inhibitor of the Proteasome, Inhibits Human Platelet Lysosomal Cathepsin A-like Enzyme. *Biochem Biophys Res Commun* **234**:729-732.
194. **Ostrowska H, Wójcik C, Wilk S, Omura S, Kozłowski L, Stokłosa T, Worowski K, Radziwon P.** 2000. Separation of cathepsin A-like enzyme and the proteasome: evidence that lactacystin/beta-lactone is not a specific inhibitor of the proteasome. *Int J Biochem Cell Biol* **32**:747–757.
195. **Geier E, Pfeifer G, Wilm M, Lucchiari-Hartz M, Baumeister W, Eichmann K, Niedermann G.** 1999. A giant protease with potential to substitute for some functions of the proteasome. *Science* **283**:978–981.

196. **Kagebein D, Gutjahr M, Grosse C, Vogel AB, Rodel J, Knittler MR.** 2014. Chlamydia trachomatis-Infected Epithelial Cells and Fibroblasts Retain the Ability To Express Surface-Presented Major Histocompatibility Complex Class I Molecules. *Infect Immun* **82**:993–1006.
197. **Sun HS, Eng EWY, Jeganathan S, Sin ATW, Patel PC, Gracey E, Inman RD, Terebiznik MR, Harrison RE.** 2012. Chlamydia trachomatis vacuole maturation in infected macrophages. *Journal of Leukocyte Biology* **92**:815–827.
198. **Turner JJ, Ewald JC, Skotheim JM.** 2012. Cell Size Control in Yeast. *Current Biology* **22**:350–359.
199. **Chien A-C, Hill NS, Levin PA.** 2012. Cell size control in bacteria. *Curr Biol* **22**:340–349.
200. **Adams DW, Errington J.** 2009. Bacterial cell division: assembly, maintenance and disassembly of the Z ring. *Nature* **7**:642–653.
201. **Jacquier N, Viollier PH, Greub G.** 2015. The role of peptidoglycan in chlamydial cell division: towards resolving the chlamydial anomaly. *FEMS Microbiol Rev* **39**:262–275.
202. **Erickson HP, Osawa M.** 2010. Cell division without FtsZ - a variety of redundant mechanisms. *Molecular Microbiology* **78**:267–270.
203. **Santi I, Dhar N, Bousbaine D, Wakamoto Y, McKinney JD.** 2013. Single-cell dynamics of the chromosome replication and cell division cycles in mycobacteria. *Nat Commun* **4**:2470–2470.
204. **Fantes PA.** 1977. Control of cell size and cycle time in *Schizosaccharomyces pombe*. *J Cell Sci* **24**:51–67.
205. **Fantes PA, Nurse P.** 1981. Control of the timing of cell division in fission yeast. *Exp Cell Res* **115**:317–329.
206. **Talia SD, Skotheim JM, Bean JM, Siggia ED, Cross FR.** 2007. The effects of molecular noise and size control on variability in the budding yeast cell cycle. *Nature* **448**:947–951.
207. **Lyons AB.** 2000. Analysing cell division in vivo and in vitro using flow cytometric measurement of CFSE dye dilution. *J Immunol Methods* **243**:147–154.
208. **Omsland A, Sager J, Nair V, Sturdevant DE, Hackstadt T.** 2012. From the Cover: Developmental stage-specific metabolic and transcriptional activity of *Chlamydia trachomatis* in an axenic medium. *PNAS* **109**:19781–19785.

209. **Campos M, Surovtsev IV, Kato S, Paintdakhi A, Beltran B, Ebmeier SE, Jacobs-Wagner C.** 2014. A constant size extension drives bacterial cell size homeostasis. *Cell* **159**:1433–1446.
210. **McCaul TF, Williams JC.** 1981. Developmental cycle of *Coxiella burnetii*: structure and morphogenesis of vegetative and sporogenic differentiations. *J Bacteriol* **147**:1063-1076.
211. **Coleman SA, Fischer ER, Howe D, Mead DJ, Heinzen RA.** 2004. Temporal Analysis of *Coxiella burnetii* Morphological Differentiation. *J Bacteriol* **186**:7344–7352.
212. **Errington J.** 1993. *Bacillus subtilis* sporulation: regulation of gene expression and control of morphogenesis. *Microbiol Rev* **57**:1–33.
213. **Solomon JM, Lazazzera BA, Grossman AD.** 1996. Purification and characterization of an extracellular peptide factor that affects two different developmental pathways in *Bacillus subtilis*. *Genes Dev* **10**:2014–2024.
214. **Feiner R, Argov T, Rabinovich L, Sigal N, Borovok I, Herskovits AA.** 2015. A new perspective on lysogeny: prophages as active regulatory switches of bacteria. *Nat Rev Microbiol* **13**:641–650.
215. **Herskowitz I, Hagen D.** 1980. The lysis-lysogeny decision of phage lambda: explicit programming and responsiveness. *Annu Rev Genet* **14**:399–445.
216. **Imamovic L, Ballesté E, Martínez-Castillo A, García-Aljaro C, Muniesa M.** 2015. Heterogeneity in phage induction enables the survival of the lysogenic population. *Environ Microbiol* doi:10.1111/1462-2920.13151.
217. **Boncompain G, Schneider B, Delevoye C, Kellermann O, Dautry-Varsat A, Subtil A.** 2009. Production of Reactive Oxygen Species Is Turned On and Rapidly Shut Down in Epithelial Cells Infected with *Chlamydia trachomatis*. *Infect Immun* **78**:80–87.
218. **Morrison SJ, Shah NM, Anderson DJ.** 1997. Regulatory mechanisms in stem cell biology. *Cell* **88**:287–298.
219. **Ossewaarde JM, De Vries A, Bestebroer T.** 1996. Application of a *Mycoplasma* group-specific PCR for monitoring decontamination of *Mycoplasma*-infected *Chlamydia* sp. strains. *Appl Environ Microbiol* **62**:328-331.
220. **Harlow E, Lane D.** 2006. Mounting samples in gelvatol or mowiol. *CSH Protoc*
221. **Zheng J-S, Tang S, Guo Y, Chang H-N, Liu L.** 2012. Synthesis of Cyclic Peptides and Cyclic Proteins via Ligation of Peptide Hydrazides. *Chembiochem* **13**:542–546.

# **Appendix**

## **Materials and Methods**

## **Cell Culture**

HeLa cells (ATCC) were grown in Advanced DMEM (4.5 g. glucose/L) (Invitrogen) supplemented with 2% fetal bovine serum (FBS) (Hyclone/Thermo Fisher) and 2mM GlutaMAX-I (Invitrogen). HEK 293T cells and retinal pigment epithelial (hTERT RPE-1) cells (both from ATCC) were cultured in DMEM (4.5 g. glucose/L) (Invitrogen) supplemented with 10% FBS. All cell lines were grown in 5% CO<sub>2</sub> at 37°C and screened for Mycoplasma contamination by PCR (219).

## ***Chlamydia* Infections**

Cell monolayers were infected with *C. trachomatis* serovar L2 (L2/434/Bu), LGV biovar, at a multiplicity of infection (MOI) of 3 in sucrose-phosphate-glutamic acid (SPG). In parallel, uninfected control experiments were performed as mock infections in SPG alone. Infections were carried out by centrifugation at 700xg in a Sorvall Legend Mach 1.6R centrifuge for 1 hour at room temperature. After centrifugation, the inoculum was replaced by fresh cell culture medium and monolayers were incubated at 37°C and 5% CO<sub>2</sub>. Chlamydial EBs (elementary bodies) were verified to be free of Mycoplasma contamination by PCR (219).

## ***Clasto-lactacystin* Treatment**

### *Clasto-lactacystin* pre-treatment

*Clasto-lactacystin*  $\beta$ -lactone (Cayman Chemical), dissolved in methyl acetate, was added to the cell culture medium at a final concentration of 150  $\mu$ M for 1 hour prior to cell processing. For example, samples of *Chlamydia*-infected cells at 36 hpi were treated with *clasto-lactacystin* at 35 hpi for 1 hour and then processed. In parallel control experiments, methyl acetate as the solvent was added to the culture medium. Treated cells were collected by trypsinization followed by lysis in RIPA buffer (as described below).

### Clasto-lactacystin in lysis buffer

*Chlamydia*-infected cells were harvested by trypsinization and cell pellets were lysed on ice for 10 minutes in RIPA buffer containing protease inhibitors (as described above, see Lysis in RIPA Buffer) and 150  $\mu$ M *clasto*-lactacystin  $\beta$ -lactone (Cayman Chemical). In parallel control experiments, methyl acetate was used instead of *clasto*-lactacystin in the RIPA buffer.

### **Cell Collection Methods**

*Chlamydia*-infected cells were collected by incubation in 500  $\mu$ L trypsin (TrypLE Express, Invitrogen) or 500  $\mu$ L accutase (Fisher Scientific) per well of a 6-well dish for 3-5 minutes at 37°C, or by scraping monolayers directly into 500  $\mu$ L 1X PBS per well of a 6-well dish. Cells were then transferred to a 15 mL conical tube on ice. The dish was washed twice with 1X PBS, and the washes were added to the 15 mL conical tube. The cells were pelleted by centrifugation at 1,500 rpm for 3 minutes at 4°C and lysed on ice for 10 minutes in 8M urea supplemented with 325 U/mL Benzonase Nuclease (Sigma-Aldrich).

### **Cell Lysis**

#### Lysis in RIPA buffer

Cells were harvested by trypsinization (TrypLE Express, Invitrogen) for 3-5 minutes at 37°C and the trypsinized cells were transferred to a 15 mL conical tube on ice. The dish was washed twice with 1X PBS and the washes were added to the 15 mL conical tube to collect any remaining cells. The cells were pelleted by centrifugation at 1,500 rpm for 3 minutes at 4°C and lysed on ice for 10 minutes in RIPA buffer (50 mM Tris [pH 7.5], 150 mM NaCl, 0.1% SDS, 0.5% sodium deoxycholate, 1% NP-40) supplemented with protease inhibitors (2 mM pepstatin, 150 mM aprotinin [both from MP Biochemicals], 1 mM leupeptin [Calbiochem], 1 mM PMSF [Acros]). The cells were resuspended by pipetting up and down in approximately 1 mL of ice-

cold lysis buffer per  $5 \times 10^6$  cells. Lysates were cleared by centrifugation at 13,000xg for 10 minutes at 4°C and protein concentrations were determined by Bradford assay (BioRad).

#### Direct Lysis in Sample Buffer

Laemmli sample buffer (50 mM Tris-HCl [pH 6.8], 10% glycerol, 2% SDS, 1%  $\beta$ -mercaptoethanol, 0.1% bromophenol blue) was added directly to cell monolayers. Lysates were pooled and boiled for 5 minutes at 95°C.

#### Direct Lysis in Urea

The monolayer of cells was washed with 1X PBS. A solution of 8M urea (or 6-7M, where indicated) was supplemented with 325 U/mL of Benzonase Nuclease (Sigma-Aldrich) and added directly to cell monolayers at a volume of 1 mL per 6-well dish for 10 minutes on ice. Lysates were then pooled and protein concentrations were determined by the DC protein assay (BioRad).

#### Lysis in Hot 1% SDS Buffer

Cells were washed with 1X PBS. 1% SDS buffer (50 mM Tris [pH 7.5], 150 mM NaCl, 1% SDS) was heated to 95°C and directly added to cell monolayers at a volume of 1 mL per 6 wells of a 6-well dish. Cells were scraped from the monolayers, and the resulting lysates from individual wells were pooled and supplemented with 325 U/mL of Benzonase Nuclease (Sigma-Aldrich). Protein concentrations were determined by the DC protein assay (BioRad).

#### **Immunoblotting**

Cell lysates were diluted into Laemmli sample buffer (50 mM Tris-HCl [pH 6.8], 10% glycerol, 2% SDS, 1%  $\beta$ -mercaptoethanol, 0.1% bromophenol blue) and incubated at 95°C for 5 minutes to denature proteins. Samples containing equal amounts of total protein were loaded and resolved by SDS-PAGE. Proteins were transferred onto nitrocellulose membranes, blocked in

5% milk PBST (5% dry powdered milk, 0.1% Tween-20, 1X PBS) and incubated in primary antibodies followed by HRP-conjugated (Jackson ImmunoResearch) or IRDye-conjugated (LI-COR) secondary antibodies. Blots were imaged by enhanced chemiluminescence (90 mM p-Courmaric acid, 250 mM 3-Aminophthalhydrazide, 100 mM Tris-HCl [pH 8.5]) or the LI-COR Odyssey SA infrared imaging system.

### **Antibodies**

The following antibodies were used in this study: rabbit anti-Bim, rabbit anti-Puma, mouse anti-keratin-8, mouse anti-keratin-18, mouse anti- $\alpha$ -tubulin, and mouse anti-vimentin (all from Sigma-Aldrich); rabbit anti-cyclin B1, mouse anti-nectin-1, mouse anti-p65/RelA and bovine anti-sheep-HRP (all from Santa Cruz Biotechnology); rabbit anti-Bik, rabbit anti-vimentin, and mouse anti-Erk 1/2 (all from Cell Signaling Technology); rabbit anti- $\alpha$ -tubulin (Abcam); mouse anti-C-Nap1 and mouse anti-caspase-3 (BD Biosciences); rabbit anti-RFX5 (Rockland Immunochemicals); mouse anti-GFP (Roche); goat anti-mouse-HRP and goat anti-rabbit-HRP (both from Jackson ImmunoResearch Laboratories); goat anti-mouse 680LT and goat anti-rabbit 800CW (both from LI-COR); AlexaFluor 488 or Alexa Fluor 594-tagged goat anti-mouse or goat anti-rabbit antibodies (Molecular Probes/Invitrogen); mouse anti-CPAFn and mouse anti-CPAFc (generous gifts from Dr. Guangming Zhong, University of Texas Health Science Center at San Antonio); rabbit anti-CPAP and rabbit anti-HsSAS-6 (generous gifts from Dr. Pierre Gönczy, École Polytechnique Fédéral de Lausanne); rabbit anti-Cep170 (kindly provided by Dr. Guilia Guarguaglini, Sapeinza University of Rome); rabbit anti-Cep192 (kind gift from Laurence Pelletier, Samuel Lunenfeld Research Institute); sheep anti-golgin-84 (generously provided by Dr. Martin Lowe, University of Manchester); rabbit anti- $\alpha$ -mannosidase II (kindly provided by Dr. Kelley Moremen, University of Georgia); mouse anti-MOMP (VD4

epitope of the major outer membrane protein from *C. trachomatis* serovar E) (kind gift from Dr. Ellena Peterson, UCI).

### **Cell-free Degradation Assays**

Uninfected and infected (36 hpi) HeLa cell lysates were prepared in RIPA buffer as described above. 25µg of uninfected lysate, as a source of host protein substrates, was incubated with a source of protease at 37°C for 1 hour in CPAF reaction buffer (25 mM Tris [pH 8.0], 150 mM NaCl, 3 mM DTT). Sources of protease included: 0.5 to 2µg of infected lysate, 5 to 10ng of purified recombinant His-CPAF (generously provided by Dr. Guangming Zhong, University of Texas Health Science Center at San Antonio), or 0.5 to 2µg of infected lysate immunodepleted of CPAF. In some experiments reactions were supplemented with 2-4mM lactacystin, or DMSO as a solvent control. All reactions were terminated by adding Laemmli sample buffer and boiling for 5 minutes. Proteins from the samples were separated by SDS-PAGE and analyzed by immunoblot using specific primary antibodies.

### **Immunodepletion**

Antibodies to GFP, CPAFn (CPAF N-terminus), or CPAFc (CPAF C-terminus) were conjugated to sepharose protein G beads (Sigma-Aldrich). *Chlamydia*-infected cell lysates were immunodepleted by three serial incubations with the antibody-conjugated beads for 1 hour at room temperature. As a control, infected lysates were mock-depleted with beads alone.

Immunodepleted infected cell lysates were then combined with uninfected cell lysates in cell-free degradation assays.

### ***In vitro* CPAF Activity Assay**

*Chlamydia*-infected HeLa cells at various times in the infection were processed by one of the methods described previously (see Cell Lysis). 4-8 µg of *Chlamydia*-infected HeLa cell

lysate, as the source of CPAF, were incubated with 12.5 µg of uninfected HeLa cell lysate, as the source of host protein substrates, at 37°C for 30 minutes in CPAF reaction buffer (25 mM Tris [pH 8.0], 150 mM NaCl, 3 mM DTT). Reactions were terminated by adding Laemmli sample buffer and boiling for 5 minutes. 16.5-20.5 µg of protein from these samples was analyzed by western blotting with specific primary antibodies.

### **Immunofluorescence**

Cells grown on glass coverslips were fixed in 4% formaldehyde or 100% ice-cold methanol for 10 minutes at room temperature. Alternatively, cells were fixed in 95% ethanol for 30 minutes on ice followed by incubation in acetone for 1 minute at room temperature. After fixation coverslips were blocked in 5% blocking buffer (0.1% Triton X-100, 5% FBS in PBS) or TBS-BSA (0.1% Tween-20, 5% BSA in TBS) for 1 hour. Cells were incubated with primary antibodies for 1 hour at room temperature or overnight at 4°C followed by Alexa-fluorochrome-conjugated secondary antibodies for 30 minutes at room temperature. Host and chlamydial DNA were stained with Hoechst 33342 (Molecular Probes/Invitrogen). Coverslips were mounted onto glass slides with gelvatol (220) or Fluoromount-G (SouthernBiotech). Cells were imaged with a Zeiss Axiovert 200M microscope (Carl Zeiss MicroImaging, Inc.) or by confocal microscopy on a Nikon Eclipse Ti-U inverted microscope fitted with a Nikon D-Eclipse confocal laser assembly and a D-Eclipse C1 controller (Nikon). Images were acquired using the Zeiss Axiovision software or Nikon EZ-C1 program and analyzed using Zeiss Axiovision, Nikon NIS Elements, and Adobe Photoshop.

### **Apoptosis Induction Assay**

Uninfected or *Chlamydia*-infected HeLa cells (MOI of 3, at 24 hpi) were incubated with 1 µM staurosporine in tissue culture medium for 3 hours. Lysates of the cell monolayers were

prepared by direct lysis in 8M urea as previously described, separated by SDS-PAGE, and analyzed by immunoblotting with antibodies to caspase-3.

### **Solid phase synthesis of protected peptide building blocks**

The protected peptide building blocks were prepared by a standard solid-phase peptide synthesis protocol, as essentially described by Zheng *et al.*, 2012 (221):

#### *General procedure for the loading of the used chloro trityl chloride resins*

The desired Fmoc-protected amino acid (1.2 eq) was dissolved in dry dichloromethane under an argon atmosphere and DIEA (4.8 eq) was added. In parallel, commercially available chloro trityl chloride resin was transferred into a reactor, kept under an argon atmosphere and washed with dry dichloromethane. The dissolved amino acid was then added to this chloro trityl chloride resin (1 eq) and shaken for 2 h at room temperature. The solution was removed and the resin was washed three times with a mixture of DCM/MeOH/DIEA (17:2:1) and then three times with DCM, twice with DMF (2x) and again three times with DCM. The loaded resin was then dried under vacuum.

#### *General procedure for the synthesis of the protected peptide synthesis fragments via an automated solid phase synthesis with a peptide synthesizer*

For solid phase peptides synthesis, the automated Peptide synthesizer Syro I from Biotage was used. This peptide synthesizer generates peptides after programming of defined peptide sequences. To this end, the synthesizer employs pre-prepared solutions for the different peptide coupling or cleavage steps: Fmoc protecting group cleavage is achieved with a 20 % piperidine in DMF solution. After each Fmoc deprotection step, the resin is washed with DMF. Coupling of Fmoc amino acids is achieved by using a mixture of the Fmoc-amino acid (4 eq) and the coupling reagents HBTU (4 eq), HOBt (4 eq) and the base DIEA (4 eq). As the last N-terminal

amino acid, a Boc-protected amino acid was used instead. After each coupling step, the resin is washed with DMF. For assembly of the different peptides, the standard protocols of the automated peptide synthesizer were used.

Cleavage of the protected peptide from the resin was achieved with a cleavage cocktail consisting of a solution of AcOH/trifluoro ethanol/DCM (2:2:6) for 2 h and the solution was filtered off from the resin. The resin was washed with DCM and again filtered. The filtrates were pooled, coevaporated with cyclohexane and dried at vacuum to give the protected peptide building blocks as a white solid.

### **Synthesis of peptide boronic acids**

The peptide boronic acids were obtained by coupling of the previously prepared boronic amino acid esters and the protected peptide fragments, as essentially described Zheng *et al.*, 2012 (221):

#### *General procedure for the synthesis of peptide boronic acid inhibitors*

The C-terminal free, otherwise fully protected peptide sequence (1 eq) obtained from the solid phase peptide synthesis approach was dissolved in DMF/DCM (1:1). Fluoro-*N,N,N',N'*-bis(tetramethylene)formamidinium hexafluorophosphate (BTFFH, 1.1 eq) and DIEA (2 eq) was added and the resulting mixture was stirred for 15 min at room temperature. The corresponding boronic amino acid esters (1.1 eq) and DIEA (2 eq) were added and stirred for further 3 h to 17 h at room temperature. The solvent was removed under reduced pressure, the residue was re-dissolved in DCM and washed twice with brine. The aqueous phase was re-extracted with DCM and the combined organic phases were dried over Na<sub>2</sub>SO<sub>4</sub>. The solvent was removed and the intermediate product dried in vacuum. For subsequent protecting group cleavage, a mixture of trifluoro acetic acid/water/triisopropyl silane (95:2.5:2.5) was added and the resulting mixture was stirred for 2 h. If peptides however featured sulfur-containing amino acids in their sequence,

protecting group cleavage was performed with trifluoro acetic acid/ethanedithiole/water/triisopropyl silane (95:2:2:1) instead. The peptide was precipitated by adding a large excess of cold diethyl ether. The resulting suspension was centrifuged (3500 rpm, 20 min) at 4 °C and the desired products were purified from the precipitate via HPLC.

### ***In vitro* screening for CPAF inhibitors**

Uninfected and infected (36 hpi) lysates were prepared in RIPA buffer as described above. Reactions of 12.5µg of uninfected lysate as a source of host proteins, 0.125µg of infected lysate as a source of CPAF, and 0.3-10µM boronate peptide inhibitors were prepared in CPAF reaction buffer then incubated at 37°C for 30 minutes. Reactions were terminated by adding Laemmli sample buffer and boiling for 5 min at 95°C. Proteins from each reaction were separated by SDS-PAGE and immunoblotted with specific antibodies to CPAF substrates p65 and nectin-1.

### **Molecular Modeling and Visualization**

The zymogen peptide CPAF crystallization structure was used as a template (PDB ID: 3DOR) – peptide amino acid substitutions were made at each P site using the “Mutate Sequence Editor” in MOE, leaving the backbone fixed. Low energy side chain rotomers were explored using the Rotamer Explorer MOE and selected to minimize Van der Waals clashes in each P site. The conversion of the zymogen proline at the P2 position was converted while maintaining the backbone torsion angles and amide nitrogen, alpha and carbonyl carbon positions. The covalent bond between Ser499 and the boronate warhead was modeled using the torsional angles and bond coordinates observed from the covalent modification with omuralide with CPAF (PDB ID: 3DPM). Once constructed, each peptide in the CPAF binding site was minimized in a multistep process with the MMFF99s force field and generalized born solvation model. Initially peptide R-

groups were unfixed with the peptide backbone fixed and the protein fixed. As a second step the peptide R-groups and protein side chains within 5.0Å were unfixed and subjected to minimization. As a final step, the peptide backbone was unfixed during the minimization as well.

### **20S Proteasome Activity Assay**

20S Proteasome Activity Assay Kit was conducted according to the manufacturer's protocol (EMD Millipore). Briefly, uninfected HeLa cell lysates (as a source of proteasomes) were incubated with LLVY-AMC substrate in the presence of inhibitors (boronate peptides, lactacystin, or solvent control) at 37°C for 2 hours. The fluorescence intensity of free fluorophore 7-amino-4-methylcoumarin (AMC) was detected by a Gemini EM Microplate Reader using a 380/460 nm filter set. The concentration of AMC in each reaction was quantified based on a standard curve generated from a dilution series of AMC alone.

### **Genome Copy Analysis**

HeLa cell monolayers were infected with *C. trachomatis* at an MOI of 3 in 6-well tissue culture dishes and harvested at different times in the infection by trypsinization. Total DNA was isolated from *Chlamydia*-infected cell pellets using the Qiagen DNeasy Blood and Tissue Kit (Qiagen, Valencia, CA) per the manufacturer's protocol. The total number of chlamydial genomes in each sample was determined by amplifying the chlamydial gene *euo* using a BioRad iCycler iQ. The amount of PCR product in each sample was quantified by converting mean critical threshold values to ng of DNA using a standard curve.

The number of infected cells in each genome copy sample was determined by counting total cells from a parallel sample then adjusting to account for infection efficiency. Cells in a parallel well within the 6-well plate were trypsinized and counted by light microscopy on a hemocytometer. In a duplicate well, cells were fixed and stained with antibodies to chlamydial

protein MOMP then analyzed to determine the infection rate. The number of infected cells was then found by multiplying the total number of cells determined by hemocytometer by the infection rate. For example, if there were  $10^6$  cells determined by hemocytometer and the infection rate was 80%, then the number of infected cells in the sample would be ( $10^6 * 0.80 = 8 \times 10^5$ ). Genome copy number was divided by the number of infected cells in the sample to determine the number of *Chlamydia* per infected cell.

### **Progeny Assay**

HeLa cells were infected with *C. trachomatis* at an MOI of 3. At the indicated times (24 or 36 hpi), cell lysates were harvested by a combination of heat shock and scraping. Infected cell plates were incubated for 15 minutes at  $-70^\circ\text{C}$  for followed by 15 minutes at  $37^\circ\text{C}$  then scraped from the plate in SPG. Serial dilutions of the lysates were applied to fresh HeLa cell monolayers and centrifuged at 700xg in a Sorvall Legend Mach 1.6R centrifuge for 1 hour at room temperature. After 36 hours, cells were fixed and chlamydial inclusions were stained with antibodies to MOMP for immunofluorescence analysis. The average number of cells containing inclusions was determined by counting 10 optical fields at 40X magnification on a Zeiss Axiovert 200M microscope (Carl Zeiss MicroImaging, Inc.) then used to calculate the number of infectious units per mL inoculum.

### **Three-dimensional Electron Microscopy**

*Chlamydia*-infected monolayers were fixed in a solution of 2% paraformaldehyde and 2.5% glutaraldehyde in 0.1M cacodylate buffer for 1 hour. Cells were washed 5X in cold 0.1M cacodylate buffer then stained in 3% potassium ferrocyanide 4% osmium tetroxide supplemented with 3mM calcium chloride for 1 hour on ice. After 5X washes in water, cells were incubated in 1% thiocarbohydrazide for 20 minutes at room temperature. Following 5X washes in water, cells

were incubated in 2% uranyl acetate at 4°C overnight then embedded in resin. Imaging was completed using automated serial sectioning on a Zeiss Sigma field-emission scanning electron microscope equipped with a 3View ultramicrotome.

### **3D-EM Segmentation and Analysis**

Complete three-dimensional reconstructions of *Chlamydia* inclusions were constructed and analyzed using the IMOD image processing software (University of Colorado, Boulder). Inclusion membrane and chlamydial forms were marked on two-dimensional electron micrographs then assembled together to build the 3D models. Numerical, volumetric, and spatial analyses were conducted using plug-ins of the IMOD software (3Dmod).

### **Mathematical Modeling**

#### Bang-Bang Model

A system of ordinary differential equations was constructed using a simple network interconnection representing RB division and RB-to-EB conversion. Each of these processes was modeled using intermediate species EB and IB respectively. All reaction rates are linear, and the reaction parameter values are outlined in Table 5.3. A preliminary optimal control analysis found that in order to maximize the number of EBs at a given time of host cell death, the optimal rate  $u(t)$  of conversion over time is given by  $u(t)=0$  for  $0 < t < t_s$ , and  $u(t)=u_{\max}$  for  $t > t_s$ , for a certain threshold value  $t_s$  that can be calculated as a function of the expected host cell death time (168). Given that real biological systems cannot be expected to change their conversion rate instantaneously, we linearly increased the conversion rate along an interval  $[t_1, t_2]$ . The solution of this system of equations was calculated numerically using Matlab.

#### Contact-Dependent Model

A spatial model was built to incorporate information about the distance between each

chlamydial form and the nearest inclusion membrane. We assumed that the inclusion is roughly spherical, and implemented 25 adjacent compartments to describe increasing distance from the membrane. On each compartment we replicated the same model described in the bang-bang time course model. Unlike that model, in this model the rate of conversion is not time-dependent but constant. Instead, the compartmental model implements a form of the contact-dependent hypothesis, by assuming that the rate of conversion is zero for cells in the first compartment (i.e. adjacent to the membrane). Chlamydial forms can also move along adjacent compartments via linear diffusion terms. All rates of motion between compartments are identical for each cell type, with the exception of motion away from the membrane-bound compartment, which is assumed to be less due to the physical contact with the membrane.

#### Stochastic RB Size Model

A discrete-time, stochastic model of cell-size dynamics was implemented and parameter-fitted using experimental data. An RB cell is assumed to divide every two hours, and its rate of growth during every two-hour period is assumed to vary stochastically. The size of the cell at the initial time has a normal distribution with mean  $1 \mu\text{m}^3$  and standard deviation  $0.2 \mu\text{m}^3$ . During each period of two hours, the cell grows at a continuous rate  $k$ , so that after two hours it has size  $\exp(2k) \cdot S$ , where  $S$  is the size in the beginning of the two hour period. The number  $k$  is normally distributed with mean 0.27 and standard deviation 0.12. For example, if  $k=0.27$  (mean value), then the cell will grow 1.76 times before dividing, consistent with the experimental data.